THERMO-MECHANICAL FINITE ELEMENT ANALYSIS AND DESIGN OF TAIL SECTION FOR A BALLISTIC MISSILE

A THESIS SUBMITTED TO
THE GRADUATE SCHOOL OF NATURAL AND APPLIED SCIENCES
OF
MIDDLE EAST TECHNICAL UNIVERSITY

BY

TOGAN KEMAL GÜLER

IN PARTIAL FULLFILLMENT OF THE REQUIREMENTS
FOR
THE DEGREE OF MASTER OF SCIENCE
IN
MECHANICAL ENGINEERING

OCTOBER 2012

Approval of the thesis:

THERMO-MECHANICAL FINITE ELEMENT ANALYSIS AND DESIGN OF TAIL SECTION FOR A BALLISTIC MISSILE

submitted by **TOGAN KEMAL GÜLER** in partial fulfillment of the requirements for the degree of **Master of Science in Mechanical Engineering Department, Middle East Technical University** by,

Prof. Dr. Canan Özgen _____
Dean, Graduate School of **Natural and Applied Sciences**

Prof. Dr. Süha ORAL _____
Head of Department, **Electrical and Electronics Engineering**

Prof. Dr. Metin AKKÖK _____
Supervisor, **Mechanical Engineering Dept., METU**

Examining Committee Members:

Prof. Dr. Suat KADIOĞLU _____
Mechanical Engineering Dept., METU

Prof. Dr. Metin AKKÖK _____
Mechanical Engineering Dept., METU

Assis. Prof. Yiğit YAZICIOĞLU _____
Mechanical Engineering Dept., METU

Assis. Prof. Gökhan O. ÖZGEN _____
Mechanical Engineering Dept., METU

M. Sc. Eng. Bülent ACAR _____
Lead Engineer, ROKETSAN Inc.

Date: 31/10/2012

I hereby declare that all information in this document has been obtained and presented in accordance with academic rules and ethical conduct. I also declare that, as required by these rules and conduct, I have fully cited and referenced all material and results that are not original to this work.

Name, Last name : Togan Kemal GÜLER

Signature :

ABSTRACT

THERMO-MECHANICAL FINITE ELEMENT ANALYSIS AND DESIGN OF TAIL SECTION FOR A BALLISTIC MISSILE

GÜLER, Togan Kemal
M.S., Department of Mechanical Engineering
Supervisor: Prof. Dr. Metin AKKÖK

October 2012, 99 pages

During the flight of missiles, depending on the flight conditions, rotation of missiles around its centerline can cause instabilities. To override this issue, missile generally is designed in 2 sections. In the missile, the rear tail section and the front section are to rotate freely by means of bearings. Tail section on which bearings are mounted is designed according to thermal loads due to flow of hot gasses through the nozzle and mechanical loads due to inertial load, interference fit and thread preload which appear during flight of missile.

The purpose of this thesis is to determine the most suitable structural parameters according to the flight conditions of missile.

The geometrical and load parameters which have effect on the results were determined. Finite element model is formed by using FEA software. After that, transient nonlinear thermo-mechanical analyses are performed and the most effective parameter on VM (Von-Mises) stress and force is determined.

DOE (Design of Experiments) method was used to determine the most suitable values for the structural parameters. Totally 27 different configurations are studied to achieve to the most suitable values for variable set.

It is observed that VM stress and force results for all configurations are within the ±%5 ranges. So this means parameters don't affect the systems response very much. By taking manufacturing processes into consideration, configuration with the highest bearing inner/outer ring interference is taken. From the comparison of the results, the most suitable configuration is obtained after checking forces and VM stress on the bearings.

Keywords: Missile Tail Section, Bearings, Finite Element Method, Nonlinear, Thermo-Mechanical Analysis

ÖZ

SONLU ELEMANLAR YÖNTEMİ İLE TERMO-MEKANİK ANALİZİ YAPILAN BALİSTİK FÜZELER İÇİN KANAT HAMİLİ TASARIMI

GÜLER, Togan Kemal
Yüksek Lisans, Makina Mühendisliği Bölümü
Tez Yöneticisi: Prof. Dr. Metin AKKÖK

Ekim 2012, 99 sayfa

Füzelerin seyri esnasında uçuş şartlarına bağlı olarak bazı durumlarda füzeler kendi ekseni etrafında dönmeleri kararsızlığa yol açmaktadır. Bu durumu gidermenin temel yöntemi füze 2 parça olarak tasarlanmaktır. Füzede arka kuyruk tarafı ve ön taraf birbirinden bağımsız olarak rulmanlar sayesinde serbestçe dönüş yapabilmektedir. Bu kapsamda rulmanların montajlanmış olduğu sistem (kanat hamili) fırlatma ve uçuş esnasında ortaya çıkan termal (İç ısınma) ve mekanik (atalet, sıkı geçme ve cıvata ön gerilme) yüklere dayanabilecek şekilde tasarlanmaktadır.

Bu tezin amacı uçuş şartlarına göre optimize edilmiş en uygun yapının belirlenmesidir.

Sonuçlar üzerinde etkisi olan geometrik ve yük parametrelerinin belirlenmiştir. Bu parametrelere göre SEY yazılımı kullanılarak sonlu elemanlar modeli oluşturulmuştur. Ardından zamana bağlı doğrusal olmayan termo-mekanik analizler yapılarak hangi parametrenin gerilme üzerinde en fazla etkiye sahip olduğu belirlenmiştir.

Deneysel tasarım yöntemi kullanılarak en iyi parametre setine ulaşılmıştır. En iyi parametre setine ulaşmak için toplam 27 farklı konfigürasyon üzerinde çalışılmıştır.

Bütün konfigürasyonlardaki gerilim ve yük değerleri incelendiğinde, değerlerin ±%5'lik aralık arasında olduğu görülmüştür. Böylece parametrelerin sistemin tepkisinde çok fazla etkisi olmamıştır. Üretim süreçleri göz önünde bulundurulduğu takdirde, en yüksek sıkı geçmeli konfigürasyon seçilmiştir. Rulmanlardaki gerilim ve yük sonuçlarının karşılaştırılmasıyla, en uygun konfigürasyon elde edilmiştir.

Anahtar Kelimeler: Füze Kanat Hamili, Rulmanlar, Sonlu Elemanlar Yöntemi, Doğrusal Olmayan, Termo-Mekanik Analiz

To My Family and Fiancée

ACKNOWLEDGEMENTS

I would like to express my deepest gratitude and appreciation to my supervisor Prof. Dr. Metin AKKÖK who inspired, encouraged and guided me at all levels of the study.

I would like to thank to ROKETSAN for partially supporting this study. I would also like to thank my colleagues in ROKETSAN for their support and discussions that expanded my horizons.

Special thanks go to Mr. Doğuş ÜNLÜ, Mr. Halil ARDIÇ and Mr. Ali YETKİN for their help during modeling and test activities.

I would like to express my sincere appreciation to Mr. Bülent ACAR for sharing his substantial knowledge in Finite Element Methods with me.

Finally, my greatest thanks go to my family and fiancée for their endless support and understanding.

TABLE OF CONTENTS

LIST OF TABLES

TABLES

LIST OF FIGURES

FIGURES

LIST OF ABBREVIATIONS

2D	Two Dimensional
3D	Three Dimensional
APDL	Ansys Programming Design Language
CoG	Center of Gravity
CAD	Computer Aided Design
CFD	Computational Fluid Dynamics
DOF	Degrees Of Freedom
FE	Finite Element
FEA	Finite Element Analysis
LC	Load Case
TM	Thermo-Mechanical
SDB	Stress Distribution for Bearings
VM	Von-Mises
VMS	Von Mises Stress

CHAPTER 1

INTRODUCTION

A missile/rocket is a weapon system used for destruction of a target. It is a structure combined of explosive material and propulsion material. Propellant term is used as a propulsion material. There are 2 main types of propellant; solid and liquid. Missile/rocket is fired by reaction of propellant. A spark is produced by igniter to start the chemical reaction for the propellant. After start of reaction, reaction speed can be controlled by changing liquid ratio for the liquid propellant. But for solid propellant reaction speed cannot be controlled. If reaction of solid propellant starts, reaction cannot be stopped and finishes when propellant finishes.

There is a difference between missiles and rockets; Rocket is an un-guided structure, missile is a guided structure. So rocket has to be guided to target area accurately, but missile doesn’t need accurate guiding.

1.1 Missile Technology

According to Newton's 3rd Law of Motion; For every action there is an equal and opposite re-action. Rocket/missile uses this principle. Reaction of the propulsion creates hot gases to the back side of rocket/missile. Hot gases push oxygen in the atmosphere. So thrust at the rear side of rocket/missile is formed by this reaction. Finally flight of rocket/missile occurs. This thrust force shall be higher to overcome weight of rocket/missile and aerodynamic forces acting on rocket/missile.

1.1.1 Historical Development of Rockets and Missiles

Historical development of rockets and missiles is given with details in reference [1] and [2]. According to these references, brief information is given below.

Most of the evidences show that invention of rocket is started in China (in 12th century) where the gunpowder was invented. This rocket was used for fireworks. In the same century rockets are started to be seen in the European wars. It is known that first usage was in the Legnica battle in 1241 by Mongols. Also there are reports for Arabs who used rocket in 1249, Peduans in 1379 and Venetians in 1380. Details of these first generation rockets aren't known. But probably case of the rocket is produced with paper layers and coated with shellac. Propellant was made of simple black powder. In 1668, it is seen that there is noticeably size and performance developments on the rockets. In Germany 60 kilograms rocket was designed. This rocket was made of wood and covered with glue-soaked sailcloth. Also this rocket contains 7 kg explosive material.

In the 18th century, India developed a rocket with an important development. For this rocket, metal cylinder is used for conserving explosive material. As discussed above, up to this point, wooden cylinders are used. Metal cylinder is made of unprocessed iron. But strength is better than paper. Higher internal pressure can be provided from propellant. These types of rockets are launched with large numbers because these rockets didn't strike to target accurately.

In the USA, Robert Hutchings Goddard was working on rocket technology. Steel cylinder and tapered nozzle is used. With this usage he improved thrust force and efficiency of rocket. In World War I, rockets didn't used very much but France used anti-balloon rockets and Germany used rockets for throwing grappling hook. In 1918, Charles F. Kettering from USA, used a gyroscope and barometer on his missile design. Gyroscope was used to control the lateral movement of the missile. Barometer was used to control the altitude of missile.

Until World War II, many experimental and design activities were performed on rockets and missiles in a number of countries. Germany was really concentrated on the rocket/missile technology. Not only government but also amateur designers worked on the rocket/missile technology. Wernher von Braun was a designer of amateur society. He was the technical leader of a work group who works on liquid propellant. The first modern ballistic missile was developed by Germany. This rocket is used liquid oxygen and had fin stabilization.

USA began to use air-to-surface guided missiles in standard aerial ammunition in the late 1950s. The first of these was "AGM". "AGM" is a rocket-powered weapon that employed visual tracking and radio-transmitted command guidance. Missile is controlled by operator commands. "AGM" is used to attack enemy radars and surface-to-air sites.

USA began to use air-to-surface guided missiles in 1947. The first was developed in 1947 named “Firebird”.

Germans were started to work on surface-to-air missiles at the World War II end. But these were not sufficient to use in the war. In the 1950s and ’60s with the rapid development occurs in the Soviet Union, USA, Great Britain, and France.

After World War II, rockets are launched from multiple-tube pods. Pods are very useful to transport rockets in one package. They are used for massive firings.

1.1.2 Sub-Systems of Missiles

Sub-systems of missiles is given with details in reference [3]. According to this study, brief information is given below.

Missile is formed as 4 main parts; the structural sub-system, the payload sub-system, the guidance sub-system, and the propulsion sub-system (Figure 1-1).

The structural sub-system is the biggest part of missile. It is the mechanical part of the missile. Structural sub-system carries all components of missile inside it. It has to be strong and it has to be manufactured by low-density material. Generally structure is designed as a cage system. Also there are fins at the rear side of missile. Fins helps missile to be stable during flight.

The payload sub-system changes according to missile’s usage area. Generally various types of explosives are used. In addition to that missiles are used for communications, forecast monitoring and space studies.

The guidance sub-system is a special designed and confidential part of the missile. This sub-system consists of special equipment like complex sensors and communication equipment. These equipment provide missile to maneuver in flight. Maneuvering method differs according to companies and countries. Countries develop different methods for that. Also the guidance sub-system has a duty to provide missile stability not to overturn in flight.

Propulsion sub-system is the biggest part of the missile. There 2 types of propulsion sub-system s; liquid and solid propellant. The structural sub-system, the payload sub-system, the guidance sub-system, and the propulsion sub-system are changes according to missile usage area. Often payload and guidance sub-system are grouped. Because designer wants to make propulsion sub-system the biggest part of missile to increase the range.

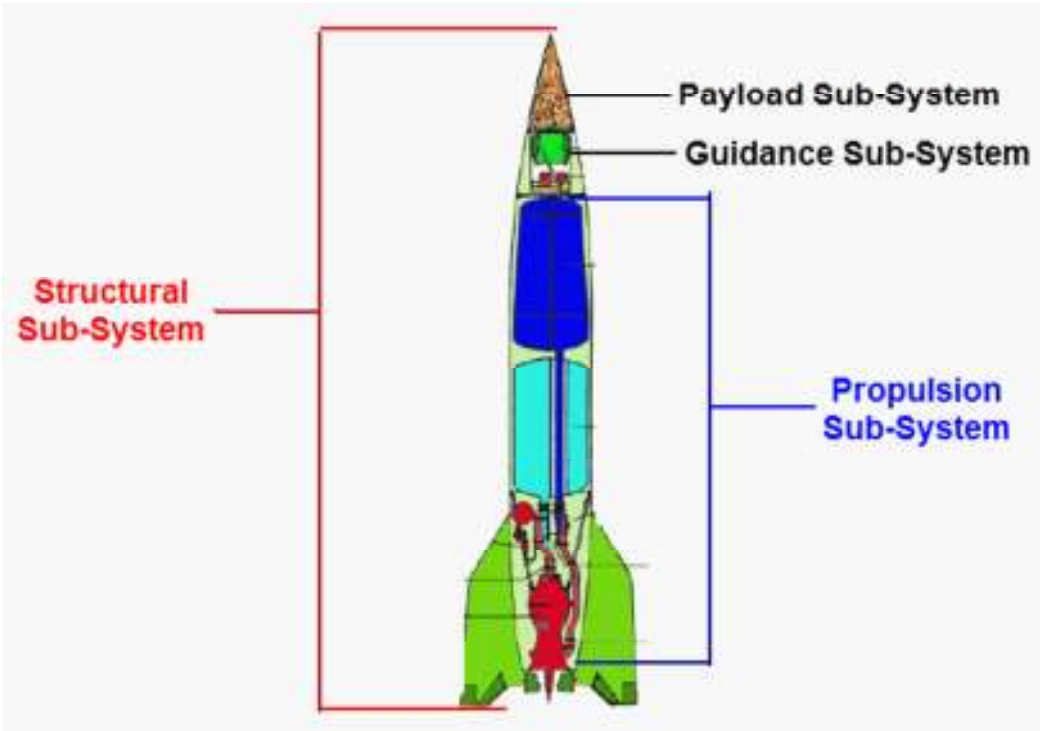

Figure 1-1. A View of Missile Sub-Systems [4]

1.1.3 Types of Missiles

1.1.3.1 Description of Cruise Missile

A cruise missile (Figure 1-2) is a guided missile towards a land-based or sea-based target. Usually cruise missiles have large payload sub-system and have long ranges. During flight cruise missiles can reach supersonic or high subsonic speeds. They have advanced guidance sub-system to reach the target accurately [1], [3].

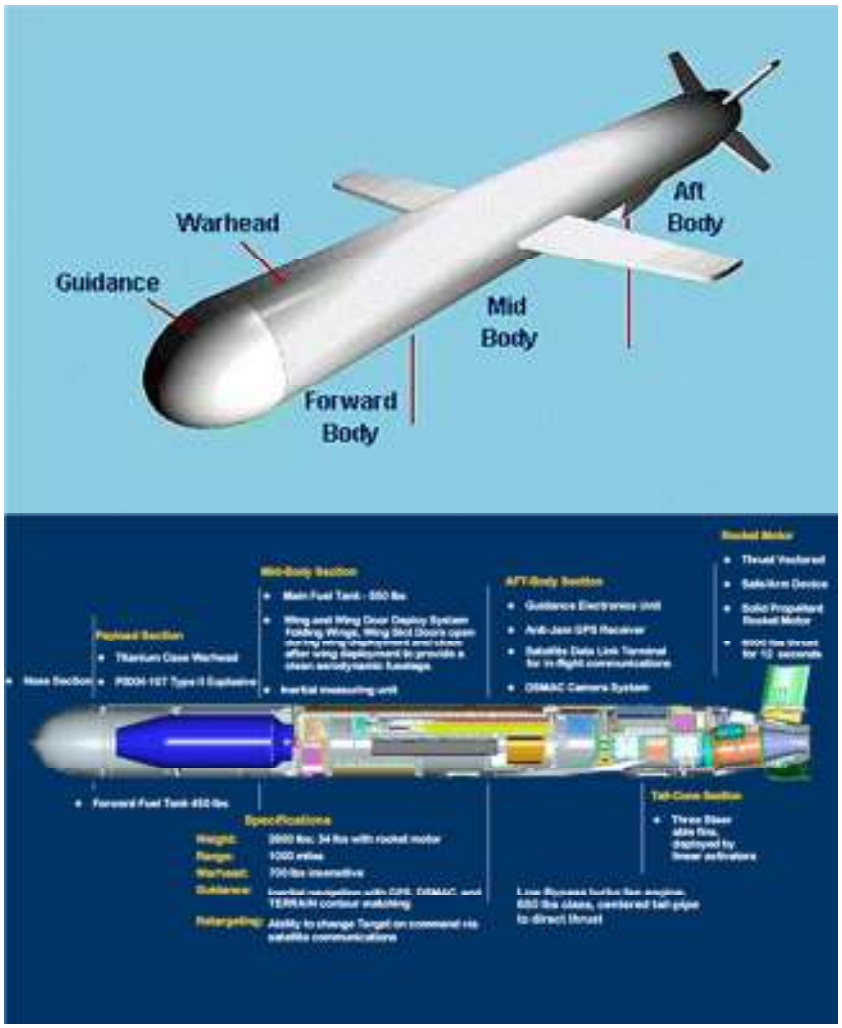

Figure 1-2. Views of Cruise Missile [5]

1.1.3.2 Description of Ballistic Missile

A ballistic missile (Figure 1-3 & Figure 1-4) is a missile that follows a set trajectory. This trajectory is determined by advanced computer software. During flight missile doesn't get out this trajectory. If missile gets out of this trajectory, missile destroys itself or it is destroyed by the operator. For ballistic missiles, guiding is used only in the thrust phase [1], [3].

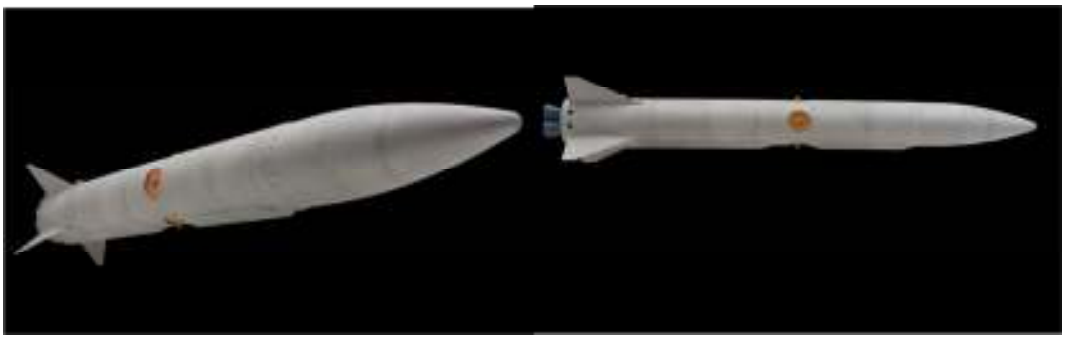

Figure 1-3. Views of a Ballistic Missile [6]

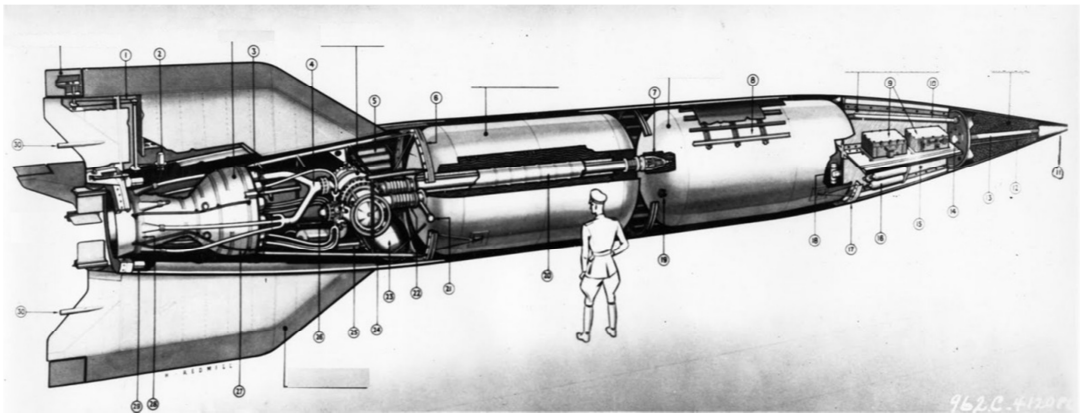

Figure 1-4. Cutaway View of a Ballistic Missile [7]

A ballistic missile trajectory consists of 3 phases; the thrust phase, the free-flight phase, and the reentry phase where the missile reenters the Earth's atmosphere. Thrust phase is the time phase in which propellant is used and missile is powered. The free-flight phase is the time phase in which missile travels freely (without thrust force) [3].

Ballistic missiles are launched from stationary areas or weapon systems (Figure 1-5 & Figure 1-6). The thrust phase duration can be variously change from seconds to minutes range. This duration change according to the propulsion sub-system of missile [3], [8], [9].

Figure 1-5. A View of a Weapon System [10]

Figure 1-6. A View of a Weapon System During Firing [10]

After thrust finishes, missile enters free-flight phase. In free-flight phase missile travels long distance than other phases.

The reentry phase starts when aerodynamic force starts to affect on the missile. Aerodynamic force slows down the missile.

1.2 Definition of the Problem

Nowadays, most of the countries work on weapon development, especially rocket/missile systems. Only large size companies (usually public companies) can work on these types of projects due to cost issues. Customers (armed forces) always want these projects to be finished as soon as possible. So designers work on the projects very intensively. During the course of the project, unpredictable problems may occur. These problems have to be solved very quickly and accurately. Special and advanced softwares are very helpful during early phase of the design.

During the flight of missile, because of the aerodynamic force mechanical loads occur on the missile. Beside the mechanical loads, thermal load occur on the tail section of missile. Details of loads acting on the missile are given in section “2.3 Loads on the Tail Section”. In this thesis, bearings in the tail section (Figure 1-7) of the missile are focused.

Under the applied transient TM (Thermo-Mechanical) loads, VM stresses and forces around the bearings are investigated by FEA. As mentioned above, there are 2 types of loads; mechanical and thermal loads. Combination of these loads is called TM loads. In order to take TM loads into account, TM analysis has to be performed. The details of the TM analysis are explained in upcoming section of the chapter.

Also some loads acting on the tail section depend on time. So TM analysis is performed with transient functionality.

Output of the FEA results are examined. It is seen that there are some important variables which have greater impact on VM stresses than other parameters. Therefore, these important variables are defined and changed within the tolerance range. These variables are the bearing inner ring interference, the bearing outer ring interference and the thread preload. By using DOE method, several finite element runs need to performed to determine the most suitable variable set. The most suitable variable set is determined by investigating VM stress and force distribution on the bearings. For VM stress distribution, firstly maximum VM stress on the bearings are controlled if it exceeds material mechanical limitations, secondly minimum value of the maximum VM stress is taken as the most suitable variable set. Beside of these controls, force distribution on the bearings is used to check if there is any separation between bearings and other parts.

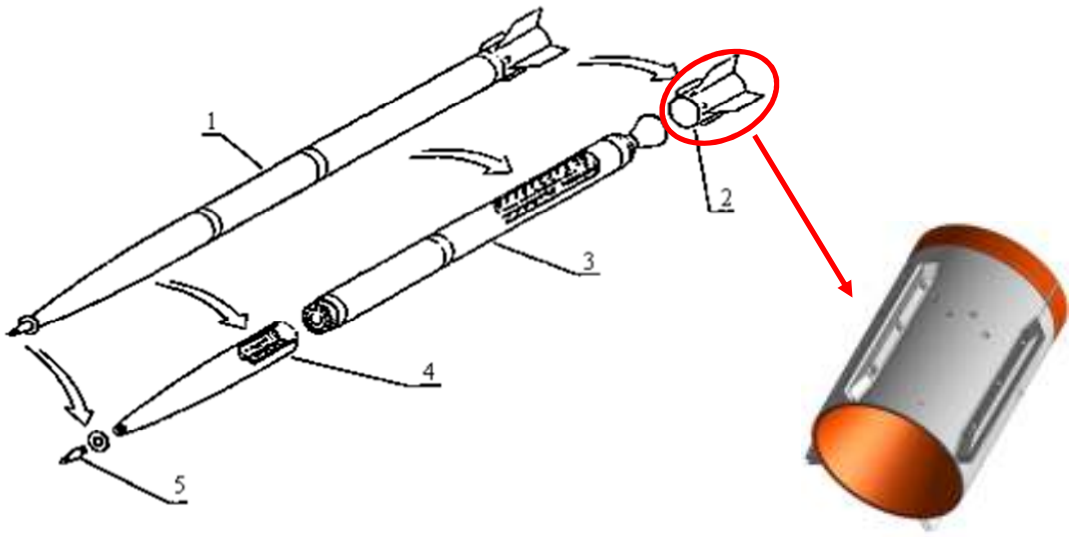

Figure 1-7. A View of a Missile Tail Section

The tail section has to meet all 5 multidisciplinary requirements given in Figure 1-8. Even if one of these 5 requirements fails, the design will be considered unsuccessfully.

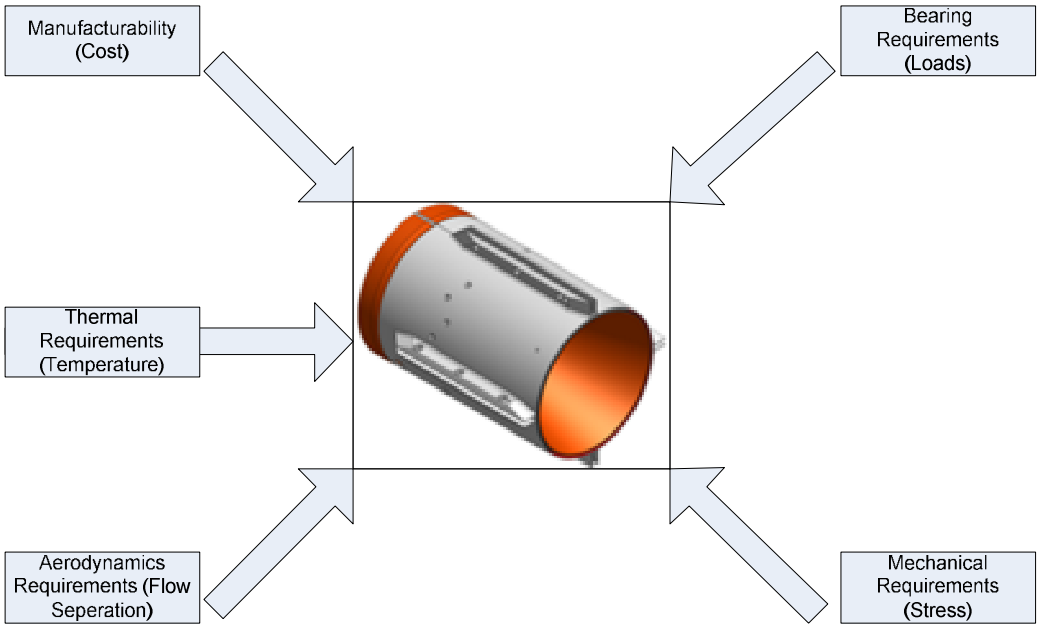

Figure 1-8. Tail Section Design Requirements

Manufacturability, thermal and aerodynamics requirements are static requirements. Bearing, thermal and mechanical requirements are dynamic requirements. Dynamic requirements are able to change according to DOE variables but static requirements aren't. So the chosen DOE variables at the end of thesis won't affect the static requirements. But for chosen DOE variables, forces and VM stresses acting on the bearing is changeable.

For manufacturability; since the chosen DOE parameters doesn't affect manufacturing process, the cost is not recalculated.

For aerodynamics requirements; because the geometry on the flow path does not change, aerodynamics requirements will not be checked after each one of iteration.

For bearing requirements; VM stresses acting on the bearings are evaluated. These VM stresses are compared with stress limitations of bearings (Limitations are taken from bearing catalogue). From this comparison the most suitable DOE parameter is used.

For thermal requirements; the temperature of the bearings are evaluated. These values are compared with temperature limitations of bearings (Limitations are taken from bearing catalogue).

For mechanical requirements; VM stresses on the bearings evaluated. These VM stresses are compared with limitations of materials. From this comparison the most suitable DOE parameter is are determined.

1.3 Outline of the Thesis

In Chapter 1, an introduction is given and the historical development for missiles is explained with details. The definition of the problem is explained and the objective of the thesis is stated clearly.

In Chapter 2, the geometrical detail of the relevant sections is shown with sub-assemblies. Mathematical discretization of the geometry is explained. Subsequently; applied loads, material and boundary conditions are presented as well.

In Chapter 3, the parameters and design of experiments logic is given. Also transient finite element results including VM stress along with temperature distribution is shown.

In Chapter 4, discussions of the results are presented and future works are given.

CHAPTER 2

FINITE ELEMENT MODELLING OF THE TAIL SECTION

For the whole design of tail section, all steps are given below with explanations; Firstly the design requirements for the missile are determined. According to the requirements mechanical design is performed by design department. By using special CFD (Computational Fluid Dynamics) software, analysis is performed on the mechanical model. Output of the CFD analysis, heat flux values are determined. Up to this point whole missile is used for calculations and analysis but after this point missile is started to be examined by its sections (such as tail section). Heat flux values are used in transient thermal analysis of the tail section.

By using the output of transient thermal analysis, the other variables coming from CFD analysis and mechanical assembling values (Preload, bearing ring interference), FEA is performed. For the first analysis, the standard mechanical assembling values given in the part catalogue of the VENDOR is used.

According to output of the analysis, mechanical assembling values are changed and new analyses are performed again. After commenting analysis results, optimum input are investigated and physical model is produced.

Experiments are performed on the physical model. If this physical model is failed during the tests, mechanical design step is studied again and all other steps are performed again until physical model passes from experimental tests. After passing tests, the physical model is manufactured for final configuration. Flow chart of the design approach is given in Figure 2-1. In this thesis blue boxes in the flow chart are considered. Other boxes are considered by other departments.

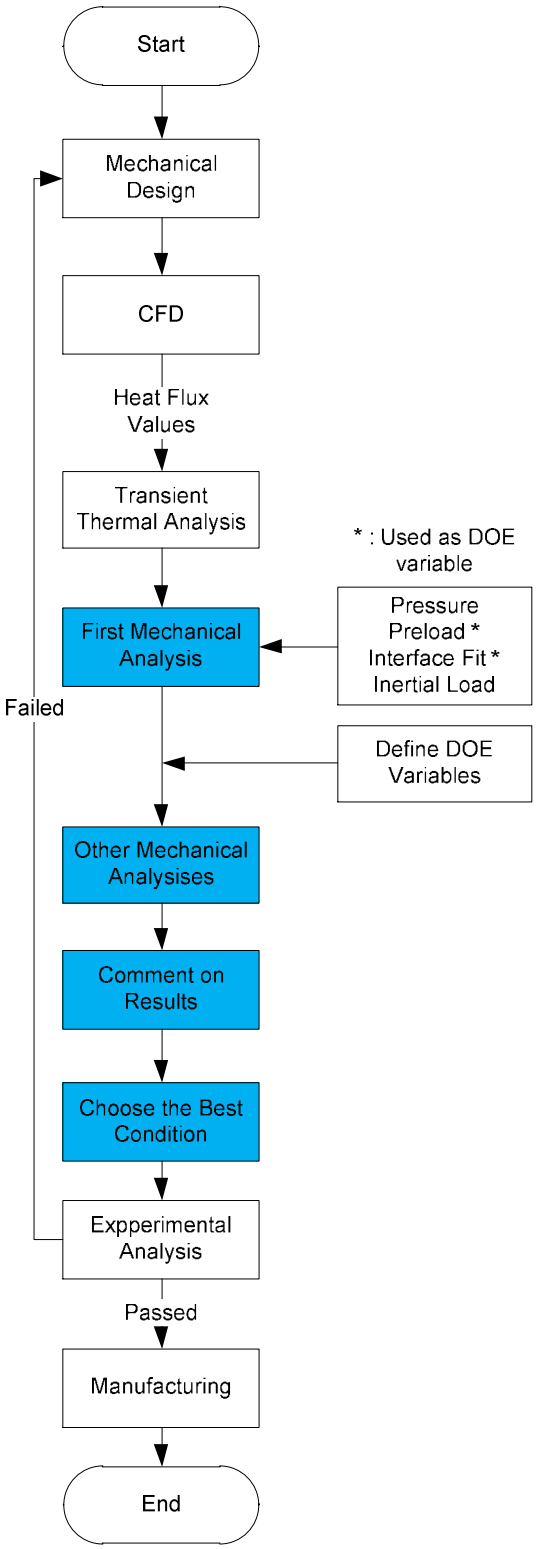

Figure 2-1. Flow Chart of the Design Approach

2.1 FEA Modeling Details

Analysis model is prepared as 2D axisymmetric elements. Mesh sizes for each part are given in section “2.6 Details of FEA Model for the Tail Section”. Because of the criticality at the thread and bearing, at these points concentrated mesh is used. Finite element model is composed of 8 node quadratic “Plane183” elements. Except bearings for all parts “Plane183" “axisymmetric” element is used.

“Plane183" (Figure 2-2) is a higher order 2-D, 8-node or 6-node element. “Plane183" has quadratic displacement behavior and is well suited to modeling irregular meshes (such as those produced by various CAD/CAM systems).

This element is defined by 8 nodes or 6 nodes having two degrees of freedom at each node: translations in the nodal x and y directions. The element may be used as a plane element (plane stress, plane strain and generalized plane strain) or as an axisymmetric element. This element has plasticity, hyperelasticity, creep, stress stiffening, large deflection, and large strain capabilities. It also has mixed formulation capability for simulating deformations of nearly incompressible elastoplastic materials, and fully incompressible hyperelastic materials. Initial state is supported. Various printout options are also available [11].

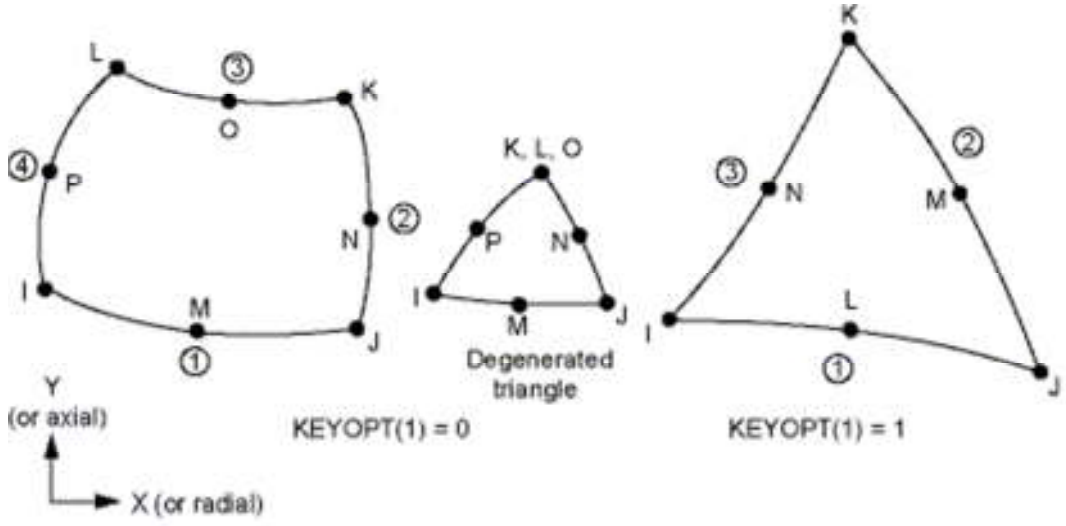

Figure 2-2. Plane183 Element

At the analysis model, there are 7284 element and 21417 nodes. The analysis is performed statically. Firstly, the analysis is run with preloads on bearings and threads. Secondly, pressure is integrated into the analysis with “Restart” command.

In reference [12], it is shown that FEA is very useful to understand the behavior of bearing under the various load conditions. The results are used to achieve improvements of the assembly which includes bearings inside. Also by discussing on the results with the bearing manufacturer, it is seen that very good improvements are gained. Because combination of manufacturer experience and FEA results build better approaches.

2.2 Boundary Conditions of the Tail Section

FEA of the tail section is solved as static. All dynamic force are converted to static forces. In FEA, there shall be some mechanical limitations (fixing point, line etc.) on the tail section model. If there is no fixing point on the model, model cannot be solved statically. To make model statically equilibrium, rear side of the tail section is fixed in Y direction (Figure 2-3).

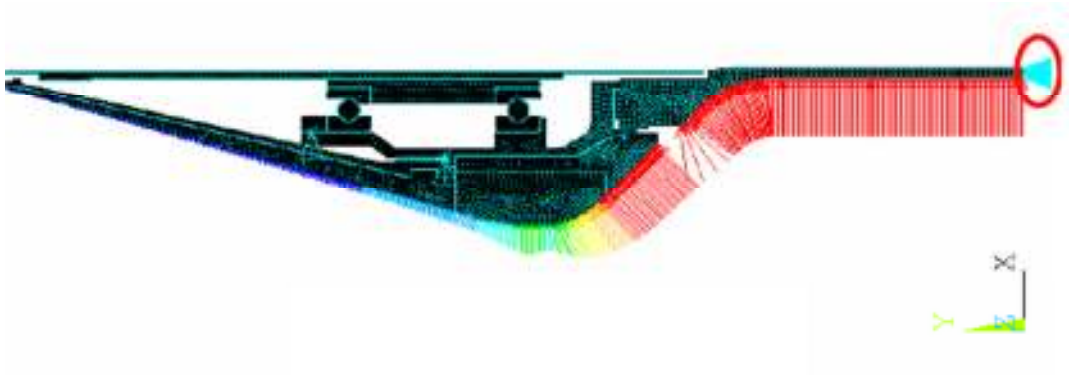

Figure 2-3. Fix Point of the Model

2.3 Loads on the Tail Section

There are 2 types of loads; thermal loads and mechanical loads. Thermal loads are occurred due to flow of hot gasses through the nozzle. Mechanical loads are occurred due to inertial load, interference fit and thread preload which appear during flight of missile. The details for loads are given below.

Variation of the loads on the tail section with time is given below. Y-axis is defined as amplitude of load, X-axis is defined as time. On time axis there t(p) and t(end) variables defined as; finish time of the chemical reaction of propellant, finish time of the missile flight, respectively.

2.3.1 Thermal Loads on the Tail Section

Launching missile starts with the burning of the propellant. During the reaction, thrust force and heat occurs. Firstly, propellant is designed. According to ingredients of propellant, CFD analysis is run. Analysis results show transient heat flux values.

Secondly, by using heat flux values, FEA is run. A view of analysis results (Figure 2-5) show mechanical effects of heat on the tail section. CFD analysis is continued until the end of propellant reaction. From the results of FEA, it is given that the load doesn't start from the start of reaction. But acting load ends at the end of reaction finishes. The thermal load versus time is given in Figure 2-4.

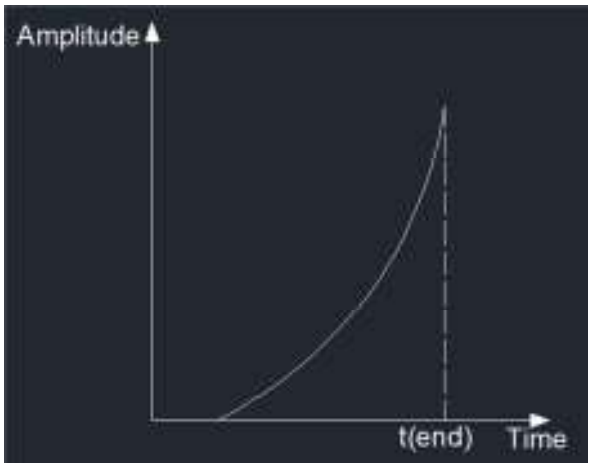

Figure 2-4. Thermal Load – Time Graph

Figure 2-5. Temperature Distribution of the Tail Section

2.3.2 Mechanical Loads on the Tail Section

2.3.2.1 Loading due to Pressure

After the start of propellant chemical reaction, pressure occurs inside the tail section. Firstly pressure increases until stabilization point. There is no change on the pressure value until chemical reaction finishes. After chemical reaction finishes, pressure goes to zero. Time graph for pressure is given in Figure 2-6. Pressure distribution is given in Figure 2-7.

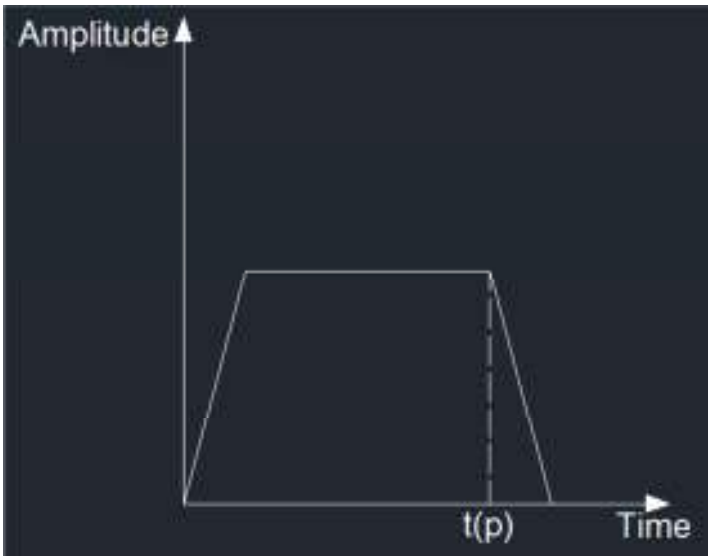

Figure 2-6. Pressure – Time Graph

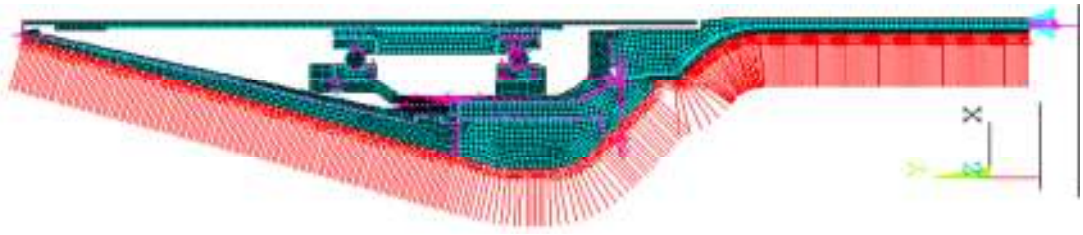

Figure 2-7. Pressure Distribution on the Tail Section

2.3.2.2 Loading due to Preloads

Preload is the term used for bolts (threaded parts). Preload affects reliability of the assembling parts. If preload is calculated very accurately, threaded parts of the assembly won't loosen. This is one of the most important variable for bolted joints. Preload can be applied by using torque wrench. When preload is given to bolt, deformation occurs on the bolt. So bolt acts as a spring and it tries to pull assembling parts [13].

Reference [14] gives information about the a classical preloaded bolted joint calculation and its insufficiencies for direct application on bearing connections. In this study, preload and working load are acted on the model and FEA is used to determine the VM stresses on the bolt.

In reference [15], thread connection response to critical pressure are focused. Various FEA methods are used to understand and choose the most efficient method. For modeling the threads 2D or 3D modeling technics are used. But the results and process show analysis with 3D modeling require long computing time. In addition to that results coming from analysis with 2D modeling are very near to 3D modeling. Also reference [16] is concentrate on pressures on the bearings. And results show that 2D modeling is much more reasonable for FEA of bearings. This is because of the same reason (computing time etc.) stated above. Time graph for preload is given in Figure 2-8. At the tail section, 2 preloads are applied; thread section (Figure 2-9) and bearing section (Figure 2-10).

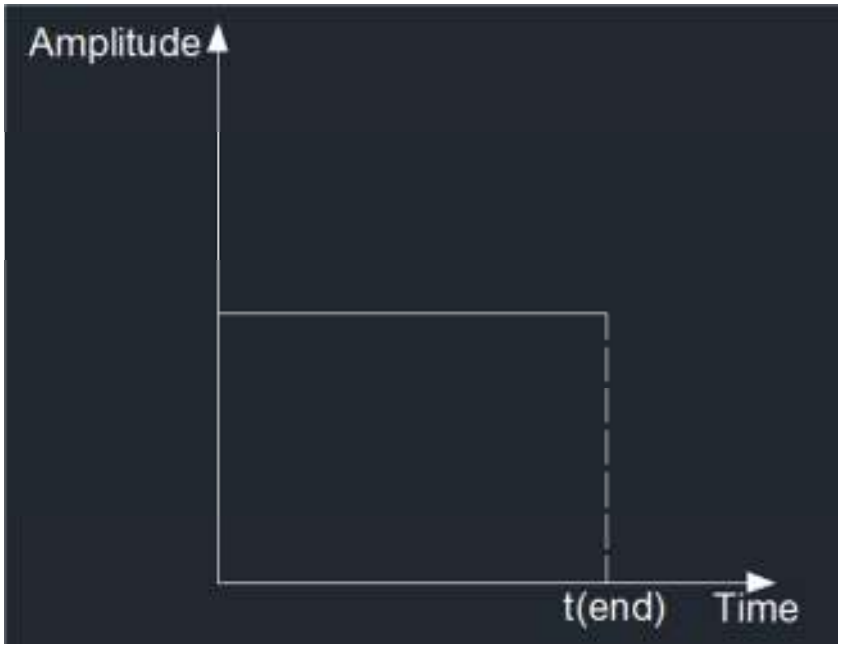

Figure 2-8. Preload (For Thread & Bearing) – Time Graph

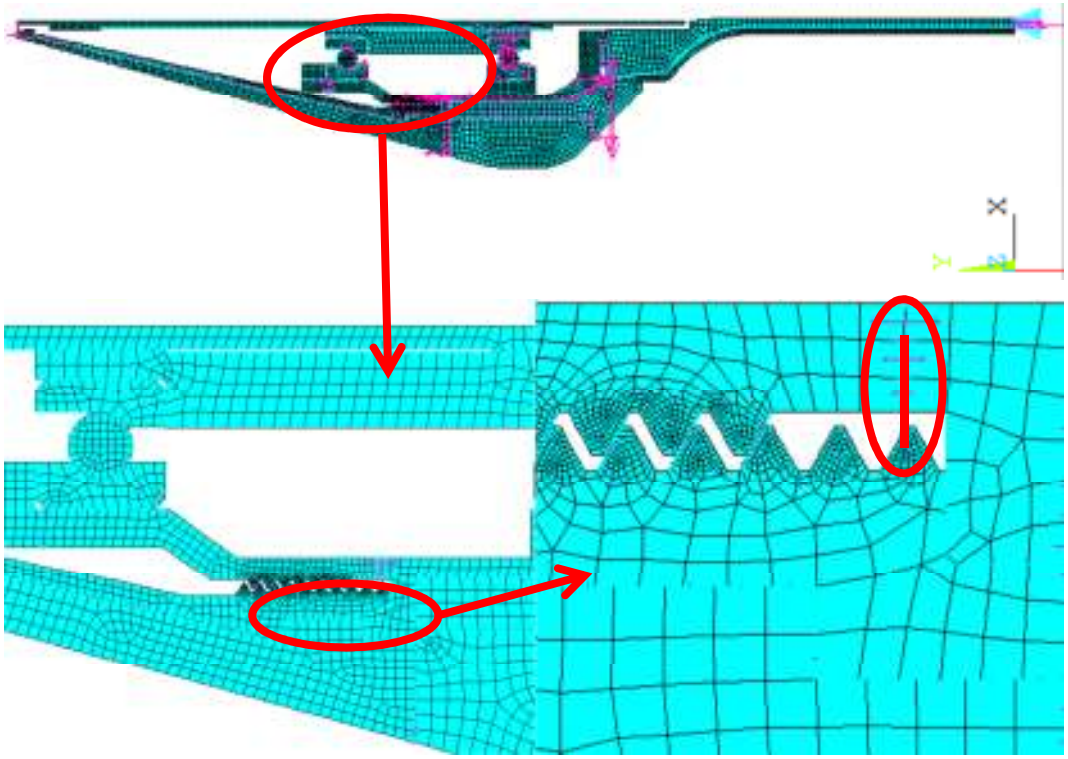

Figure 2-9. Preload @ Thread

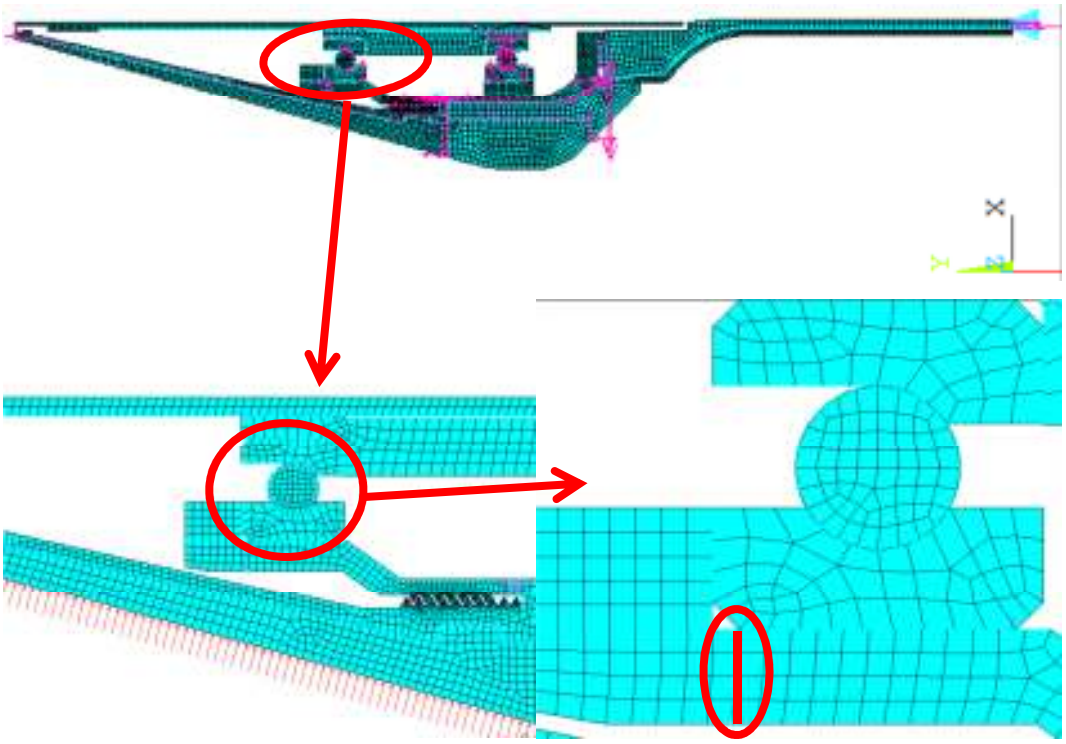

Figure 2-10. Preload @ Bearing

2.3.2.3 Loading due to Interference Fit

One of the objectives of proper bearing installation is to achieve radial holding of the bearing rings with shaft or housing bore. Bearings are used with a shaft or housing bore. To combine bearing with other part (shaft or housing bore), interference fit is used. The interference fit is described as a value of tightness between the shaft and bearing bore or the housing bore and bearing outside diameter. There are 3 types of interference fit types available; loose fit, light interference fit and interference fit.

The purpose of interface fit is to prevent creeping. Temperature increases to high temperatures because of creeping. Once this happens, considerable wear occurs on the fitting surface and both shaft and housing are damaged. So usage life of parts will be lower. Also during bearing operation there will be noise increase because of abrasion.

Normally a large interference fit prevents creeping, but it is necessary to select the interference fit type according to working conditions of bearing. Because operation temperature and the acting forces on the bearing affects working of bearing very much [17], [18], [19]. Time graph for interference fit is given in Figure 2-11. Interference fit locations are given in Figure 2-12. Bearing inner/outer ring interference which is given in Table 3-1, is acted on the interference fit locations.

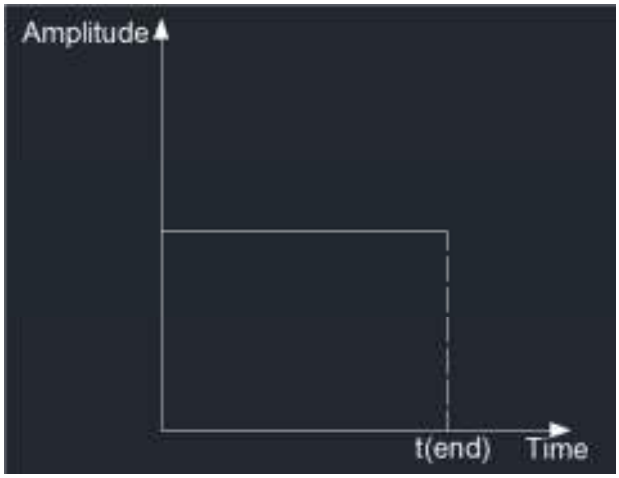

Figure 2-11. Interference Fit – Time Graph

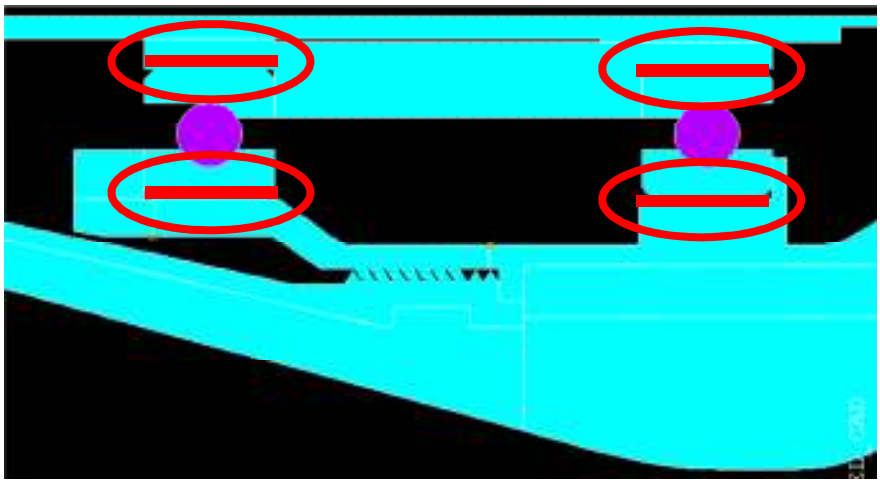

Figure 2-12. Interference Fit Locations

2.3.2.4 Loading due to Inertial Load

After the start of propellant chemical reaction, inertial load occurs inside the tail section until the end of flight. In reality, inertial load changes according to speed, altitude and direction of missile. But generally the maximum value is taken and for all the flight time maximum load is applied.

The CoG (Center of Gravity) of the outer race of the tail section is taken from the 3D modeling software. The inertial load is applied to this point as an acceleration term. Time graph for the inertial load is given in Figure 2-13. The inertial load application point is given in Figure 2-14.

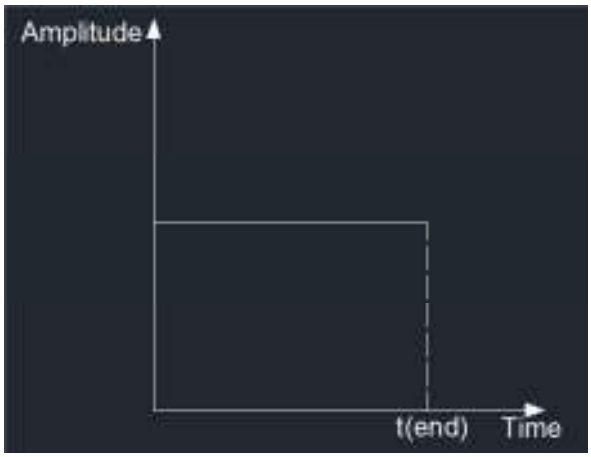

Figure 2-13. Inertial Load – Time Graph

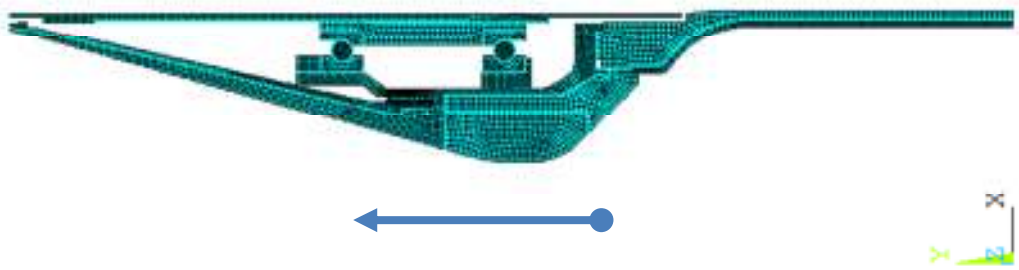

Figure 2-14. Inertial Load Application Point

2.4 Load Cases for FEA Model of Tail Section

As mentioned in “2.3 Loads on the Tail Section” section, various types of loads act on the tail section. All loads given above are combined in one graph (Figure 2-15) to understand the comparison of loads.

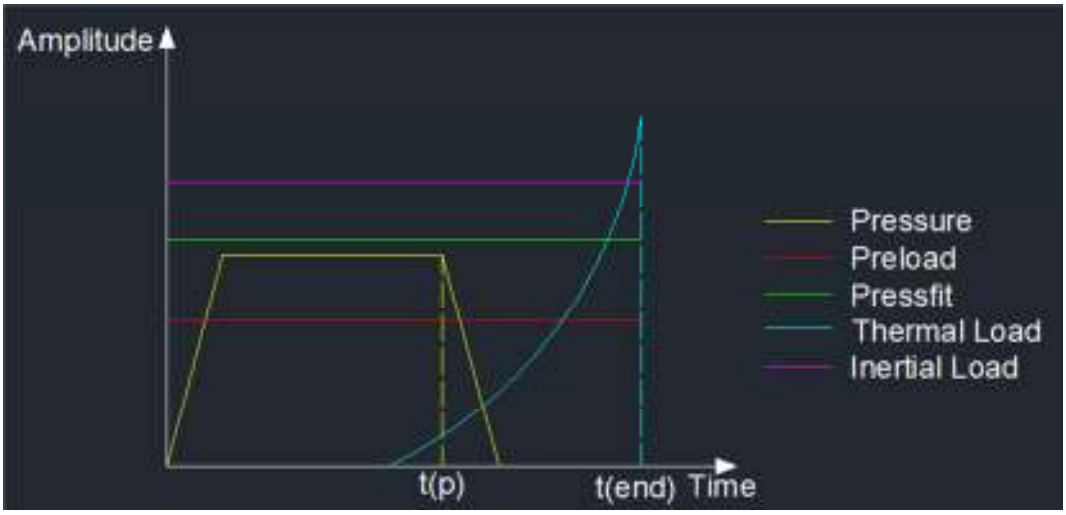

Figure 2-15. Combination of Thermal and Mechanical Loads

Also these loads are applied on the model in different time domains. Different time domains are applied to FEA model as different load cases. Definitions of load cases are given in Table 2-1.

Table 2-1. Definitions of Load Cases

	Definition	Loads on the Tail Section
LC-1	Interference fit (IF) and Preload (PL) are applied	IF+PL
LC-2	Pressure (P) is applied	IF+PL+P
LC-3	Inertial load (IL) is applied	IF+PL+IL+P
LC-4	Thermal load (TL) is applied	IF+PL+IL+P+TL
LC-5(End of burning)	Pressure is removed	IF+PL+IL+TL
LC-6	This is the end of flight	IF+PL+IL+TL

2.5 Geometry and Material Properties of the Tail Section

The tail section CAD (Computer Aided Drawing) model is prepared by the design department in ROKETSAN using IDEAS software. Most of the model is designed as axisymmetric except the fin holder and the bearings which are taken into consideration with special methods (described in 4.6 assumptions section) for the analysis. A view of The tail section CAD model is given in Figure 2-16.

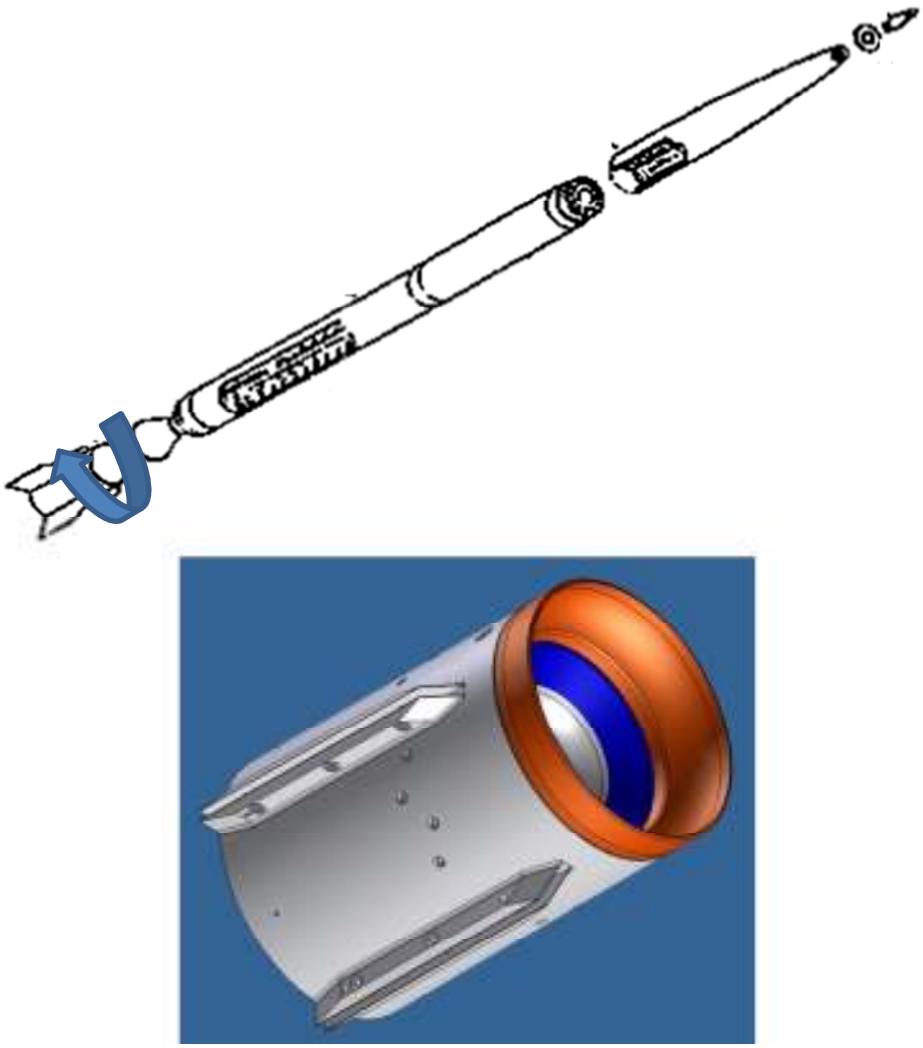

Figure 2-16. A View of the Tail Section

Before making the analysis, some modifications are performed to CAD model. Firstly, the cross-sectional view which is taken from the CAD model including all the parts in the tail section is given in Figure 2-17.

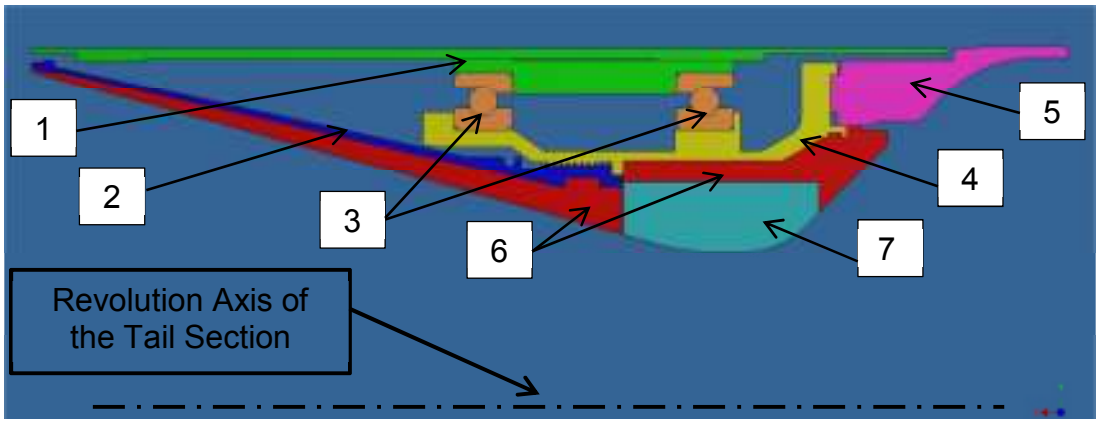

Figure 2-17. Cross-Section of the Tail Section

The parts shown with number 6 and 7 in Figure 2-17 are made of special insulation non-metallic material to prevent the heat conduction to steel materials. The insulation material is able to resist to high temperatures due to the chemical reaction in combustion gases. The Insulation materials are attached to steel material by bonding material on all the contacting surfaces. Also the insulation materials are attached to each other by bonding material with the same principle. The parts shown with number 2 to 5 in Figure 2-17 are made of steel. The parts shown with number 1 are made of aluminum. For the analysis, the materials are modeled as linear elastic with isotropic, property.

The part number 1 in Figure 2-17 is the outer case of the tail section which rotates freely during flight. This part on which the fins are fixed, is mounted by means of 2 bearings (Parts numbered with 3 given in Figure 2-17) and assembled from the right and left. The outer race and bearings are assembled with interface fit.

The part numbered with 4 (Figure 2-17) is the front nozzle of the tail section. The front nozzle and bearings are assembled with interface fit. Part numbered with 2 (Figure 2-17) is the rear nozzle of the tail section. The front and rear nozzles are assembled with threaded mechanical connection.

Part numbered with 5 (Figure 2-17) is the rear dome of the tail section. Front nozzle and rear dome are assembled with mechanical joining elements. The geometric data of the bearings on the tail section are given in Table 2-2.

Table 2-2. Dimensions of the Bearings

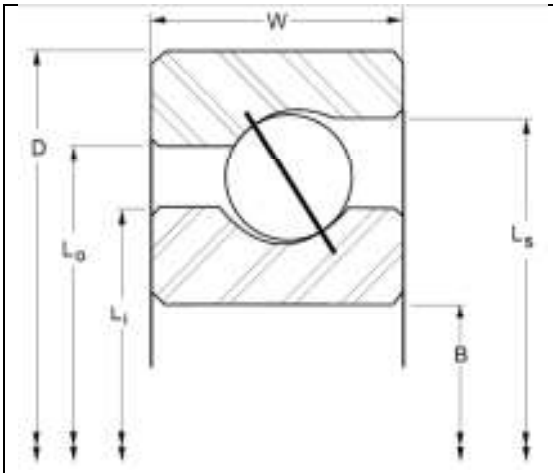	B : 1 inch D : 1,4 inch W : 0,2 inch L_i : 1,15 inch Lo : 1,25 inch Ls : 1,3 inch Ball diameter : 0,1 inch Ball quantity : 8 Raceway Radius : 0,11 inch

The variation of the Specific heat (C), thermal conductivity (KXX), thermal expansion coefficient (ALPX) and elastic modulus (EX) values with temperature of the materials are entered to FEA software to have sensitive results. These graphs are obtained by testing the materials to authorized companies.

Graphs for steel are given in Figure 2-18 to Figure 2-20.

Graphs for insulation material are given in Figure 2-21 to Figure 2-23.

Graphs for aluminum are given in Figure 2-24 to Figure 2-26.

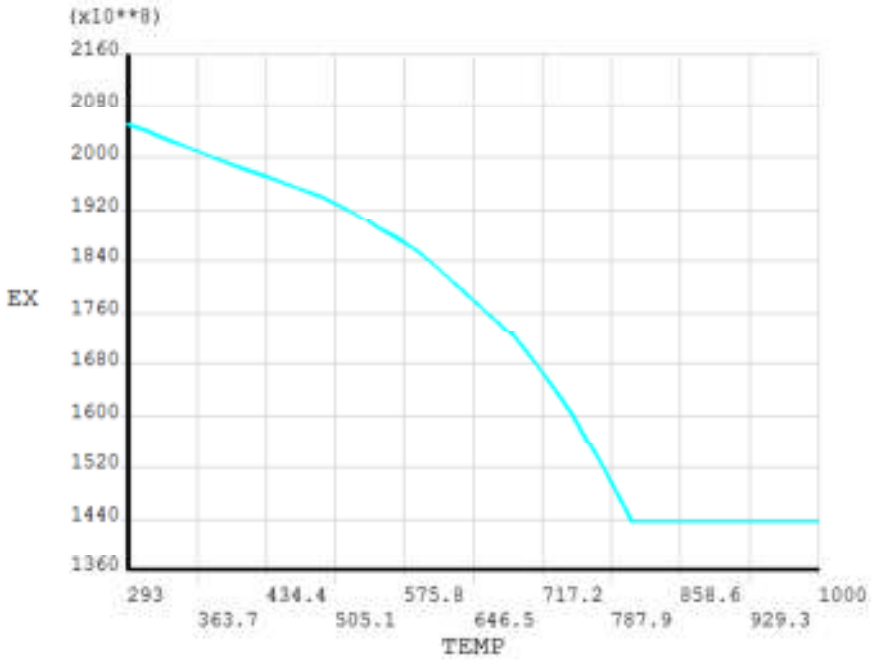

Figure 2-18. Variation of the Elastic Modulus of Steel with Temperature

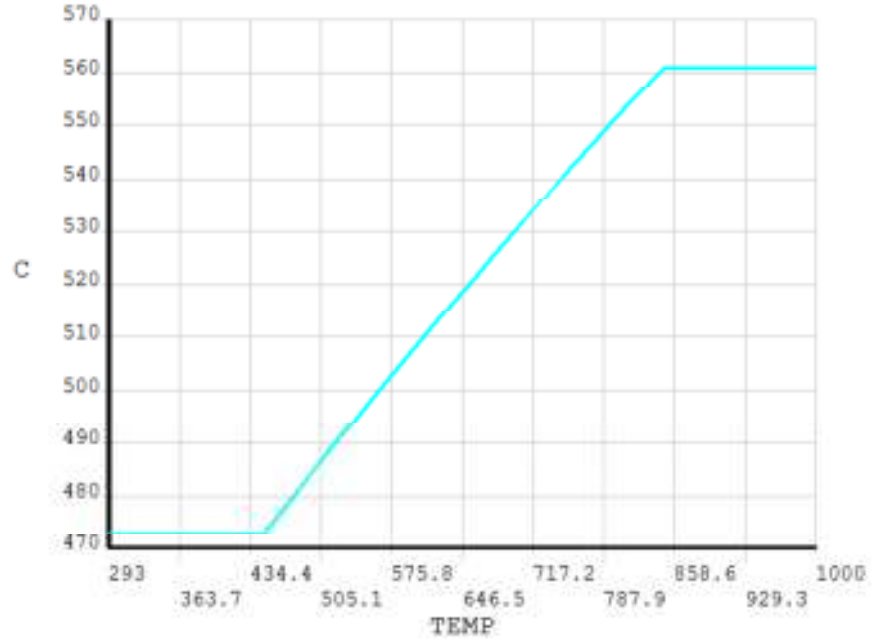

Figure 2-19. Variation of the Specific Heat of Steel with Temperature

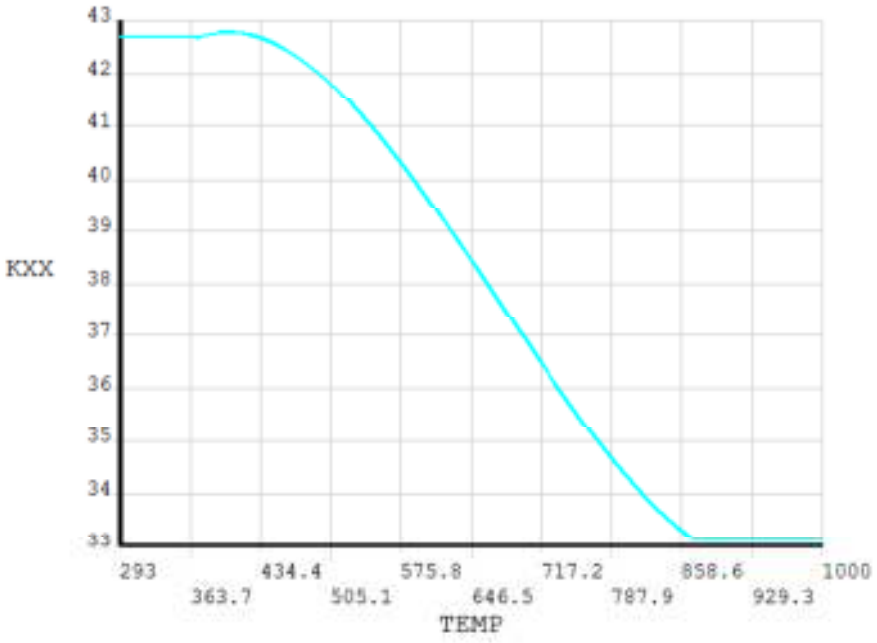

Figure 2-20. Variation of the Thermal Conductivity of Steel with Temperature

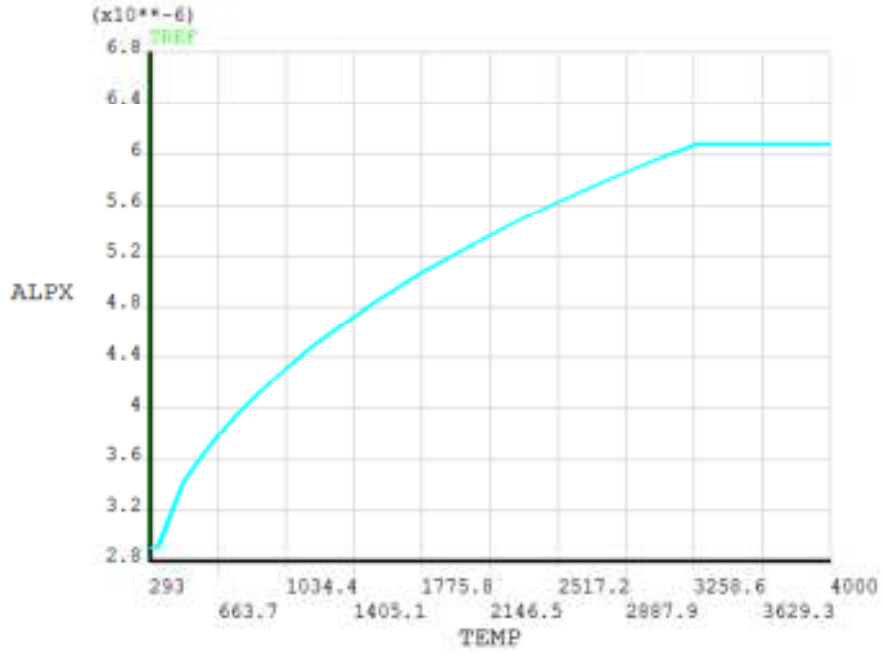

Figure 2-21. Variation of the Thermal Expansion Coefficient of Insulation Material with Temperature

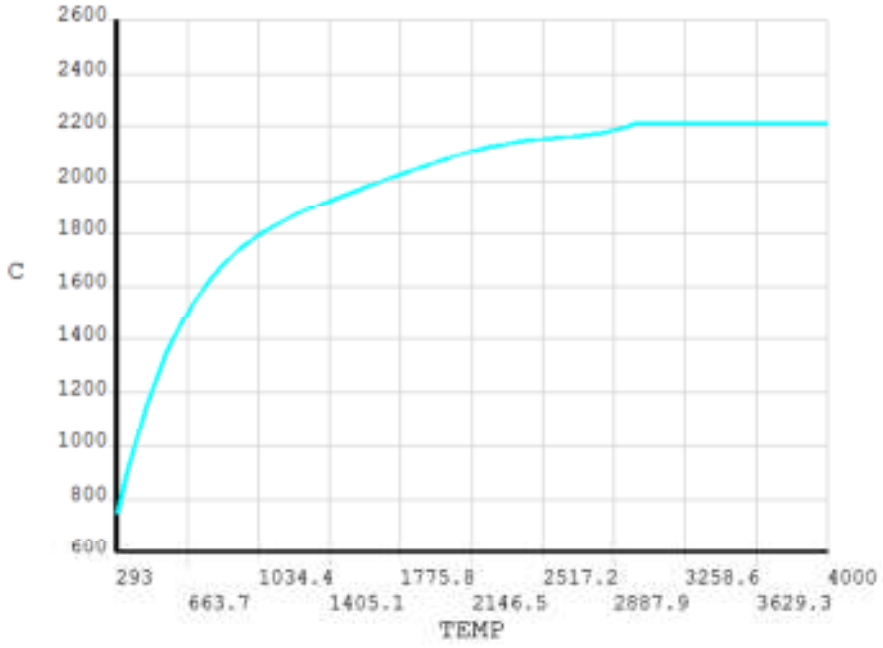

Figure 2-22. Variation of the Specific Heat of Insulation Material with Temperature

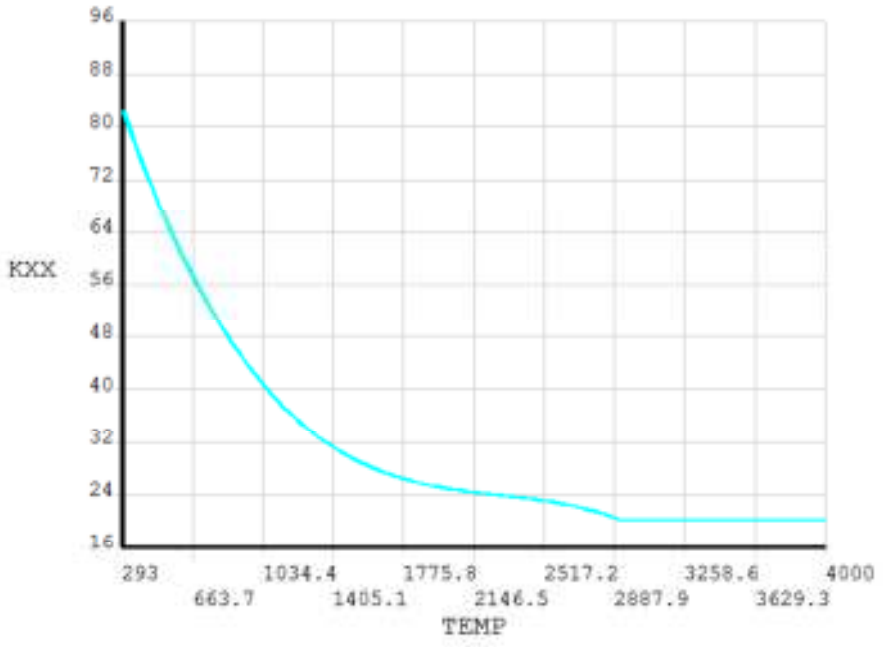

Figure 2-23. Variation of the Thermal Conductivity of Insulation Material with Temperature

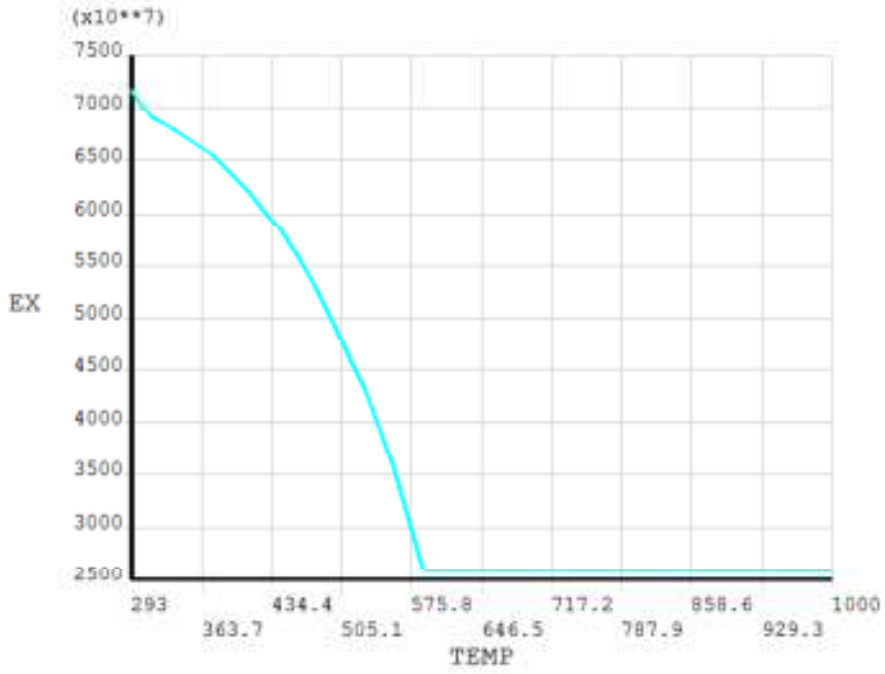

Figure 2-24. Variation of the Elastic Modulus of Aluminum with Temperature

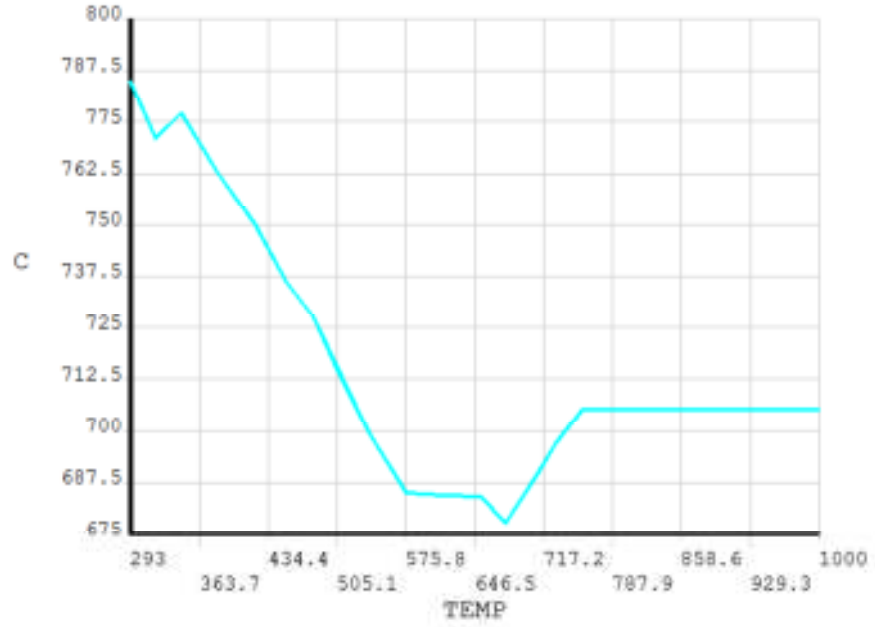

Figure 2-25. Variation of the Specific Heat of Aluminum with Temperature

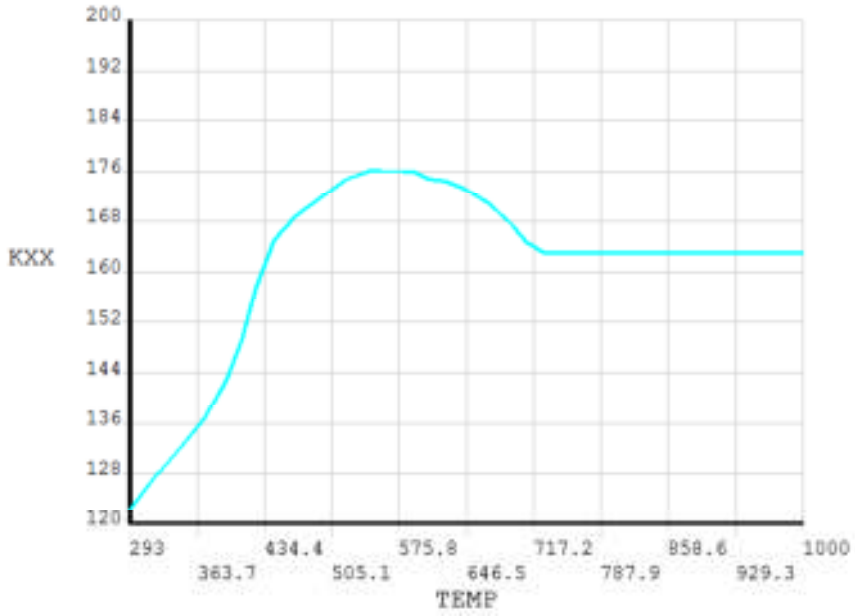

Figure 2-26. Variation of the Thermal Conductivity of Aluminum with Temperature

2.6 Details of FEA Model for the Tail Section

For the tail section, several calculations are performed. According to Von-Mises stress and force results the optimum mesh size is evaluated. As seen from Figure 2-27, the results don't change decreases as the mesh density is increased. If the change of result is less than %5 of lower result that means mesh density is optimum. The mesh optimization is performed to minimize analysis time. According to the mesh optimization, the model is prepared for analysis. The mesh structures for all parts are given in Figure 2-32 to Figure 2-28.

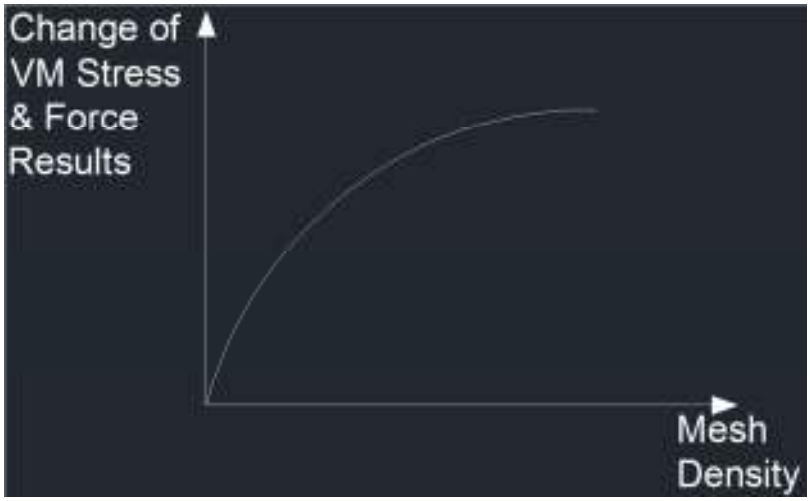

Figure 2-27. Mesh Density – Change of Results

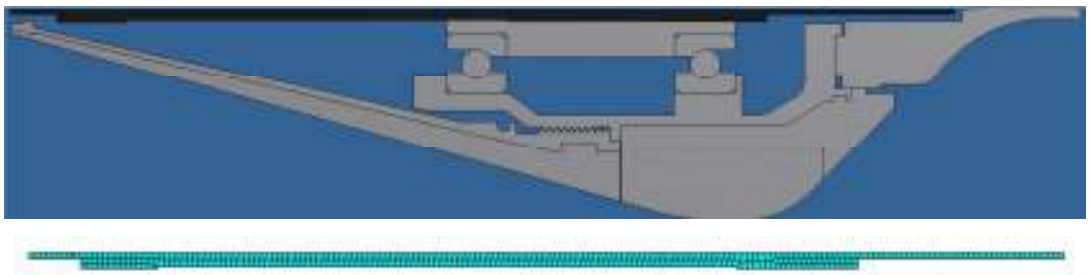

Figure 2-28. Mesh Structure for Part – 1 (Outer Part)

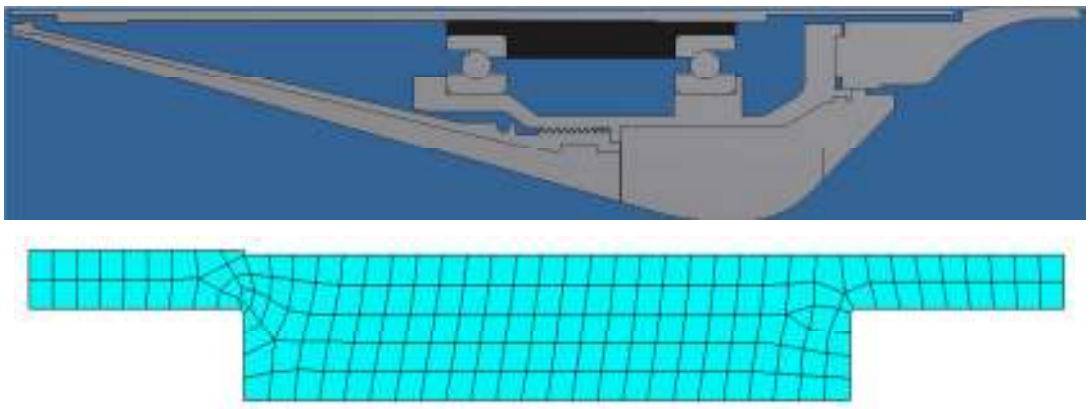

Figure 2-29. Mesh Structure for Part – 1 (Inner Part)

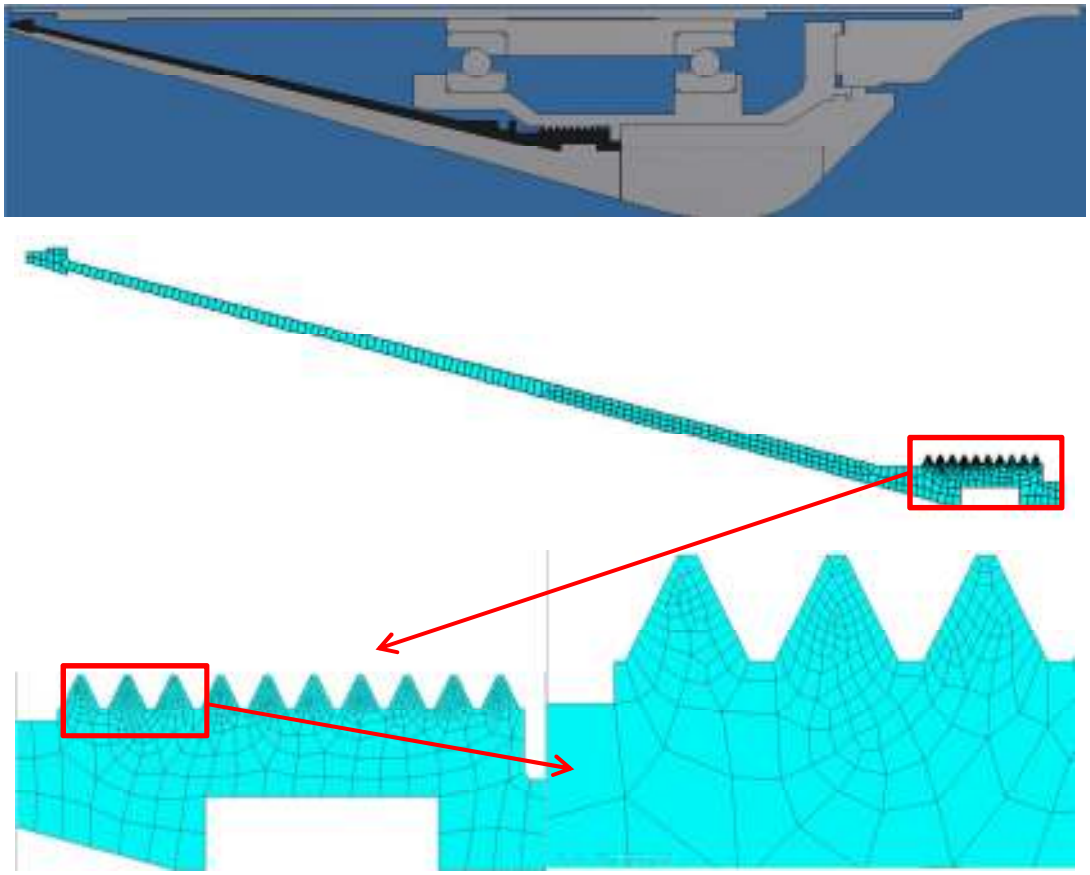

Figure 2-30. Mesh Structure for Part – 2

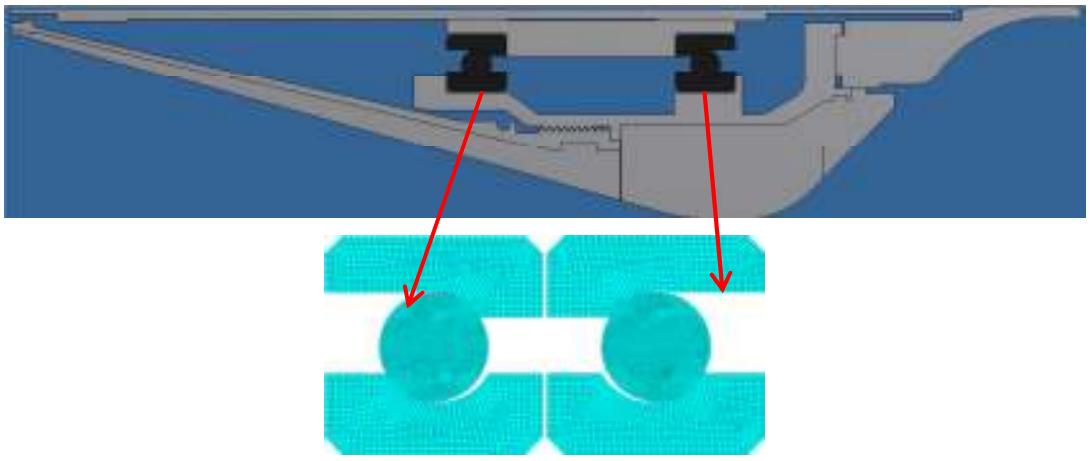

Figure 2-31. Mesh Structure for Part – 3

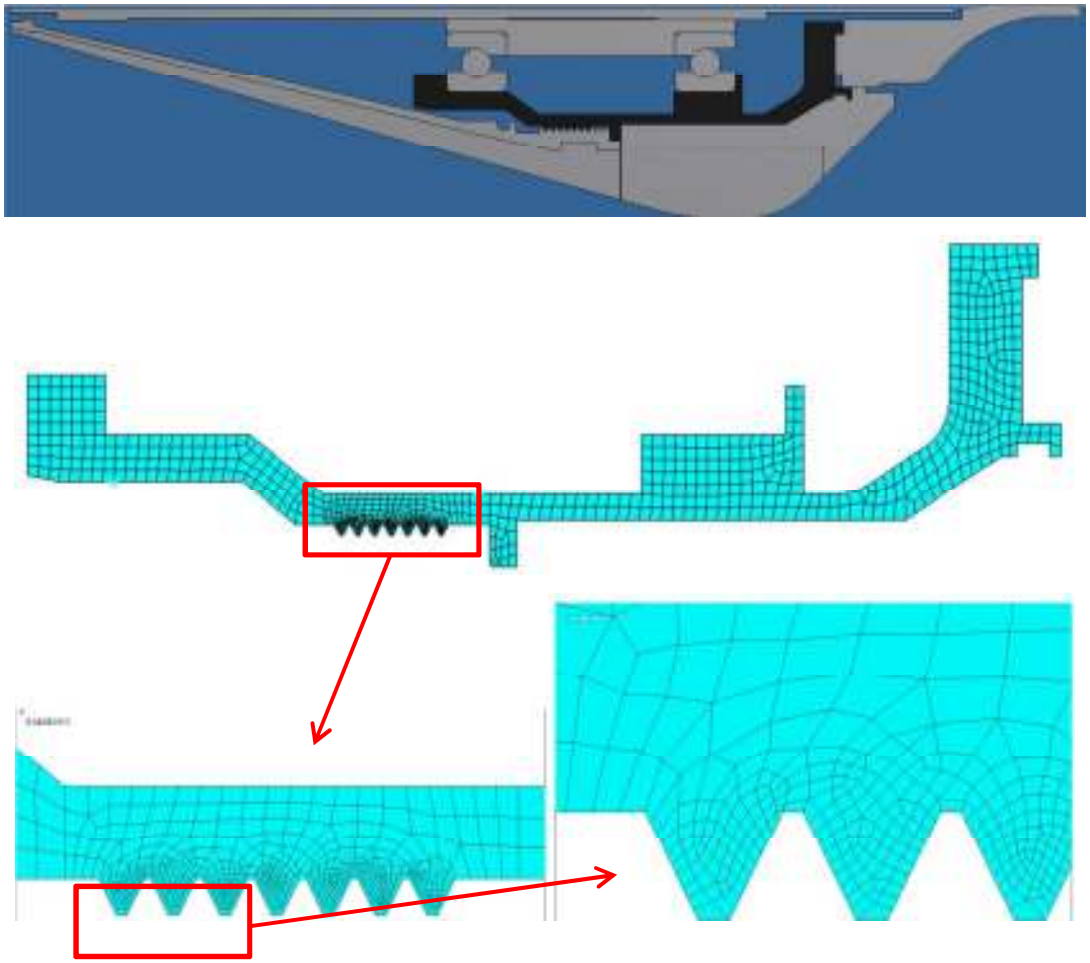

Figure 2-32. Mesh Structure for Part – 4

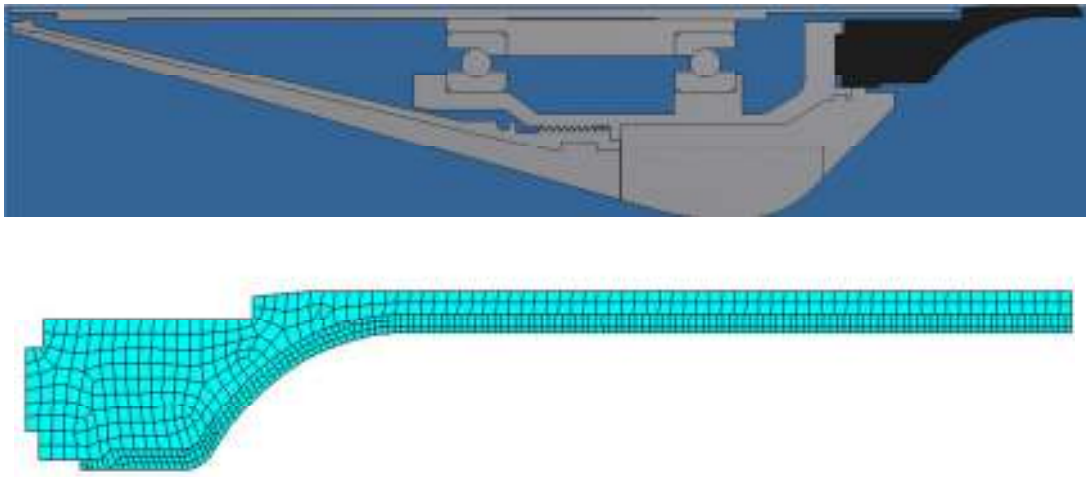

Figure 2-33. Mesh Structure for Part – 5

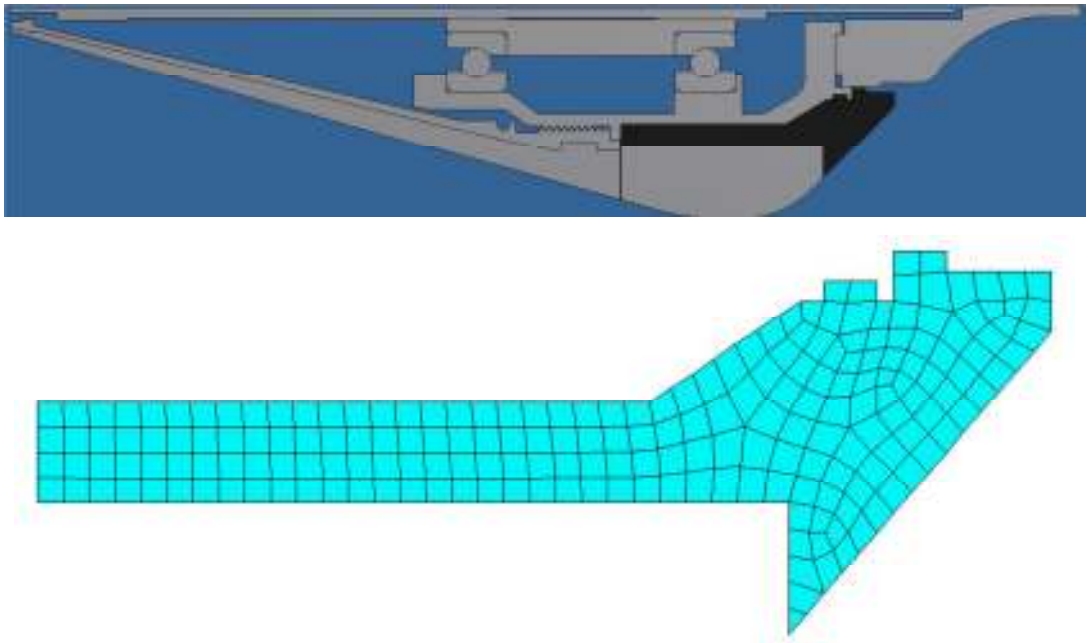

Figure 2-34. Mesh Structure for Part – 6 (Front)

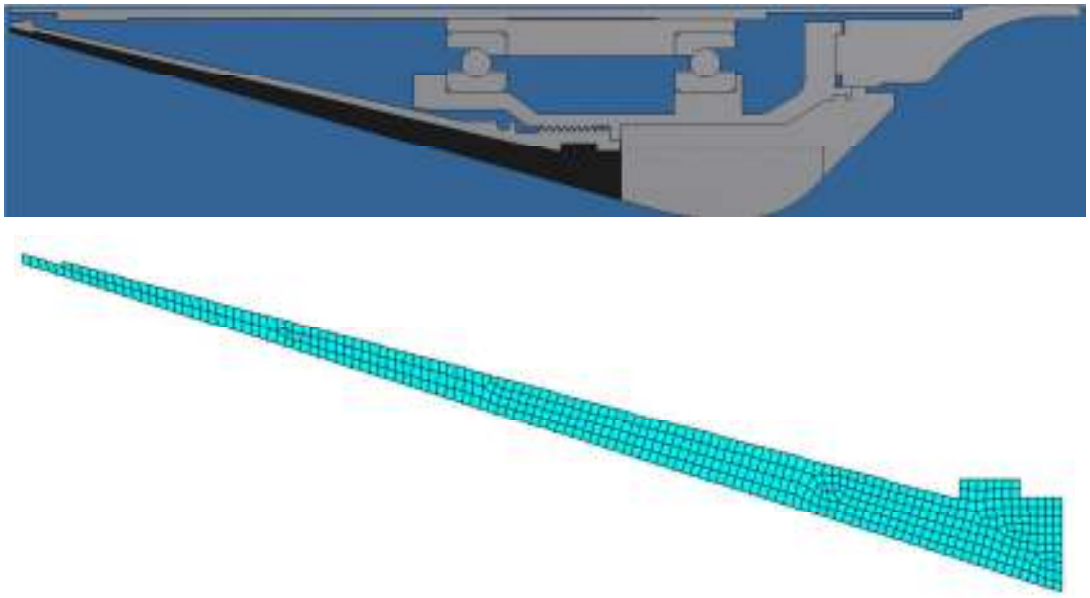

Figure 2-35. Mesh Structure for Part – 6 (Rear)

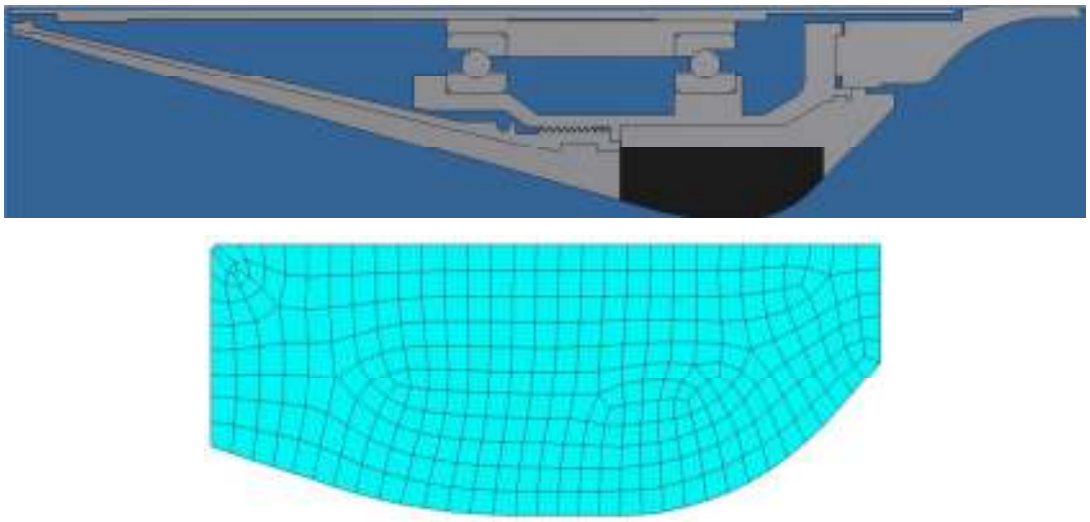

Figure 2-36. Mesh Structure for Part – 7

2.7 Contact Properties on the Tail Section FEA Model

2 types of contact algorithm are used; “Standard” and “Bonded (Always)”. If there is no bonding material between the parts and the parts touch each other by contact, “Standard” type is used. In this contact type, the parts contact each other with “Default” tolerances. There won’t be force transfer if parts contact exceeds the given tolerance values. Also normal pressure equals zero if separation occurs.

If the parts are assembled with a bonding material between parts, “Bonded (Always)” type is used. In “Bonded (Always)” contact type, the target and contact surfaces are bonded in all directions (once contact is established) for the remainder of the analysis.

Contact lines for all parts are given in Figure 2-37. Blue lines refer to “Standard” contact with 0.2 friction coefficient. Red lines refer to “Bonded (Always)” contact. The finalized contact lines are given in Figure 2-38. There are 24 contact elements in the model as given in Figure 2-39. Also contact input deck is given in Figure 2-40.

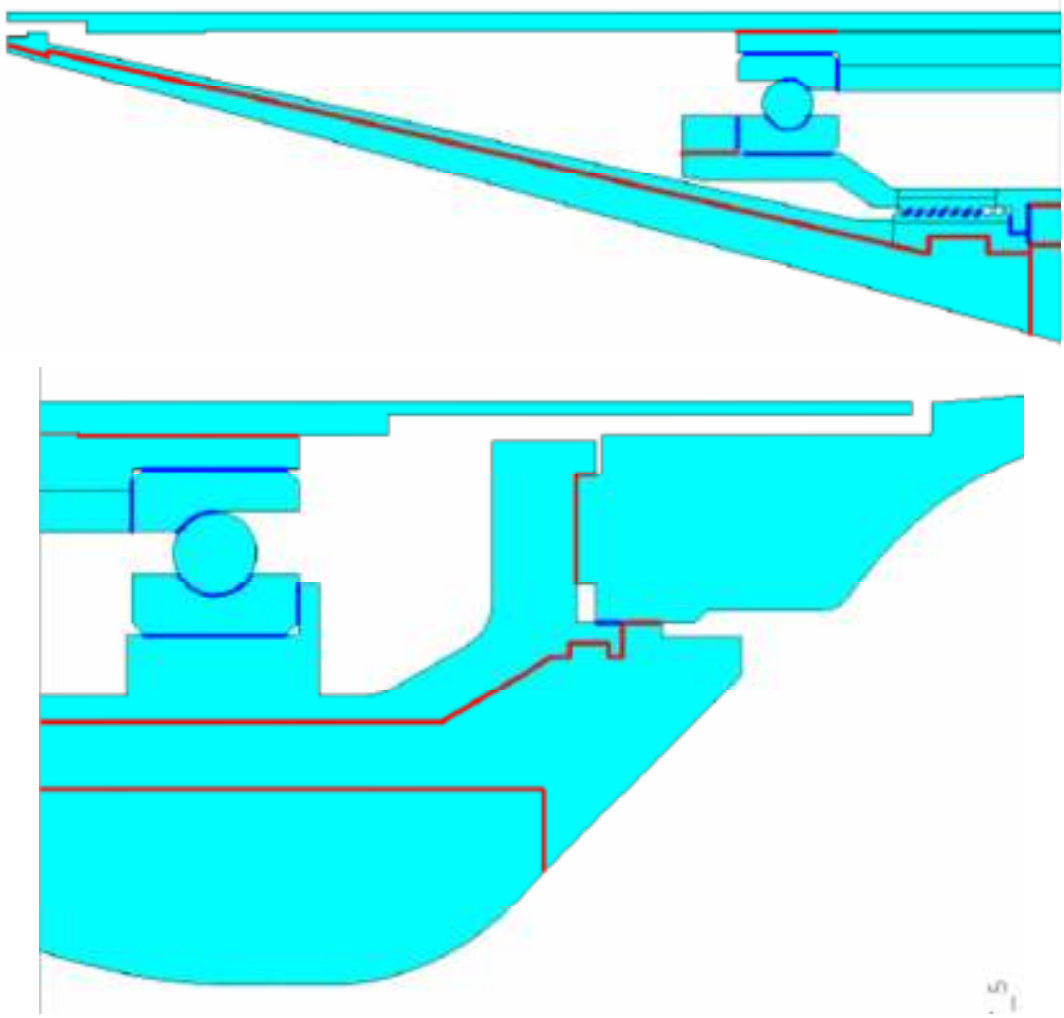

Figure 2-37. Contact Types Used on Parts

Figure 2-38. Contact Surfaces of the Parts

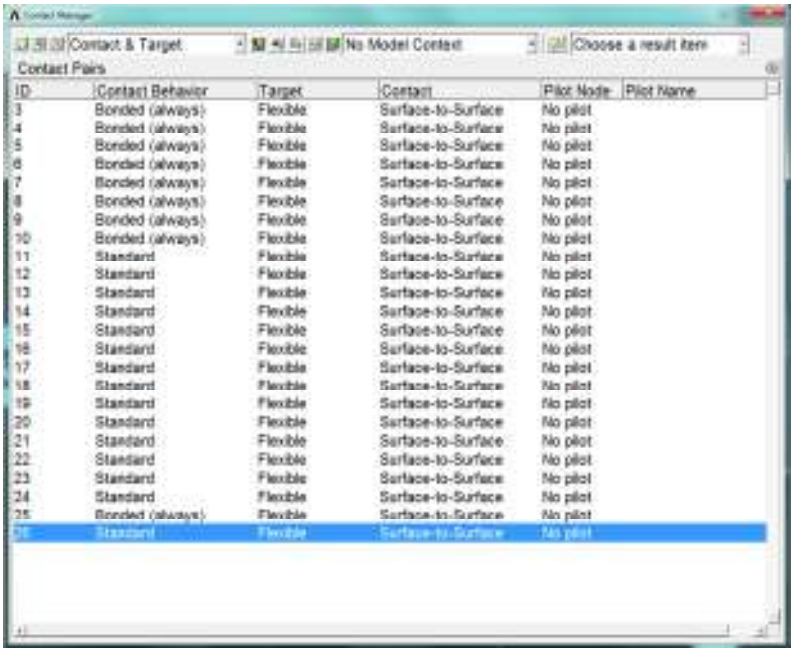

Figure 2-39. Contact List of the Parts

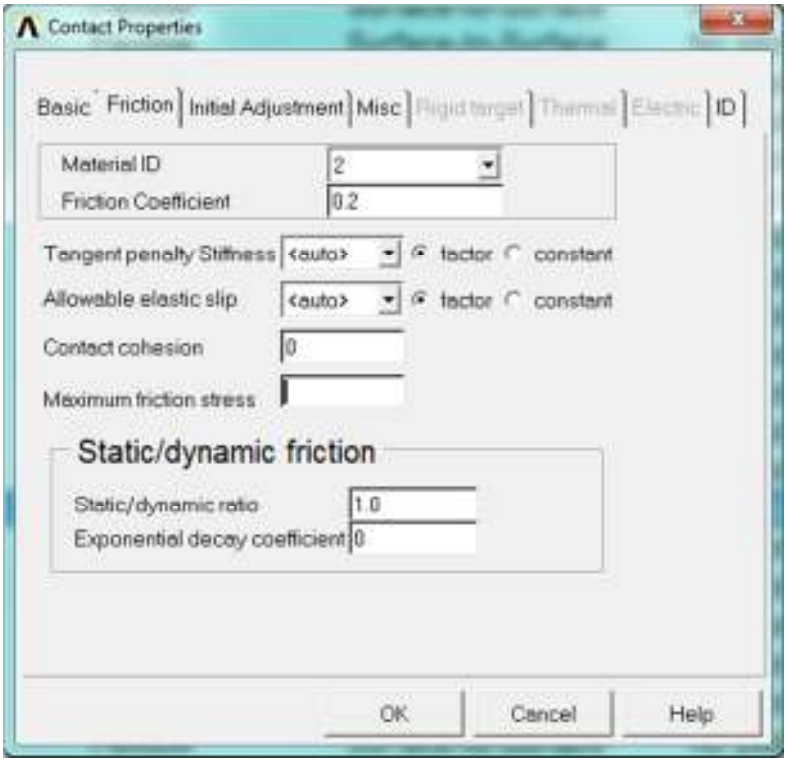

Figure 2-40. Contact Input Deck

2.8 Assumptions for FEA Analysis

To reduce the analysis time, some assumptions are integrated FEA model. If these assumptions weren't used, analysis hasn't been converged. Because making FEA model complex, hardens the calculation of analysis. Assumptions used in the analysis are given below;

- Friction between metal parts has an important effect on the analysis results. Friction coefficient is taken as 0.2.

- Bearings cannot be modeled as axisymmetric element. So for bearings, "plane strs w/thk" element is used. For "plane strs w/thk", equivalent thickness value is entered to software. For calculation of equivalent thickness formula given below is used;

$$\frac{4}{3}\pi r^3 N = 2\pi \mathrm{rT}$$

r : Radius of the balls
N : Number of the balls
T : Equivalent thickness of the cylinder

Left side of the formula means the total volume of the balls. The volume is changed to equivalent cylinder volume. T is the equivalent thickness of cylinder.

For the check of this assumption 2 analyses are performed. Firstly, section of a bearing is taken and analysis is performed on this 3D model. Then analysis is performed on the 2D model of bearing section by using this assumption. Deformation values on the bearing are compared. Results show that deformation values are very near to each other and within the ±10 range. Deformation values similarity proves that this assumption doesn't affect force results for the bearings. Bearing models used in 2 analyses is given in Figure 2-41. Deformation results and their comparison is given in Figure 2-43, Figure 2-44 and Figure 2-42.

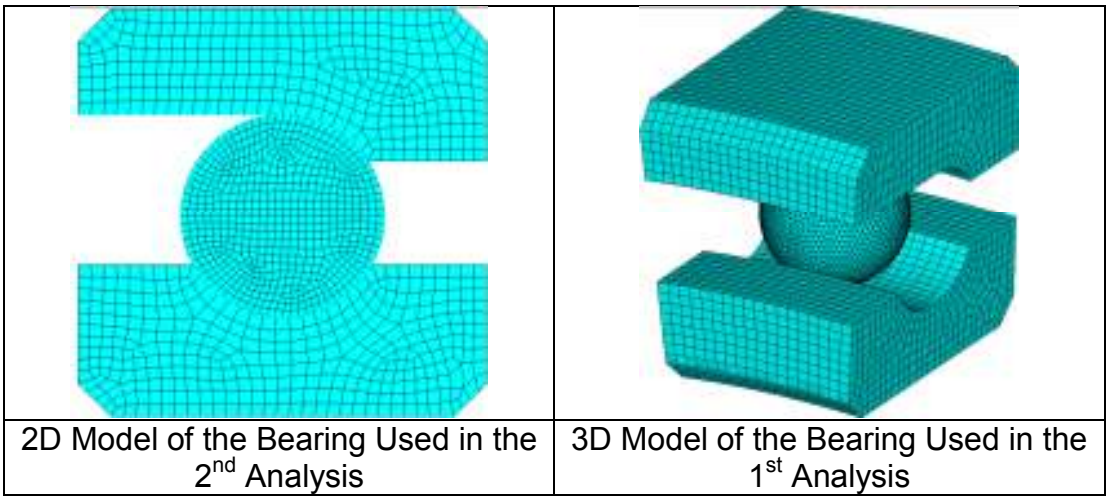

2D Model of the Bearing Used in the 2nd Analysis	3D Model of the Bearing Used in the 1st Analysis

Figure 2-41.2D & 3D Model of the Bearing

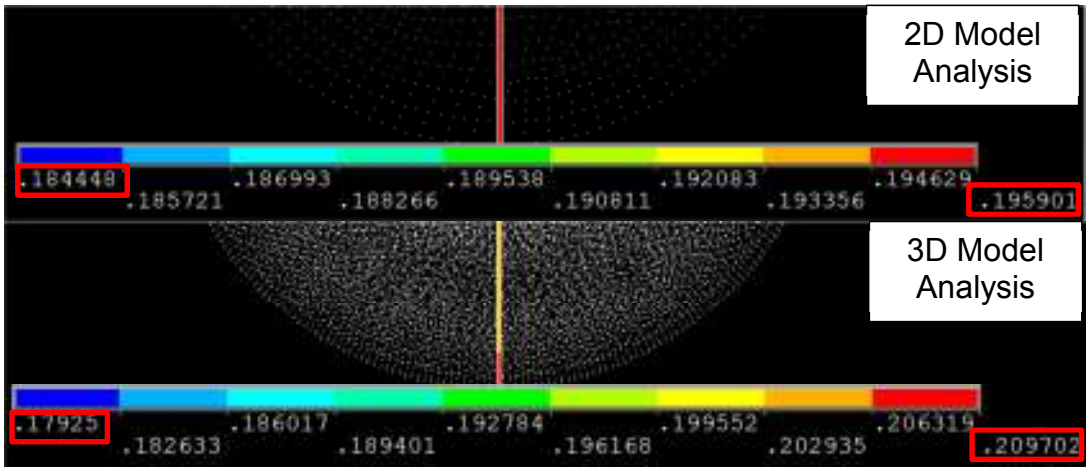

Figure 2-42. Comparison of the Deformation on the Bearing Ball

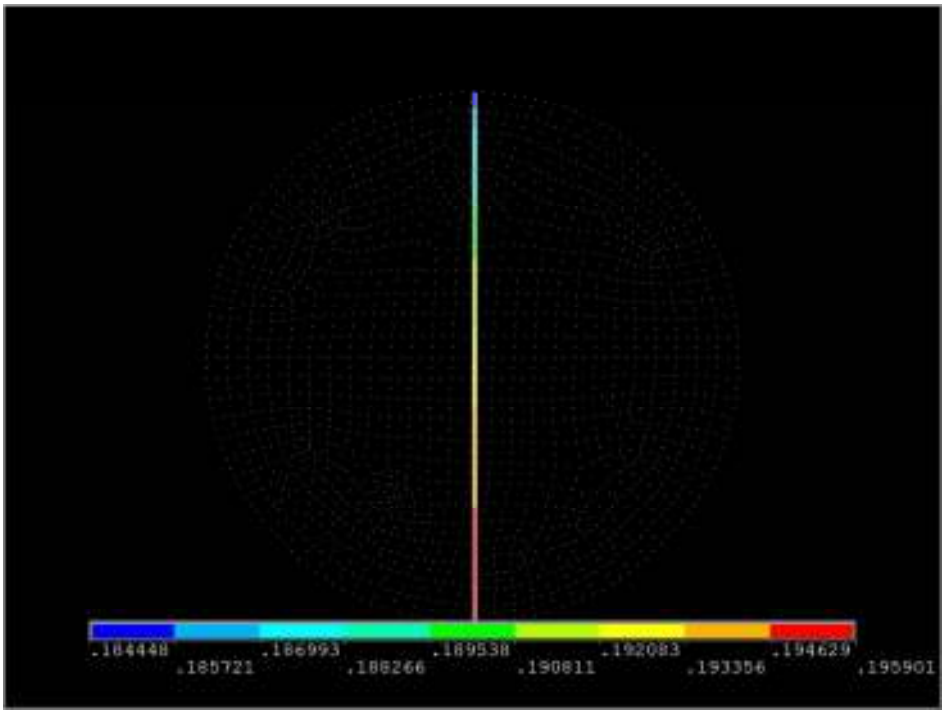

Figure 2-43.Deformation on the Bearing Ball with 2D Model

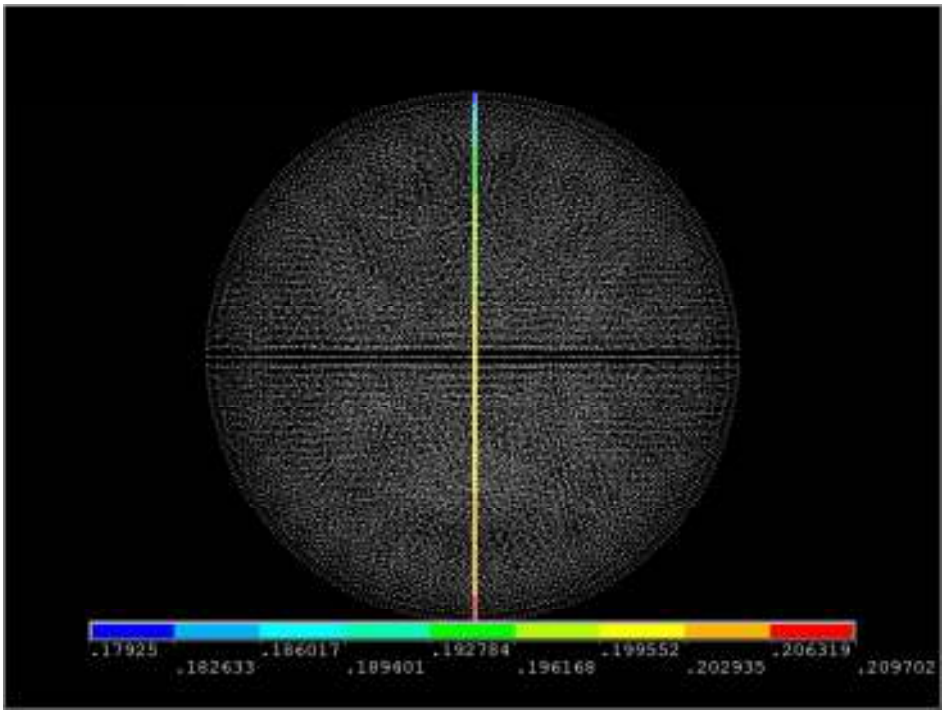

Figure 2-44. Deformation on the Bearing Ball with 3D Model

- During the flight of missile, pitching radial loads acting on the bearings are very low comparing to pressure.
- Fin supporters (Figure 2-45) on the outer race of the tail section cannot be modeled as axisymmetric element. So fin supporters didn't considered into analysis because it has very low effect on the analysis results. But mass of fin supporters is included into outer race weight.

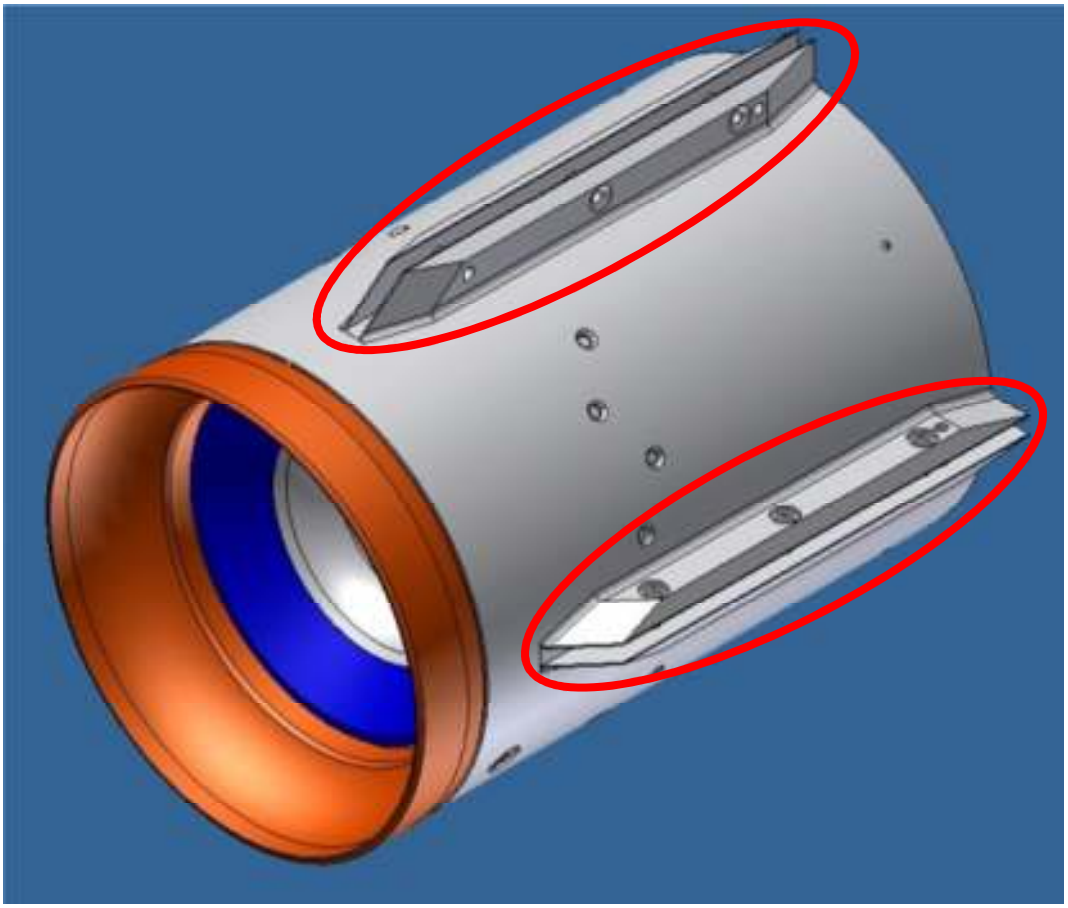

Figure 2-45. A View of the Fin Supporters

CHAPTER 3

FEA RESULTS WITH DOE VARIABLES

Up to this point all inputs (except DOE variables) for FEA are determined and entered to FEA software. In this section, DOE variables are defined and according to these defined variables analyses are run. Also results of the analysis are given.

3.1 Design of Experiments Procedure on the Tail Section

3.1.1 Introduction to Design of Experiments

DOE is used to examine the response of a system or process. Every test is performed to the system according to systematic plan. Outputs of the tests are reviewed by the combination of results. DOE is the systematic way to gain the best information and results from the experiment. In every step one (or more) variable is changed to understand which variable affects the system and how much affects the system. DOE evaluate most of the dependencies of the variables. So the most suitable results are taken from the experiment [20].

Firstly, purpose of the experiment is cleared and after that changing variables are defined. After making experiment with the first variable, the output point where the output values will be taken, is cleared. Then by changing the variables, all the output values are taken from the same point. So the experiment is reliable [20].

DOE principle is given in Figure 3-1. Firstly mechanical design of the tail section is finished. Secondly, this model is used for FEA model and meshing is performed. After that FEA is run and according to results of FEA there should be some changes on the mechanical design. Than other steps are repeated until the most suitable values for the variables are obtained.

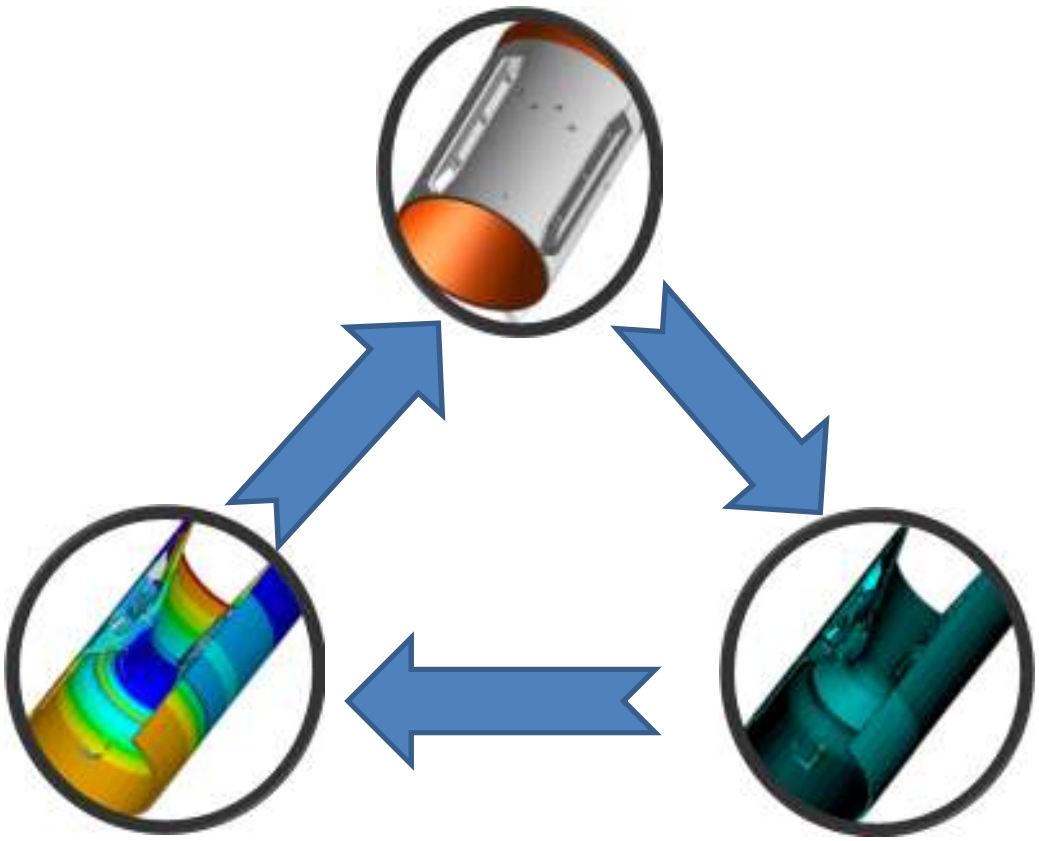

Figure 3-1. DOE Principle

3.1.2 Definitions of Variables

Three variables are determined for DOE. Those are; bearing inner ring interference, bearing outer ring interference and preload on the threaded part. Geometry of the parts cannot be changed but these variables can be changed.

Three different values are assigned for each one of the three variables (totally there are 9 values). For each variable, the initial value (Value-2) is selected from the manufacturer's catalogue. The other two values are called minimum and maximum values which are determined by adding and subtracting to the initial value. Generally in DOE, for one variable two values (Minimum and maximum) are defined. To make the DOE analysis more reliable, addition to minimum and maximum values, also initial value is defined. So three values are determined for each variable.

Table 3-1. DOE Values for Each Variable

	Value(1)	Value(2)	Value(3)
Bearing Inner Ring Interference (BI)	0 µm	10 µm	20 µm
Bearing Outer Ring Interference (BO)	20 µm	30 µm	40 µm
Preload	1250 N	1750 N	2250 N

3.1.3 Running Various Analyses

After defining the variables and the values that will change in the analyses; according to DOE principles, analysis configurations are determined. According to DOE; totally V^N times analysis shall be performed where V is the number of values assigned for each variable, N is the number of variables (Bearing inner ring interference, bearing outer ring interference and preload). So in this thesis 3^3=27 analyses are performed. The configurations are given in Table 3-2.

These various analyses are performed by using APDL (ANSYS Parametric Design Language technique. Firstly FEA model is prepared. But none of the changing variables didn't include into model. For changing variables codes are prepared. By using this method, only some codes are changed for different configurations. The reason is that using APDL shortens the analysis preparing time.

APDL stands for ANSYS Parametric Design Language, a scripting language that one can use to automate common tasks or even build the model in terms of parameters (variables). While all ANSYS commands can be used as part of the scripting language, the APDL commands discussed here are the true scripting commands and encompass a wide range of other features such as repeating a command, macros, if-then-else branching, do-loops, and scalar, vector and matrix operations [11]. APDL used in this thesis is given in APPENDIX A.

Table 3-2. Inputs for the Variables in DOE

	Bearing Inner/Outer Ring Interference		**Threaded Part Preload**
	Inner Ring	**Outer Ring**	
Configuration-1	0 μm	20 μm	1250 N
Configuration-2	0 μm	20 μm	1750 N
Configuration-3	0 μm	20 μm	2250 N
Configuration-4	0 μm	30 μm	1250 N
Configuration-5	0 μm	30 μm	1750 N
Configuration-6	0 μm	30 μm	2250 N
Configuration-7	0 μm	40 μm	1250 N
Configuration-8	0 μm	40 μm	1750 N
Configuration-9	0 μm	40 μm	2250 N
Configuration-10	10 μm	20 μm	1250 N
Configuration-11	10 μm	20 μm	1750 N
Configuration-12	10 μm	20 μm	2250 N
Configuration-13	10 μm	30 μm	1250 N
Configuration-14	10 μm	30 μm	1750 N
Configuration-15	10 μm	30 μm	2250 N

Configuration-16	10 µm	40 µm	1250 N
Configuration-17	10 µm	40 µm	1750 N
Configuration-18	10 µm	40 µm	2250 N
Configuration-19	20 µm	20 µm	1250 N
Configuration-20	20 µm	20 µm	1750 N
Configuration-21	20 µm	20 µm	2250 N
Configuration-22	20 µm	30 µm	1250 N
Configuration-23	20 µm	30 µm	1750 N
Configuration-24	20 µm	30 µm	2250 N
Configuration-25	20 µm	40 µm	1250 N
Configuration-26	20 µm	40 µm	1750 N
Configuration-27	20 µm	40 µm	2250 N

3.2 Results of FEA

For configuration-1, forces and the maximum VM stresses on the bearings are investigated. Forces and maximum VM stresses are given for each load case. Definitions of the forces on the bearing ball are given in Figure 3-2. Forces acting on the bearing ball for configuration-1 are given in Table 3-3 and Table 3-4. The VM stress distributions of the bearings for configuration 1 are given in Figure 3-4 and Figure 3-6. Also the most critical points are marked with red circles. The maximum VM stress values on the bearings are given in Table 3-5 and Table 3-6. After checking all the results given in Table 3-3 to Table 3-6, it is seen that LC-6 is the most critical load case. So for other configurations only LC-6 is investigated. Calculated forces acting on the bearing ball for all configurations are given in Table 3-7 to Table 3-10. For force tables, “X” means force acting on the X direction, “Y” means force acting on the Y direction, “X & Y” means total force calculated by squareroot of sum of squares of forces in X and Y direction.

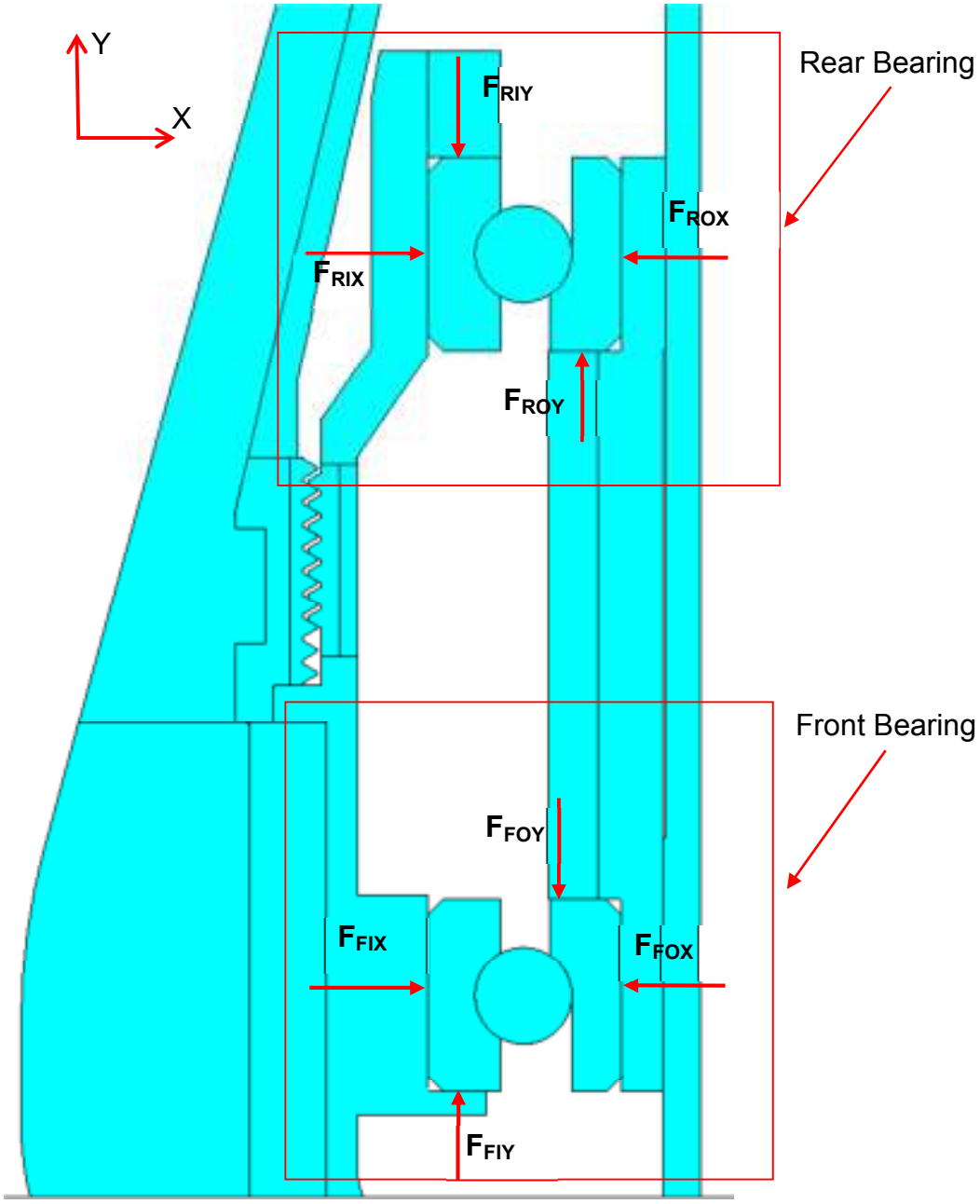

Figure 3-2. Definition of the Forces on the Bearing Ball

Table 3-3. Calculated Forces Acting on the Rear Bearing Ball for Configuration-1

	Rear Bearing					
	Inner Ring			Outer Ring		
	X (F_{RIX})	Y (F_{RIY})	X & Y	X (F_{ROX})	Y (F_{ROY})	X & Y
LC - 1	475 N	2434 N	2480 N	-78 N	67 N	103 N
LC - 2	5417 N	3624 N	6517 N	-6639 N	5820 N	8829 N
LC - 3	9234 N	4612 N	10322 N	-11871 N	10602 N	15916 N
LC - 4	9449 N	9955 N	13725 N	-10910 N	9588 N	14524 N
LC - 5	8977 N	9457 N	13039 N	-10365 N	9109 N	13798 N
LC - 6	22789 N	19515 N	30003 N	-22672 N	18453 N	29232 N

Table 3-4. Calculated Forces Acting on the Front Bearing Ball for Configuration-1

	Front Bearing					
	Inner Ring			Outer Ring		
	X (F_{FIX})	Y (F_{FIY})	X & Y	X (F_{FOX})	Y (F_{FOY})	X & Y
LC - 1	53 N	-15 N	55 N	-76 N	-67 N	101 N
LC - 2	6452 N	-1110 N	6547 N	-6972 N	-5820 N	9082 N
LC - 3	2844 N	-2406 N	3725 N	-1999 N	-1612 N	2568 N
LC - 4	1733 N	-8800 N	8969 N	-776 N	-599 N	980 N
LC - 5	1646 N	-8360 N	8521 N	-737 N	-569 N	931 N
LC - 6	20388 N	-7005 N	21558 N	-16475 N	-9464 N	19000 N

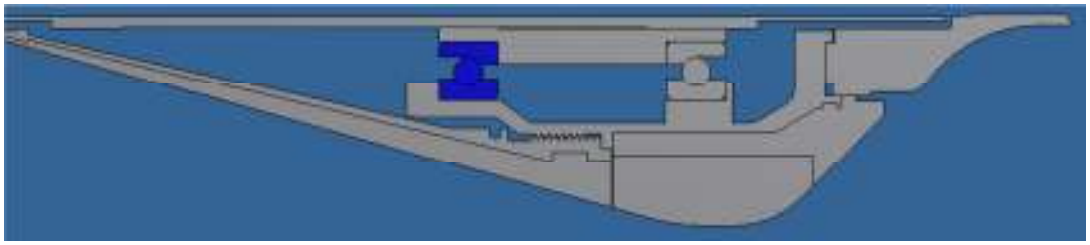

Figure 3-3. Rear Bearing

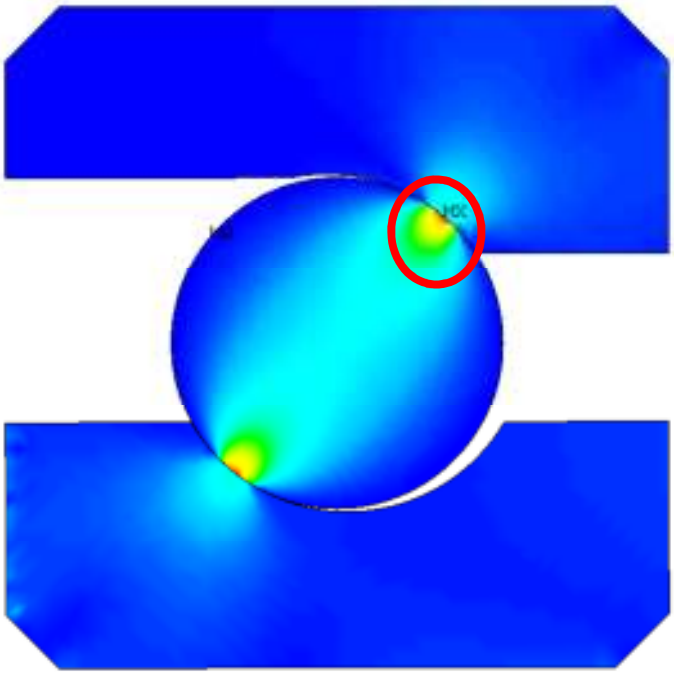

Figure 3-4. Von-Mises Stress Distribution for the Rear Bearing

Table 3-5. Maximum Von-Mises Stresses Calculated on the Rear Bearing for Configuration-1

	Rear Bearing		
	Inner Ring	Ball	Outer Ring
LC - 1	1,1 MPa	1,2 MPa	0,5 MPa
LC - 2	11,9 MPa	34,9 MPa	11,7 MPa
LC - 3	15,7 MPa	50,4 MPa	15,2 MPa
LC - 4	15,0 MPa	47,3 MPa	14,8 MPa
LC - 5	14,3 MPa	44,9 MPa	14,1 MPa
LC - 6	23,6 MPa	68,0 MPa	21,8 MPa

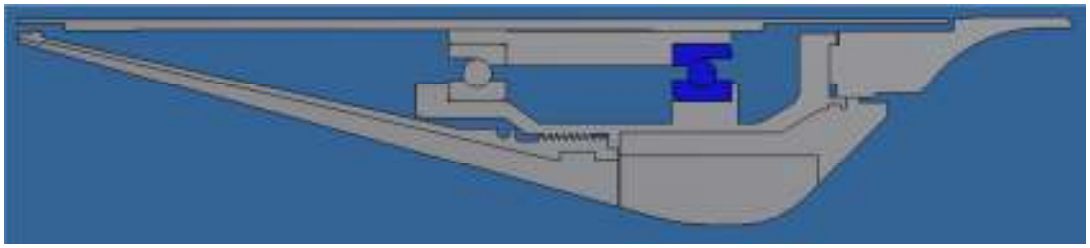

Figure 3-5. Front Bearing

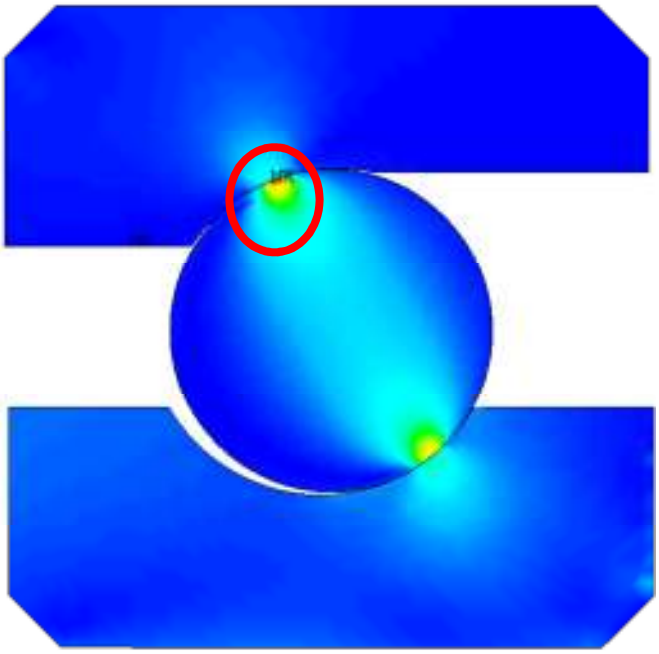

Figure 3-6. Von-Mises Stress Distribution for the Front Bearing

Table 3-6. Maximum Von-Mises Stresses Calculated on the Front Bearing for Configuration-1

	Front Bearing		
	Inner Ring	Ball	Outer Ring
LC - 1	0,4 MPa	1,1 MPa	0,3 MPa
LC - 2	13,2 MPa	34,2 MPa	11,1 MPa
LC - 3	7,3 MPa	15,5 MPa	5,1 MPa
LC - 4	5,4 MPa	10,5 MPa	2,6 MPa
LC - 5	5,1 MPa	10,0 MPa	2,4 MPa
LC - 6	22,6 MPa	58,8 MPa	17,1 MPa

Table 3-7. Calculated Forces Acting on the Rear Bearing Ball for LC-6

	Rear Bearing					
	Inner Ring			Outer Ring		
	X	Y	X & Y	X	Y	X & Y
Conf. - 1	22789 N	19515 N	30003 N	-22672 N	18453 N	29232 N
Conf. - 2	22833 N	20465 N	30662 N	-22510 N	18312 N	29018 N
Conf. - 3	22794 N	21396 N	31263 N	-22237 N	18075 N	28656 N
Conf. - 4	23672 N	21586 N	32036 N	-23407 N	19102 N	30212 N
Conf. - 5	22833 N	20465 N	30662 N	-22510 N	18312 N	29018 N
Conf. - 6	22971 N	21435 N	31419 N	-22474 N	18283 N	28972 N
Conf. - 7	22431 N	19438 N	29681 N	-22194 N	18034 N	28597 N
Conf. - 8	22833 N	20465 N	30662 N	-22510 N	18312 N	29018 N
Conf. - 9	23020 N	21445 N	31461 N	-22539 N	18339 N	29057 N
Conf. - 10	22721 N	19501 N	29942 N	-22582 N	18374 N	29113 N
Conf. - 11	22834 N	20465 N	30663 N	-22511 N	18313 N	29019 N
Conf. - 12	22971 N	21434 N	31418 N	-22473 N	18282 N	28970 N
Conf. - 13	22806 N	19519 N	30018 N	-22694 N	18473 N	29262 N
Conf. - 14	22833 N	20465 N	30662 N	-22510 N	18312 N	29018 N
Conf. - 15	22972 N	21435 N	31419 N	-22475 N	18283 N	28972 N
Conf. - 16	22781 N	19514 N	29996 N	-22661 N	18444 N	29218 N
Conf. - 17	22833 N	20465 N	30662 N	-22509 N	18312 N	29017 N
Conf. - 18	23334 N	21513 N	31738 N	-22958 N	18708 N	29615 N
Conf. - 19	23151 N	19594 N	30330 N	-23154 N	18877 N	29874 N
Conf. - 20	22833 N	20465 N	30662 N	-22510 N	18313 N	29018 N
Conf. - 21	23011 N	21443 N	31453 N	-22528 N	18330 N	29043 N
Conf. - 22	22856 N	19530 N	30064 N	-22761 N	18532 N	29351 N
Conf. - 23	22833 N	20465 N	30662 N	-22510 N	18313 N	29018 N
Conf. - 24	23284 N	21502 N	31694 N	-22891 N	18649 N	29526 N
Conf. - 25	22721 N	19501 N	29942 N	-22581 N	18374 N	29112 N
Conf. - 26	22833 N	20465 N	30662 N	-22510 N	18313 N	29018 N
Conf. - 27	22975 N	21435 N	31421 N	-22479 N	18287 N	28978 N

Table 3-8. Calculated Forces Acting on the Front Bearing Ball for LC-6

	Front Bearing					
	Inner Ring			Outer Ring		
	X	Y	X & Y	X	Y	X & Y
Conf. - 1	20388 N	-7005 N	21558 N	-16475 N	-9464 N	19000 N
Conf. - 2	20027 N	-7009 N	21218 N	-16220 N	-9323 N	18708 N
Conf. - 3	19888 N	-7021 N	21091 N	-15781 N	-9085 N	18209 N
Conf. - 4	21246 N	-6964 N	22358 N	-17656 N	-10113 N	20347 N
Conf. - 5	20207 N	-7009 N	21388 N	-16220 N	-9323 N	18708 N
Conf. - 6	20172 N	-7005 N	21354 N	-16164 N	-9293 N	18645 N
Conf. - 7	19836 N	-7033 N	21046 N	-15719 N	-9045 N	18136 N
Conf. - 8	20207 N	-7009 N	21388 N	-16220 N	-9323 N	18708 N
Conf. - 9	20251 N	-7000 N	21427 N	-16269 N	-9350 N	18764 N
Conf. - 10	20294 N	-7008 N	21470 N	-16340 N	-9385 N	18843 N
Conf. - 11	20208 N	-7009 N	21389 N	-16221 N	-9324 N	18710 N
Conf. - 12	20171 N	-7006 N	21353 N	-16163 N	-9293 N	18644 N
Conf. - 13	20410 N	-7005 N	21579 N	-16509 N	-9484 N	19039 N
Conf. - 14	20207 N	-7009 N	21388 N	-16219 N	-9323 N	18708 N
Conf. - 15	20173 N	-7006 N	21355 N	-16165 N	-9294 N	18646 N
Conf. - 16	20376 N	-7006 N	21547 N	-16459 N	-9454 N	18981 N
Conf. - 17	20207 N	-7009 N	21388 N	-16220 N	-9323 N	18708 N
Conf. - 18	20696 N	-6990 N	21845 N	-16912 N	-9718 N	19505 N
Conf. - 19	20913 N	-6988 N	22050 N	-17222 N	-9887 N	19858 N
Conf. - 20	20208 N	-7009 N	21389 N	-16220 N	-9323 N	18708 N
Conf. - 21	20223 N	-7007 N	21403 N	-16242 N	-9340 N	18736 N
Conf. - 22	20479 N	-7003 N	21643 N	-16609 N	-9542 N	19155 N
Conf. - 23	20208 N	-7009 N	21389 N	-16221 N	-9324 N	18710 N
Conf. - 24	20615 N	-6993 N	21769 N	-16800 N	-9660 N	19379 N
Conf. - 25	20294 N	-7008 N	21470 N	-16339 N	-9384 N	18842 N
Conf. - 26	20207 N	-7009 N	21388 N	-16220 N	-9323 N	18708 N
Conf. - 27	20177 N	-7005 N	21358 N	-16171 N	-9297 N	18653 N

Table 3-9. Maximum Von-Mises Stresses on the Rear Bearing for LC-6

	Rear Bearing		
	Inner Ring	Ball	Outer Ring
Conf. - 1	23,6 MPa	68,2 MPa	21,9 MPa
Conf. - 2	23,5 MPa	67,9 MPa	21,8 MPa
Conf. - 3	23,3 MPa	67,4 MPa	21,6 MPa
Conf. - 4	24,1 MPa	69,5 MPa	22,2 MPa
Conf. - 5	23,5 MPa	67,9 MPa	21,8 MPa
Conf. - 6	23,5 MPa	67,8 MPa	21,8 MPa
Conf. - 7	23,3 MPa	67,3 MPa	21,6 MPa
Conf. - 8	23,5 MPa	67,9 MPa	21,8 MPa
Conf. - 9	23,5 MPa	67,9 MPa	21,8 MPa
Conf. - 10	23,6 MPa	68,0 MPa	21,8 MPa
Conf. - 11	23,5 MPa	67,9 MPa	21,8 MPa
Conf. - 12	23,5 MPa	67,8 MPa	21,8 MPa
Conf. - 13	23,6 MPa	68,2 MPa	21,9 MPa
Conf. - 14	23,5 MPa	67,9 MPa	21,8 MPa
Conf. - 15	23,5 MPa	67,8 MPa	21,8 MPa
Conf. - 16	23,6 MPa	68,2 MPa	21,9 MPa
Conf. - 17	23,5 MPa	67,9 MPa	21,8 MPa
Conf. - 18	23,8 MPa	68,7 MPa	22,0 MPa
Conf. - 19	24,0 MPa	69,1 MPa	22,1 MPa
Conf. - 20	23,5 MPa	67,9 MPa	21,8 MPa
Conf. - 21	23,5 MPa	67,9 MPa	21,8 MPa
Conf. - 22	23,7 MPa	68,3 MPa	21,9 MPa
Conf. - 23	23,5 MPa	67,9 MPa	21,8 MPa
Conf. - 24	23,8 MPa	68,6 MPa	22,0 MPa
Conf. - 25	23,6 MPa	68,0 MPa	21,8 MPa
Conf. - 26	23,5 MPa	67,9 MPa	21,8 MPa
Conf. – 27	23,5 MPa	67,8 MPa	21,8 MPa

Table 3-10. Maximum Von-Mises Stresses on the Front Bearing for LC-6

	Front Bearing		
	Inner Ring	Ball	Outer Ring
Conf. - 1	2,5 MPa	58,6 MPa	17,2 MPa
Conf. - 2	22,3 MPa	60,4 MPa	17,2 MPa
Conf. - 3	22,5 MPa	59,2 MPa	17,0 MPa
Conf. - 4	23,5 MPa	60,8 MPa	17,5 MPa
Conf. - 5	22,3 MPa	60,4 MPa	17,2 MPa
Conf. - 6	22,3 MPa	60,3 MPa	17,2 MPa
Conf. - 7	22,5 MPa	58,9 MPa	16,9 MPa
Conf. - 8	22,3 MPa	60,4 MPa	17,2 MPa
Conf. - 9	22,5 MPa	59,7 MPa	17,2 MPa
Conf. - 10	22,6 MPa	58,8 MPa	17,1 MPa
Conf. - 11	22,3 MPa	60,4 MPa	17,2 MPa
Conf. - 12	22,3 MPa	60,3 MPa	17,2 MPa
Conf. - 13	22,5 MPa	58,8 MPa	17,2 MPa
Conf. - 14	22,3 MPa	60,4 MPa	17,2 MPa
Conf. - 15	22,3 MPa	60,3 MPa	17,2 MPa
Conf. - 16	22,5 MPa	58,7 MPa	17,2 MPa
Conf. - 17	22,3 MPa	60,4 MPa	17,2 MPa
Conf. - 18	23,1 MPa	60,8 MPa	17,3 MPa
Conf. - 19	22,9 MPa	60,4 MPa	18,0 MPa
Conf. - 20	22,3 MPa	60,7 MPa	17,2 MPa
Conf. - 21	22,1 MPa	60,7 MPa	17,1 MPa
Conf. - 22	22,5 MPa	58,7 MPa	17,3 MPa
Conf. - 23	22,3 MPa	60,4 MPa	17,2 MPa
Conf. - 24	22,1 MPa	60,0 MPa	17,2 MPa
Conf. - 25	22,6 MPa	58,8 MPa	17,1 MPa
Conf. - 26	22,3 MPa	60,4 MPa	17,2 MPa
Conf. – 27	22,3 MPa	60,4 MPa	17,2 MPa

The Variation of the forces acting on the bearing ball for different configurations are given in Figure 3-7 and Figure 3-8.

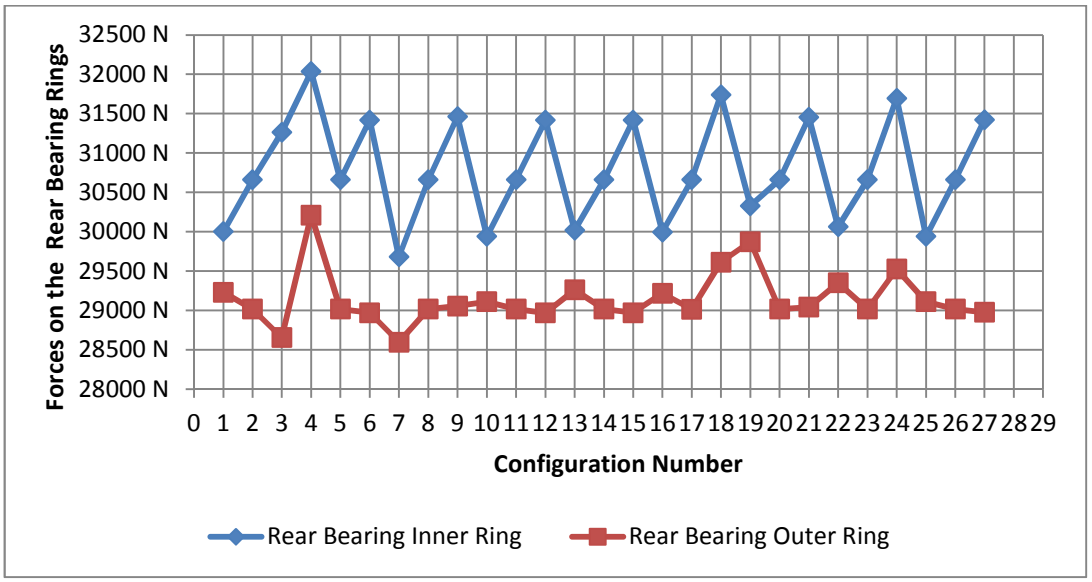

Figure 3-7. The Variation of the Forces on the Rear Bearing Ball for Different Configurations for LC-6

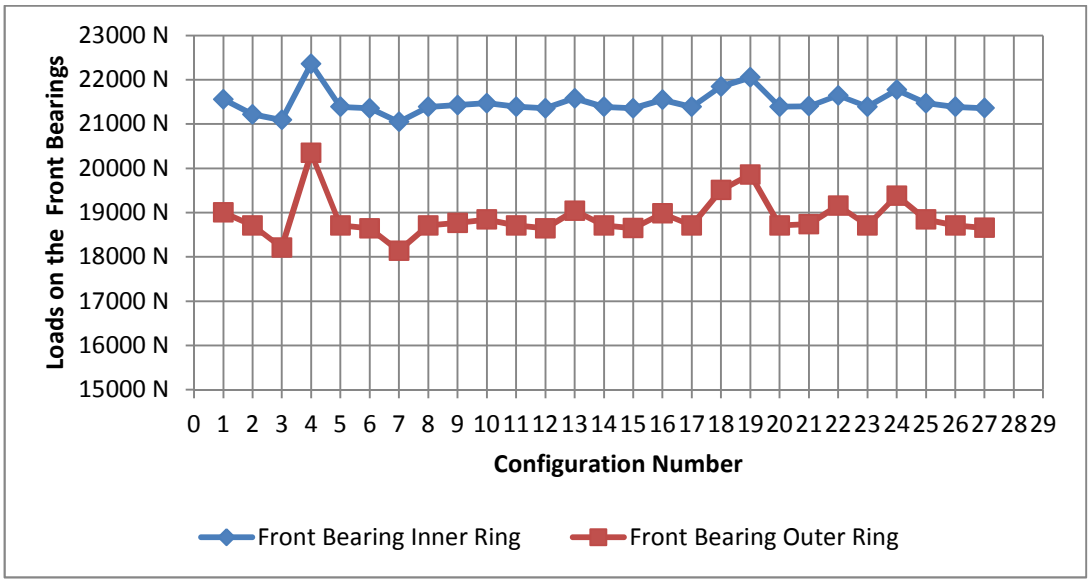

Figure 3-8. The Variation of the Forces on the Front Bearing Ball for Different Configurations for LC-6

By investigating the forces on the bearing ball given in Figure 3-7 and Figure 3-8, it is observed that the inner ring forces are higher than the outer ring forces. Because the difference value of inner and outer ring is transferred to Z direction. The free body diagram for the force transfer is given in Figure 3-9 where F(1) is the outer ring force, F(2) is the inner ring force and F(Z1)X and F(Z2)X are the forces acting on a ball at the Z direction. F(Z1)X and F(Z2)X values are the same. So F(Z)X values cancel each other. Finally F(2) is calculated by adding F(Z1)Y and F(Z2)Y to F(1).

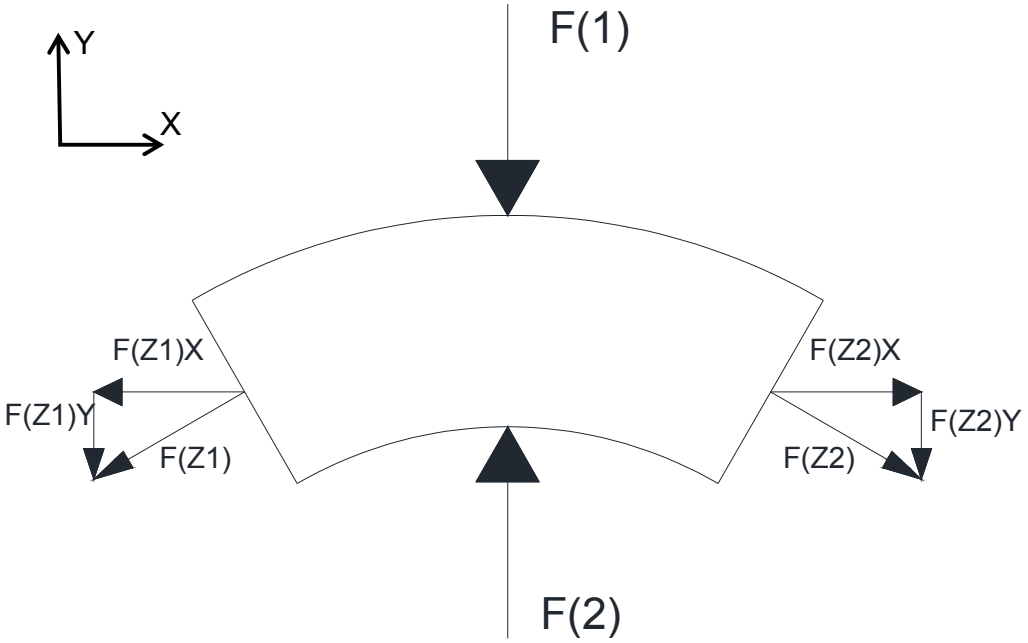

Figure 3-9. Free Body Diagram for the Force Transfer

To have a better understanding, the VM stress distribution on the tail section is given as splitting into three parts. FEA results for configuration-25 (VM stress distribution) are given in “APPENDIX B”.

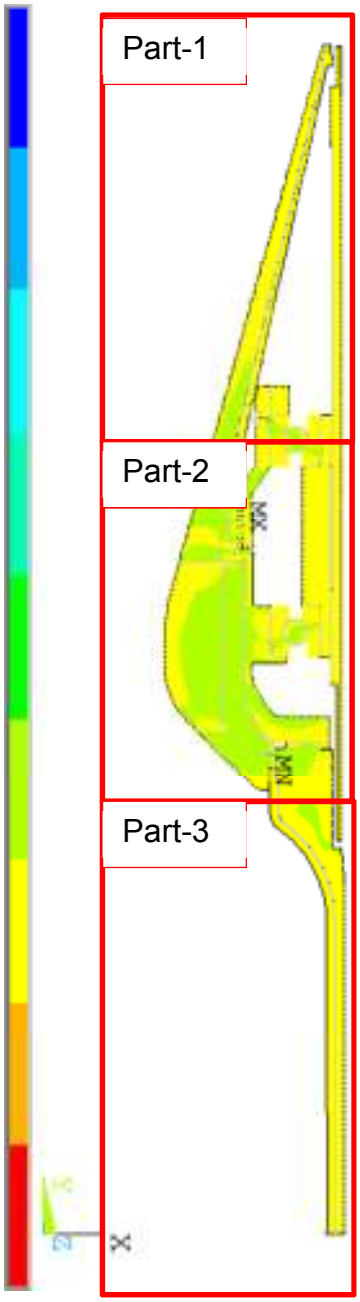

Figure 3-10. Von-Mises Stress Distribution of the Tail Section for LC-6 and Configuration-25

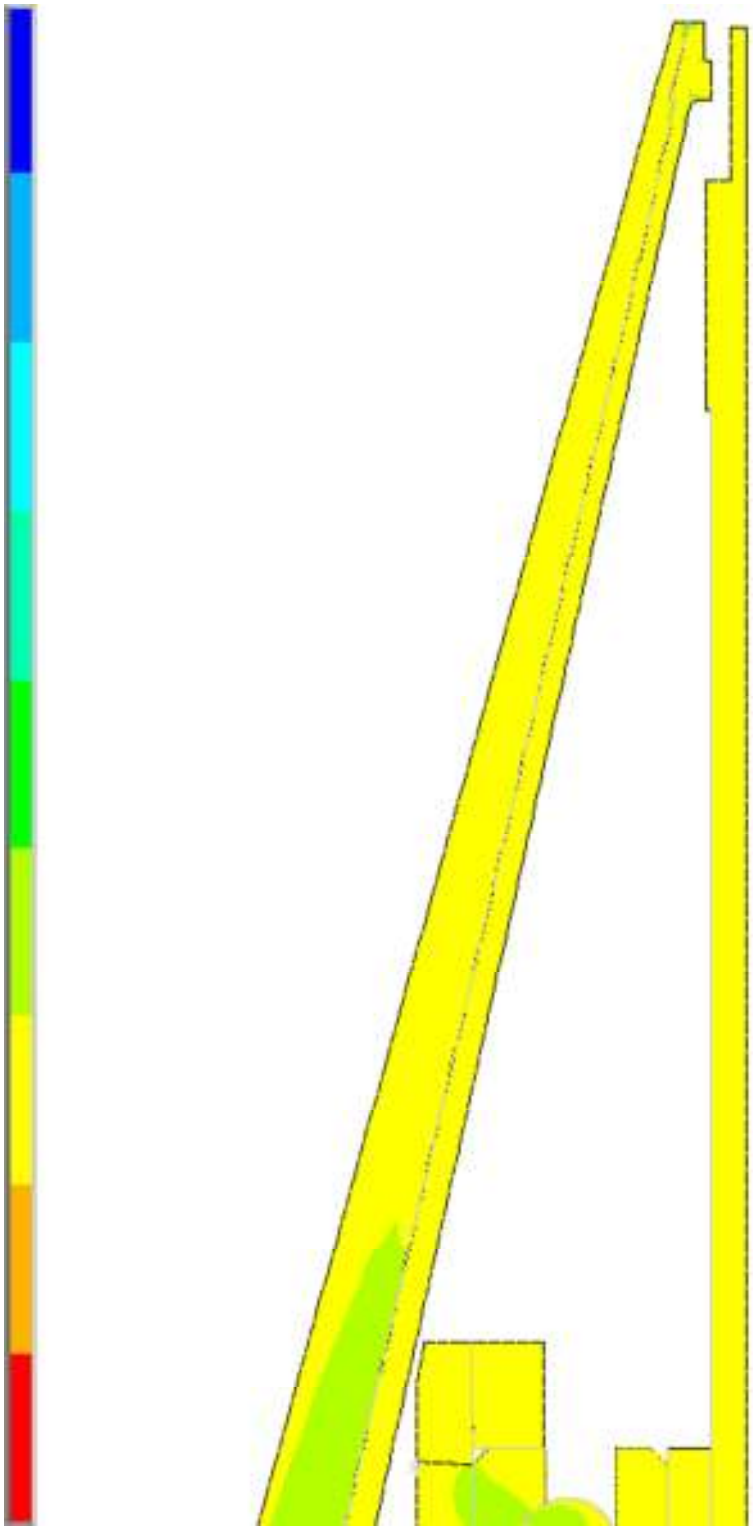

Figure 3-11. Von-Mises Stress Distribution of the Tail Section for LC-6 and Configuration-25 – Part-1

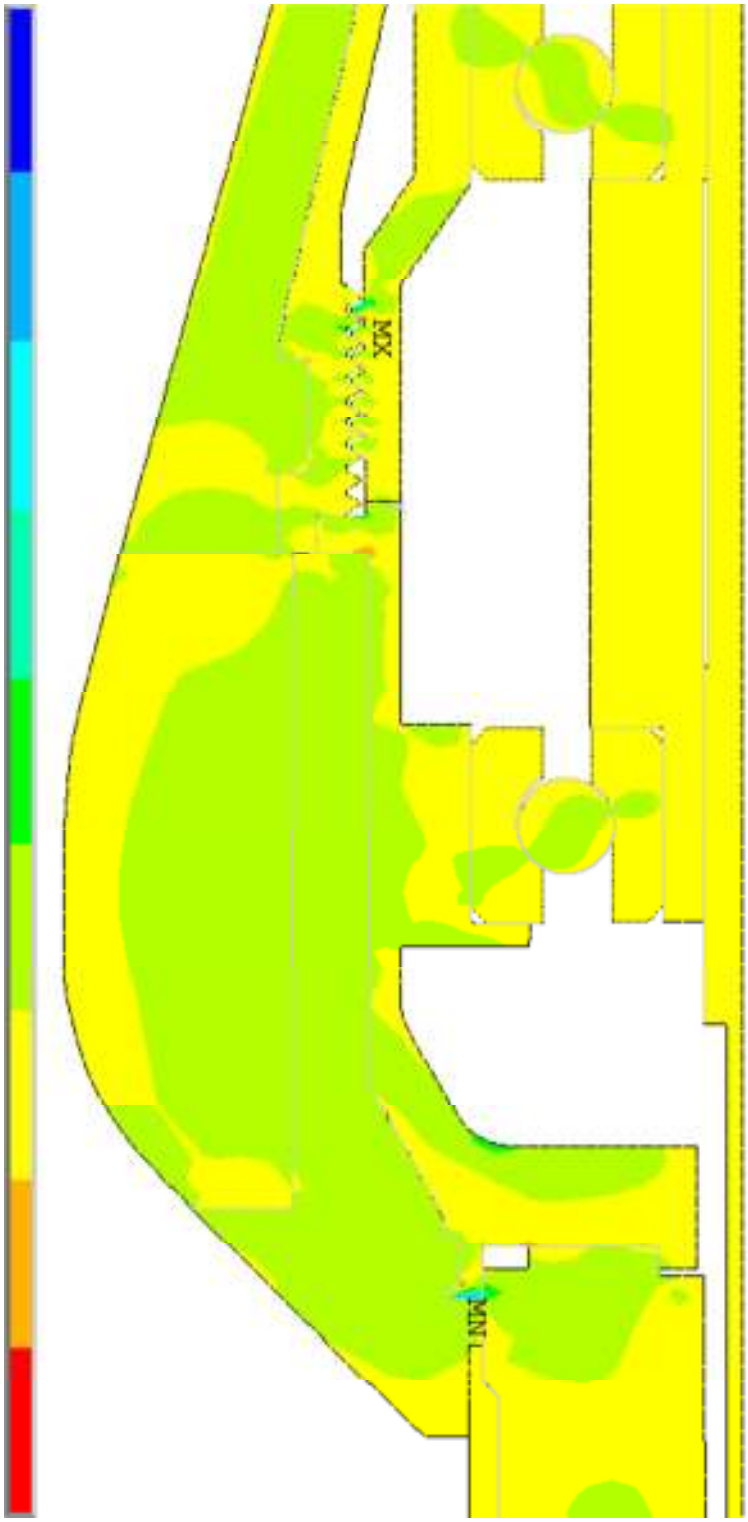

Figure 3-12. Von-Mises Stress Distribution of the Tail Section for LC-6 and Configuration-25 – Part-2

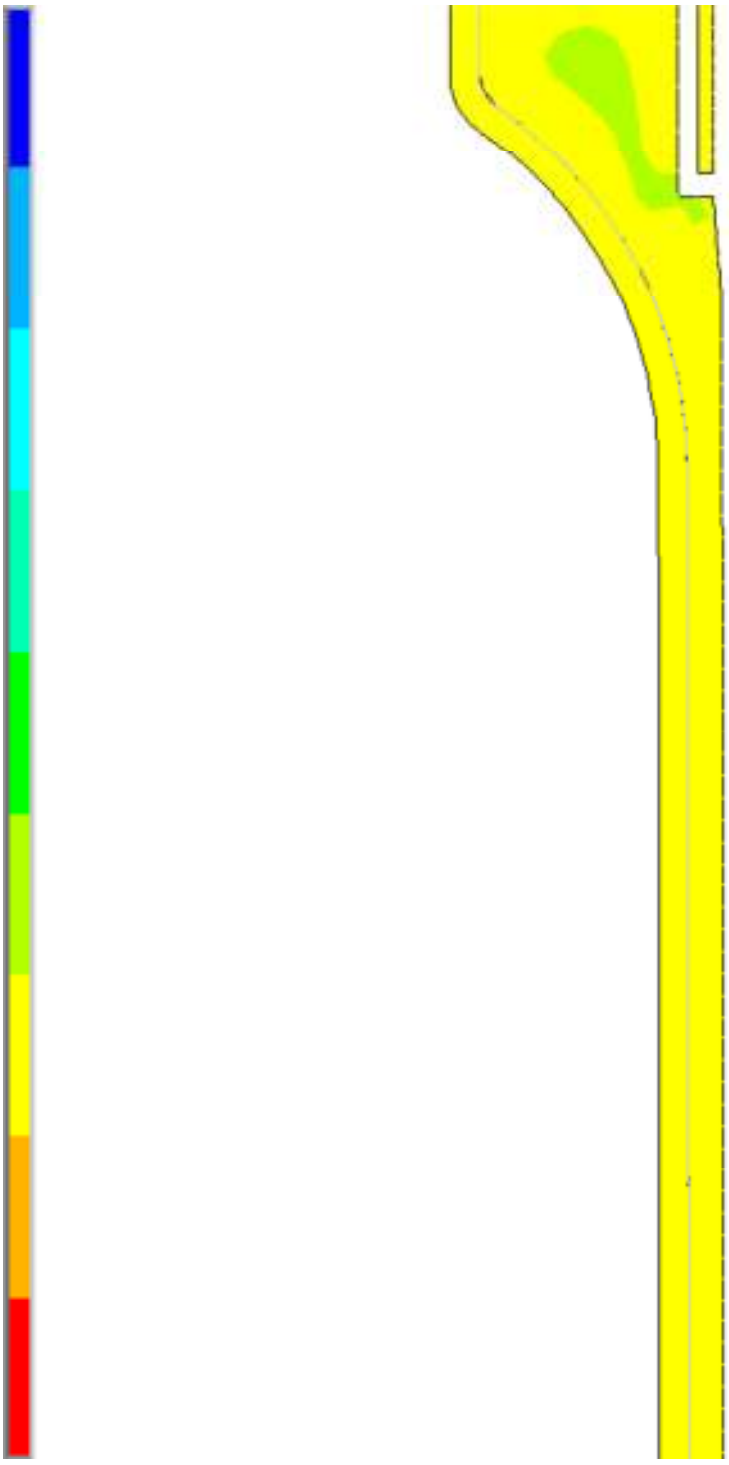

Figure 3-13. Von-Mises Stress Distribution of the Tail Section for LC-6 and Configuration-25 – Part-3

The deformation of the tail section is given as splitting to 3 parts. Model with colors means final position of tail section. Model with only lines means initial position of tail section

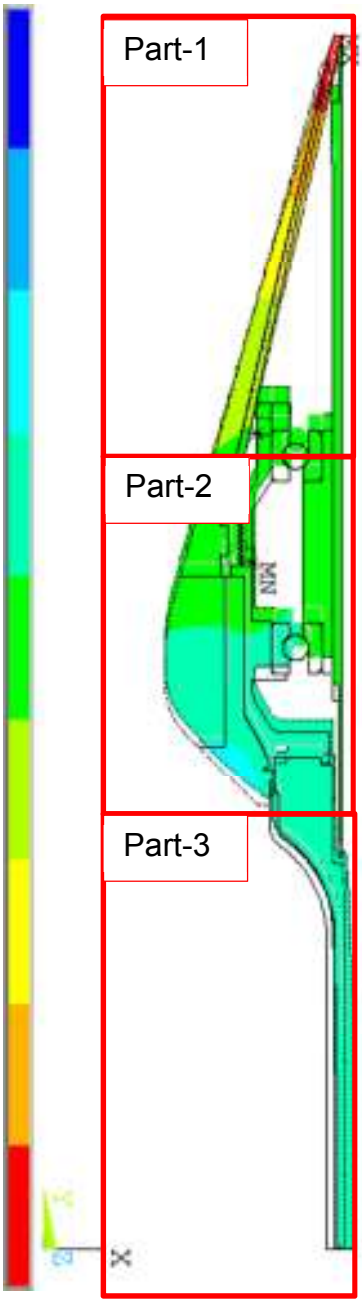

Figure 3-14. Deformation of the Tail Section for LC-6 and Configuration-25

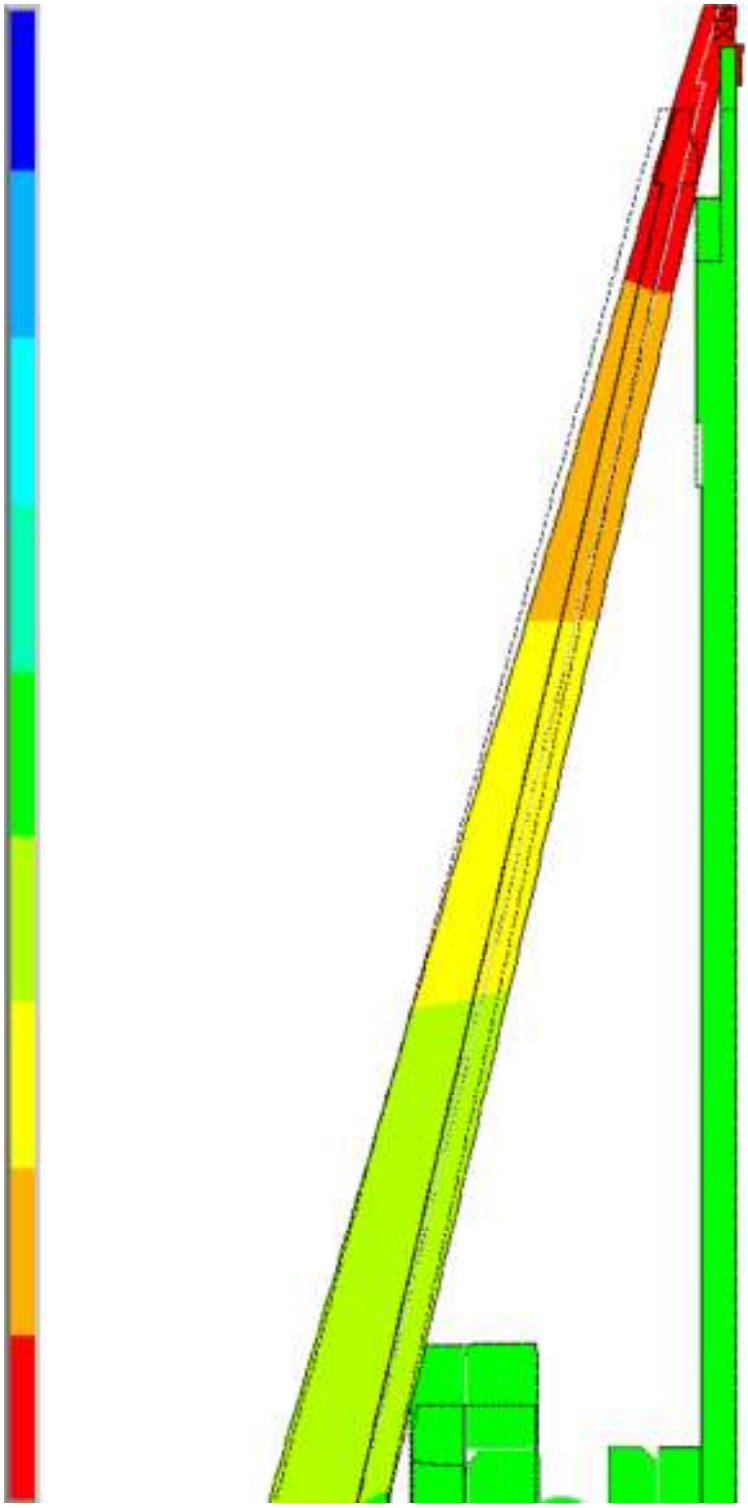

Figure 3-15. Deformation of the Tail Section for LC-6 and Configuration-25 – Part-1

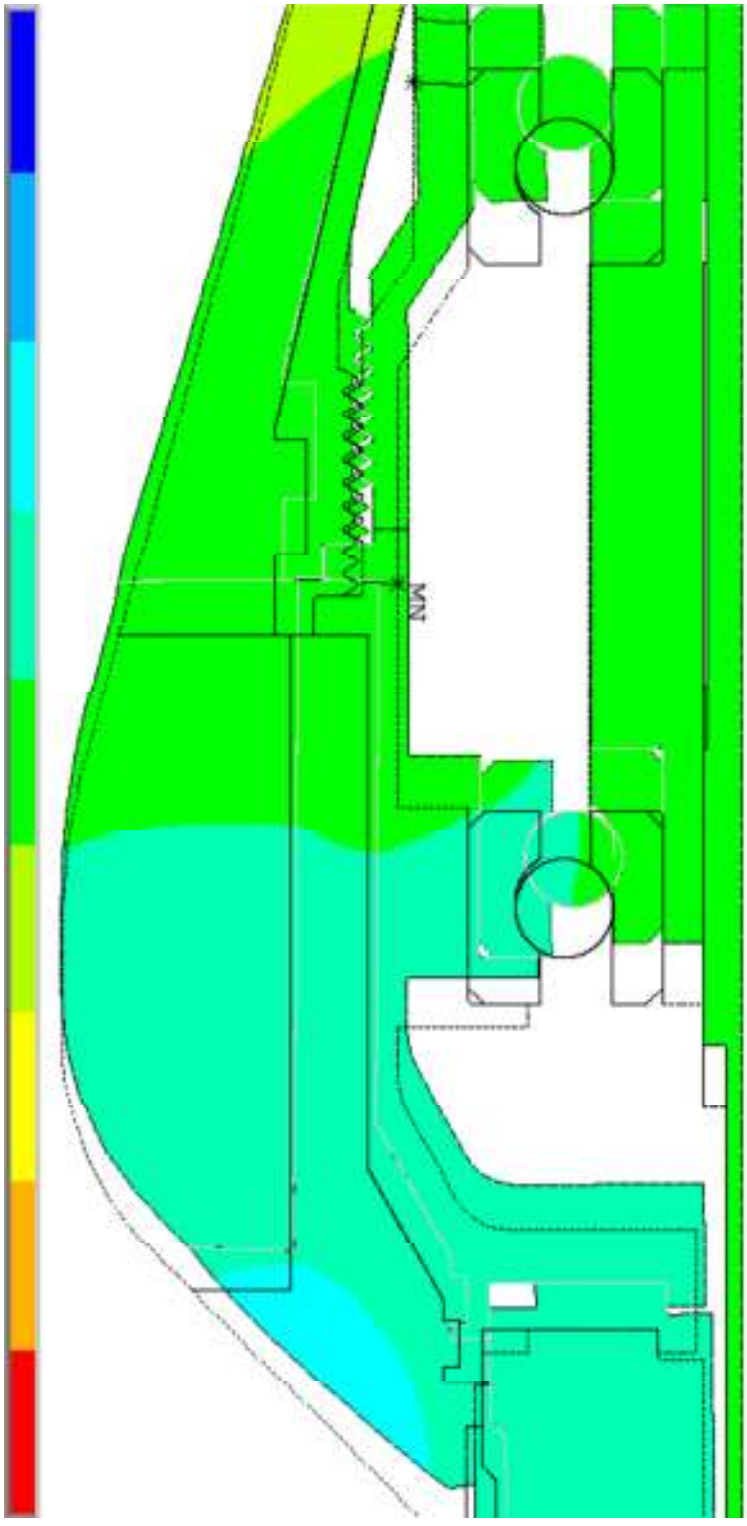

Figure 3-16. Deformation of the Tail Section for LC-6 and Configuration-25 – Part-2

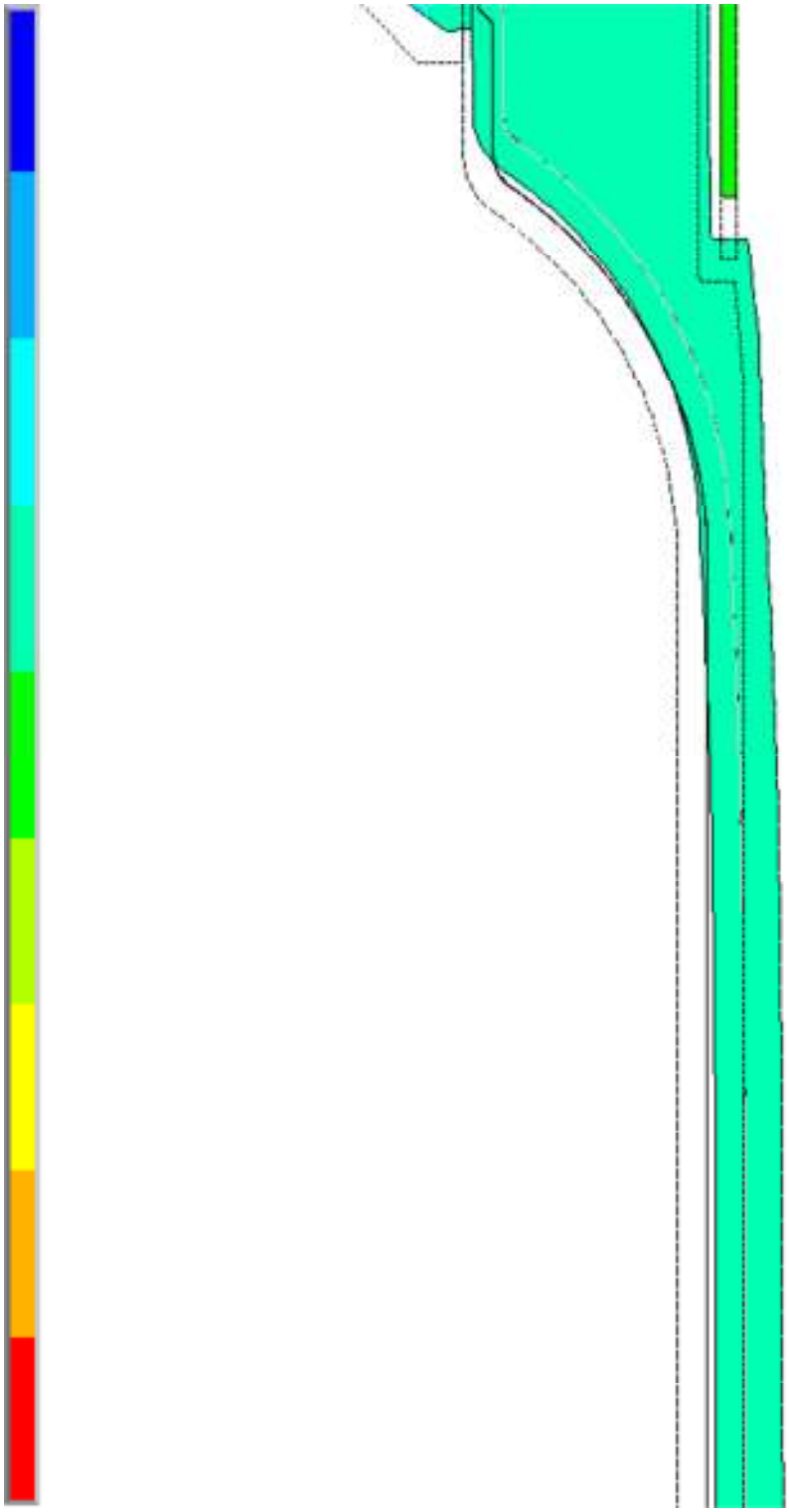

Figure 3-17. Deformation of the Tail Section for LC-6 and Configuration-25 – Part-3

To examine the FEA results by DOE method, special software is used. FEA inputs (Table 3-1 and Table 3-2) and FEA results (Table 3-7 and Table 3-8) are used as an input of the DOE software. The Output of the DOE software is given in Table 3-11.

Table 3-11. ANOVA Table for the Forces Occurred on the Bearing Rings

Source	Sum of Squares	df	Mean Square	F Value	P-value Prob > F
Model	9,8E+06	18	5,5E+05	2,87	0.0658
A-Bearing Inner Ring	1,0E+05	2	5,2E+04	0,27	0.7665
B-Bearing Outer Ring	4,0E+05	2	2,0E+05	1,05	0.3921
C-Preload	7,3E+06	2	3,6E+06	19,08	0.0009
AB	7,9E+05	4	2,0E+05	1,04	0.4457
AC	5,1E+05	4	1,3E+05	0,67	0.6306
BC	7,6E+05	4	1,9E+05	1,00	0.4611
Residual	1,5E+06	8	1,9E+05		
Cor Total	1,1E+07	26			

Sum of Squares: Total of the sum of squares for the terms in the model, as reported in the Effects List for factorials and on the Model screen for RSM, MIX and Crossed designs.

DF: Degrees of freedom for the model. It is the number of model terms, including the intercept, minus one.

Mean Square: Estimate of the model variance, calculated by the model sum of squares divided by model degrees of freedom.

F Value: Test for comparing model variance with residual (error) variance. If the variances are close to the same, the ratio will be close to one and it is less likely that any of the factors have a significant effect on the response. Calculated by Model Mean Square divided by Residual Mean Square.

Prob > F: Probability of seeing the observed F value if the null hypothesis is true (there is no factor effect). Small probability values call for rejection of the null hypothesis. The probability equals the proportion of the area under the curve of the F-distribution that lies beyond the observed F value. The F distribution itself is determined by the degrees of freedom associated with the variances being compared.

Effects of the variables on the force results is given in Figure 3-18, Figure 3-19 and Figure 3-20. DOE software prepares a formula from the given force inputs. This formula evaluates the average (predicted) value for the force value. In graphs prisms show the predicted values evaluated from formula. Points indicate real values obtained from FEA results. If point is red, this means that the real value is above the predicted value; if the point is pink, this means that the real value is below the predicted value. If the graphs given examined, one can see that most of the real values are very close to the predicted values.

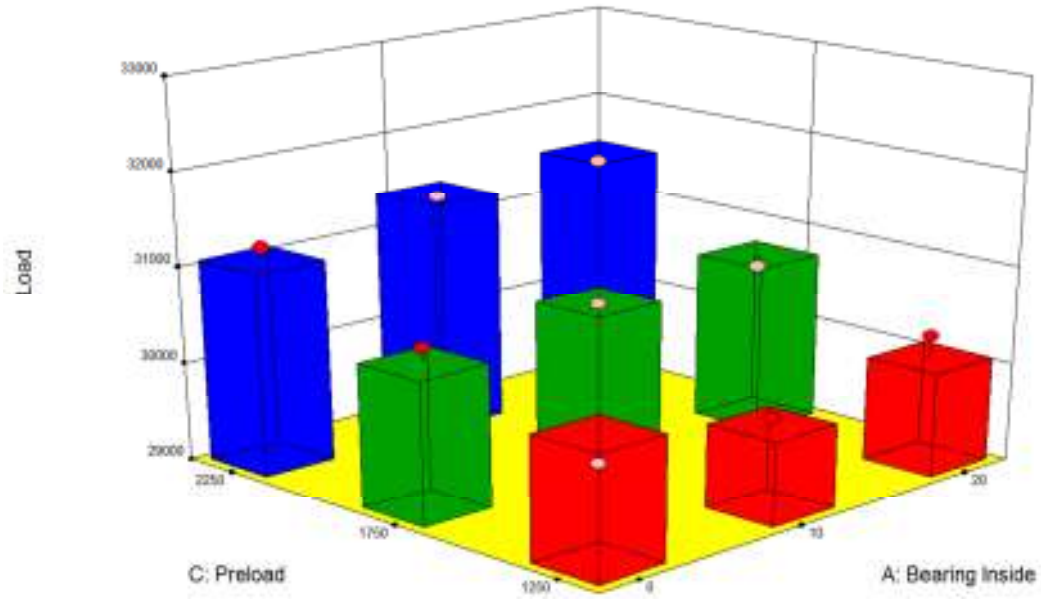

Figure 3-18. 3D Graph for the Effect of the Variables on the Force Results for BO of 20μm

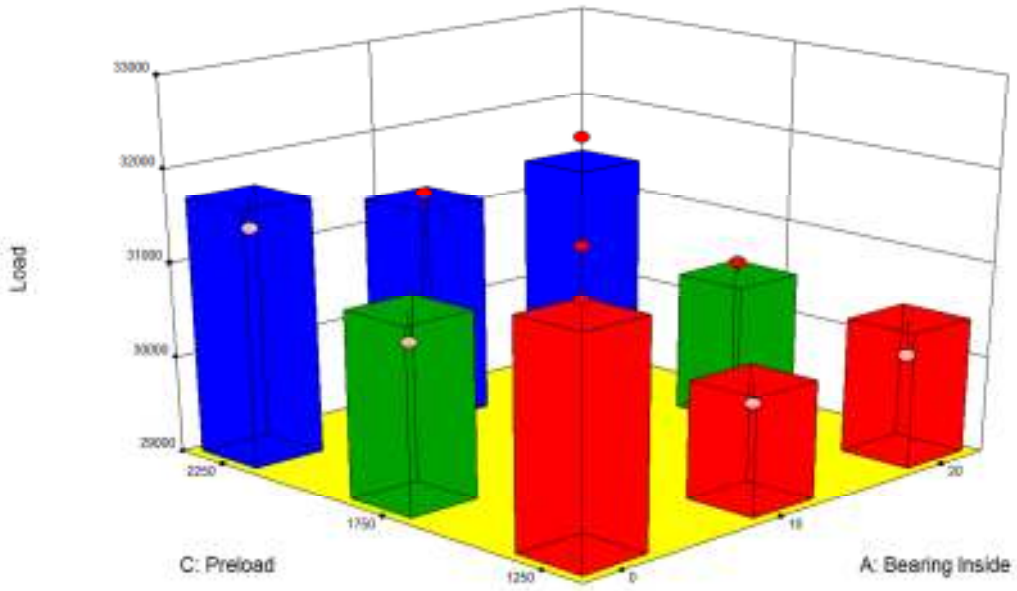

Figure 3-19. 3D Graph for the Effect of the Variables on the Force Results for BO 30µm

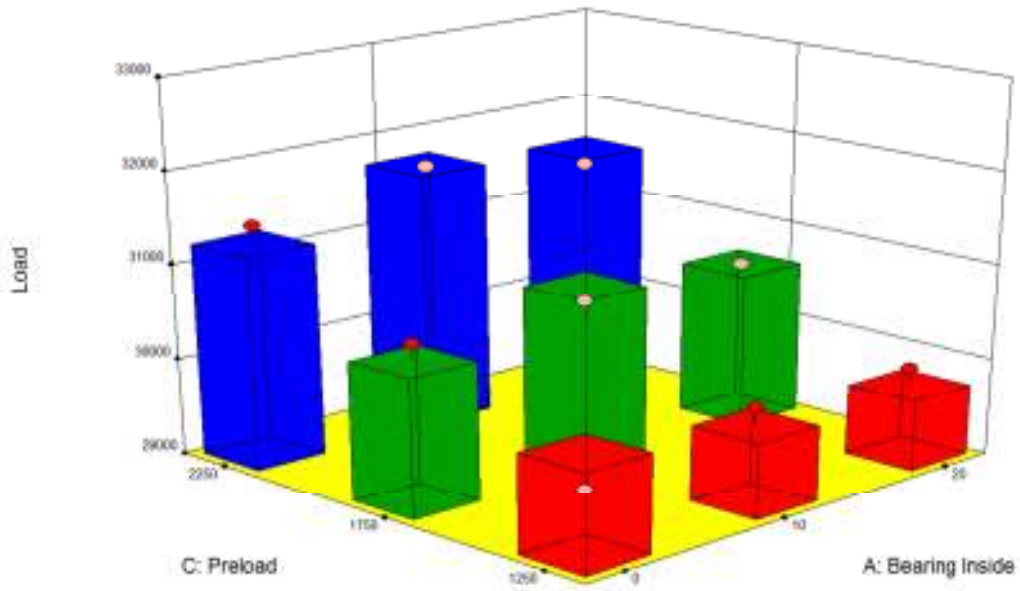

Figure 3-20. 3D Graph for the Effect of the Variables on the Force Results for BO 40µm

It is obvious from Table 3-11 that bearing inner/outer ring interference values don't affect system's response very much. Because for α=%90 reliability level, statistically only between preload and force values there is a significant difference. This situation is understood by comparing P values. The other variables don't affect the system very much. So for the other two variables, any value can be chosen for the most suitable configuration.

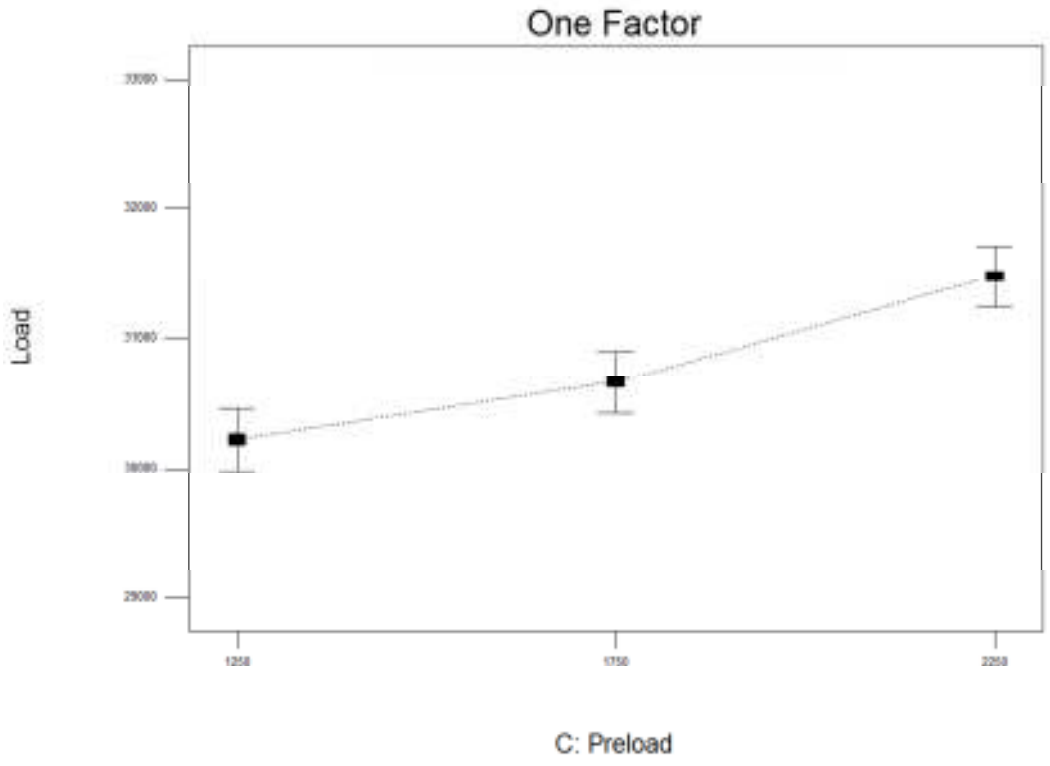

Figure 3-21. Effect of Preload Parameter on the Front Bearing Force Results (BI=10μm, BO=30μm)

One can see from Figure 3-21 that if the preload value increases, force value increases. That's why configuration with minimum preload value (configuration-25) is chosen as the most suitable configuration.

Effects of the variables on the force results is given in Figure 3-18, Figure 3-19 and Figure 3-20. DOE software prepares a formula from the given load inputs. This formula evaluates the average (predicted) value for the force. In graphs prisms show the predicted values evaluated from formula. Points indicate real values obtained from FEA results. If point is red, this means that the real value is above the predicted value; if the point is pink, this means that the real value is below the predicted value. If the graphs given examined, one can see that most of the real values are very close to the predicted values.

CHAPTER 4

CONCLUSIONS AND FUTURE WORKS

4.1 Conclusions

For the weapon systems, rocket/missile systems are very critical issue. So to validate the design of rocket/missile, FEA shall be performed for all the steps. In this thesis, tail section of the missile is examined. During the flight of missile, the thermal and mechanical loads (pressure because of propulsion, thread preload, inertial load because of aerodynamic forces and interference fit values of the bearings) occur on the missile. Also nonlinearities like concentrated contacts between the parts, large deformations, the mechanical behavior of materials (plasticity)) are included to FEA to predict the correct behavior of bearings.

After the first analysis, DOE variables are determined. By using these variables several analysis are performed. By taking all the results into consideration, the most suitable values for the variable set are determined. Totally 27 different configurations are studied to achieve to the most suitable variable set.

The most suitable variable configuration is determined by investigating VM stress and force distribution on the bearings. For VM stress distribution, firstly maximum VM stress on the bearings are controlled if it exceeds material mechanical limitations, secondly minimum value of the maximum VM stress is taken as most suitable variable set. Beside of these controls, force distribution on the bearings is used to check if there is any separation between bearings and other parts. The assembly investigated has the following pairs located at the front and back side of the tail section; 2 outer rings, 2 balls and 2 inner rings.

After examining the VM stresses and loads given in tables in section “3.2 Results of FEA”, it is seen that results for all configuration are in the ±%5 range. So this means our parameters don’t affect the systems response very much.

So taking manufacturing processes into consideration, configuration with the highest bearing inner/outer ring interference is taken as the most suitable configuration among others. For bearing inner ring interference is 20 μm; for bearing outer ring interference is 40μm are the highest interference value in the configurations. But there are three configurations with these values; configuration 25, 26 and 27. So these configurations are compared with each other. The comparison shows that the configuration 25 is the most suitable one, if forces and VM stress on the bearings are checked.

Generally the manufacturer of the bearing (or whatever part) makes many tests on the bearing to choose the most suitable input values for the bearing. However it is understood that even if the manufacturer makes many tests on the bearing, these values may not be used for extreme operations. So FEA shall be performed to check the catalogue values are useable or not.

For extreme operations, specially designed bearings are used. So this means that bearings used for extreme operations aren't standard bearings. So cost for the design time and manufacturing processes is very important. FEA method is used to decrease these costs.

Bearing inner/outer ring interference values are effective to manufacturing process. Because for low interference fit values, expensive benches shall be used and long manufacturing time is needed. From the FEA results, one can see that for this tail section model, bearing inner/outer ring interference values don't have considerable impact on the forces and VM stresses.

Based on the VM stress analysis for balls (located at the front and back side of the tail section), the more critical ball is located at the rear side and is exposed to 68 MPa for configuration 25. On the other hand, if outer rings (located at the front and back side of the tail section) are examined, it is shown that the more critical part is the outer ring which is located at the rear side and is exposed to 21,8 MPa for configuration 25. In addition to that the more critical inner ring is located at the rear side and is exposed to 23,6 MPa for configuration 25. As a conclusion, if the VM stress and force results are investigated carefully, configuration 25 gives the most suitable solution for the current design.

4.2 Recommendations for Future Work

After performing FEA and selecting the most suitable values for the parameter set, as a next step, the design is to be validated by testing the system. The test system is to simulate thermal loads and mechanical loads (pressure and inertial load) stated in section “2.3 Loads on the Tail Section”. The thermal loads are to be applied by heater resistance. Mechanical loads are to be applied by dummy weights. After applying all loads to system, the sensors are to measure loads on the bearings. Output of the sensors and FEA results are to be compared.

REFERENCES

[1] Encyclopædia Britannica, Rocket and Missile System, “http://www.britannica.com”, Last Access Date: 12.07.2012.

[2] Crouch, Tom D.-Spencer, Alex M. [eds.], History of Rocketry and Astronautics, 1993.

[3] Encyclopædia Britannica, Missile, “http://www.britannica.com”, Last Access Date: 03.07.2012.

[4] National Aeronautics and Space Administration, “http://www.grc.nasa.gov”, Last Access Date: 11.07.2012

[5] Defense Industry Daily, “http://www.defenseindustrydaily.com”, Last Access Date: 11.07.2012

[6] Space Daily, “http://www.spacedaily.com”, Last Access Date: 11.07.2012

[7] Imperial War Museum, “http://www.iwm.org.uk”, Last Access Date: 11.07.2012

[8] IHS Jane's: Defense & Security Intelligence & Analysis, Jane’s Military Vehicles and Logistics, 2010-2011.

[9] IHS Jane's: Defense & Security Intelligence & Analysis, Jane’s Armour and Artillery, 1996-1997.

[10] Roketsan, “http://www.roketsan.com.tr/”, Last Access Date: 11.07.2012

[11] ANSYS, User Manual. Version 14.0, Last Access Date: 16.07.2012.

[12] Dr. Ing. Claudio Gianini: Formula One Car Wheel Bearings: an FE Approach, ABAQUS Users' Conference, 2007

[13] National Aeronautics and Space Administration, Criteria for Preloaded Bolts, 1998.

[14] Göncz, P. & Glodez, S.: Calculation Model for Pre-Stressed Bolted Joints of Slewing Bearings, Advanced Enginerring, 3(2009)2, 175-186

[15] Allan Zhong: Thread Connection Response to Critical Pressures, ABAQUS Users' Conference, 2007

[16] Luca Furbatto, Stephen M King: Investigation Into the Distribution of Contact Pressure in Roller Bearings Used for High Speed Automative Applications, ABAQUS Users' Conference, 2007

[17] Bearing Installation — Fitting Practice, BSA Educational Services Committee, 2000.

[18] McGraw-Hill, Shigley's Mechanical Engineering Design, 2007.

[19] Harold A. Rothbert," Mechanical Design Handbook", McGraw-Hill Professional Publishing; Rev Sub edition, November 1, 1995.

[20] The Quality Portal, Design of Experiments, Overview, "http://thequalityportal.com", Last Access Date: 20.07.2012.

APPENDIX A

Ansys Programming Design Language

APDL stands for ANSYS Parametric Design Language, a scripting language that you can use to automate common tasks or even build your model in terms of parameters (variables). While all ANSYS commands can be used as part of the scripting language, the APDL commands discussed here are the true scripting commands and encompass a wide range of other features such as repeating a command, macros, if-then-else branching, do-loops, and scalar, vector and matrix operations [11]. APDL used in this thesis is given in below;

```
/prep7
/SOL
LSCLEAR,…
LSCLEAR, …
LSCLEAR, …
SLOAD, …
ANTYPE, …
NSUBST, …
NLGEOM, …
TIME, …
TUNIF, …
DL, …
*DEL, …
*DIM, …
*SET, …
```

*DO, …
SLOAD, …
*ENDDO
*DEL, …
*DIM, …
*SET, …
*DO, …
SLOAD, …
*ENDDO
*DEL, …
*DIM, …
*SET, …
*DO, …
SLOAD, …
*ENDDO
solve
finish
/SOL
ANTYPE, …
NSUBST, …
TIME, …
OUTRES, …
SFL, …
SFL, …
SFL, …
SFL, …
SFL, …
SFL, …
SFL, …
SFL, …
SFL, …
SFL, …
SFL, …
SFL, …
solve
finish
/SOL
ANTYPE, …
NSUBST, …
TIME, …
OUTRES, …
ACEL, …
solve
finish
/SOL

```
ANTYPE, …
NSUBST, …
TIME, …
OUTRES, …
LDREAD, …
solve
finish
/SOL
ANTYPE, …
NSUBST, …
TIME, …
OUTRES, …
SFL, …
SFL, …
SFL, …
SFL, …
SFL, …
SFL, …
SFL, …
SFL, …
SFL, …
SFL, …
solve
finish
/SOL
ANTYPE, …
DELTIM, …
TIME, …
OUTRES, …
LDREAD, …
solve
finish
```

APPENDIX B

Results for Bearings of the Tail Section

B.1. Von-Mises Stress Distribution for Bearings

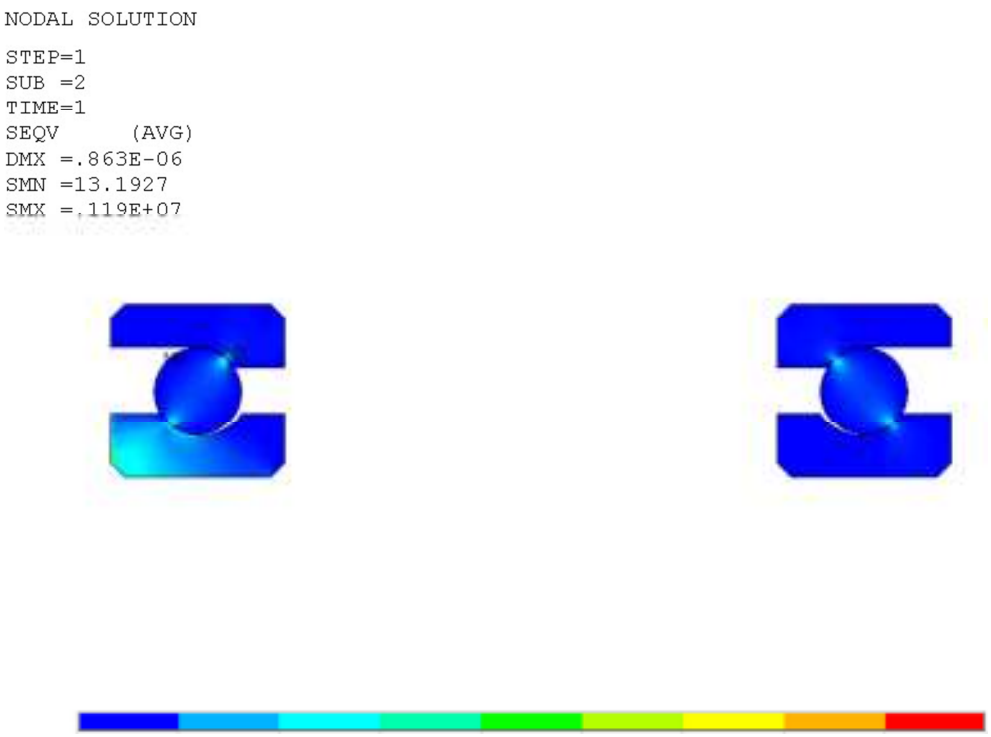

Figure B. 1. Von-Mises Stress Distribution for Bearings Load Case – 1

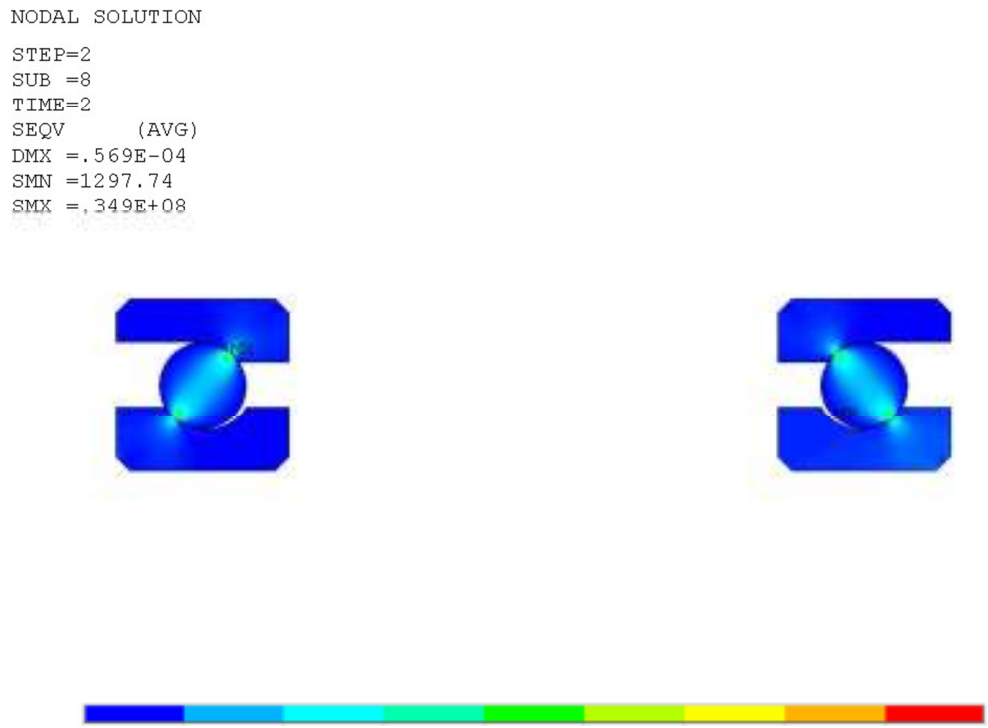

Figure B. 2. Von-Mises Stress Distribution for Bearings Load Case – 2

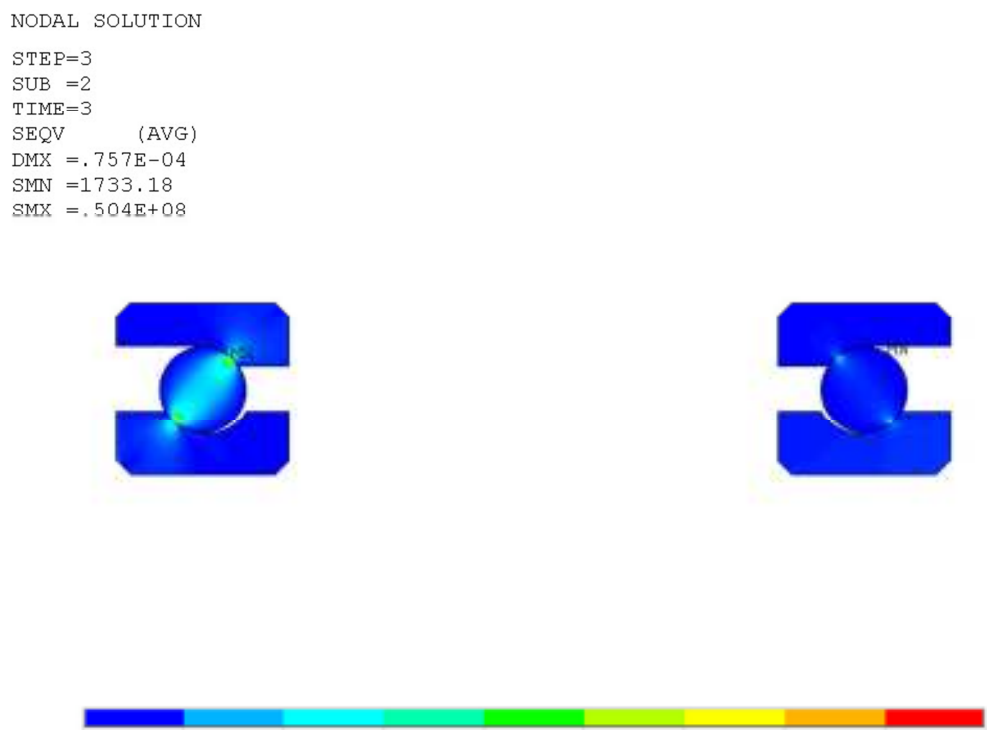

Figure B. 3. Von-Mises Stress Distribution for Bearings Load Case – 3

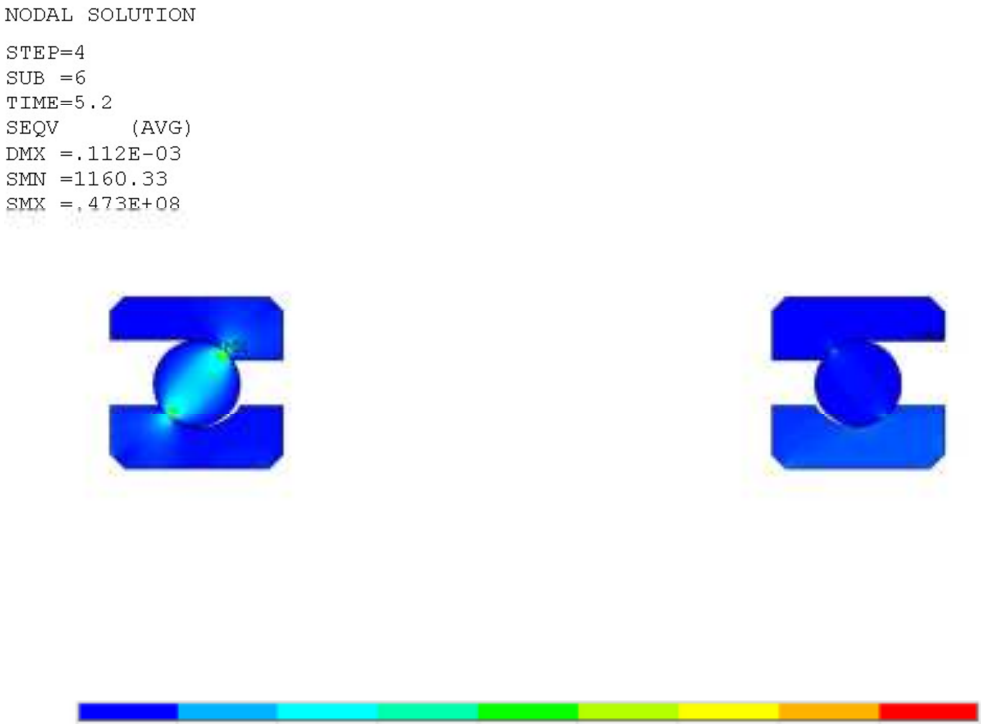

Figure B. 4. Von-Mises Stress Distribution for Bearings Load Case – 4

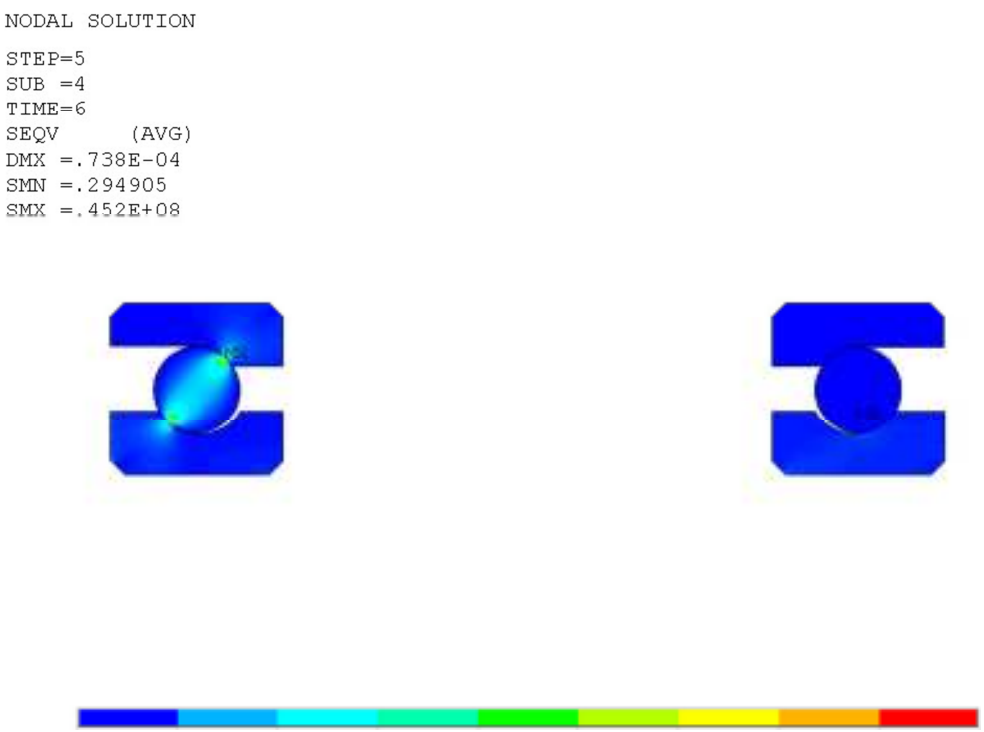

Figure B. 5. Von-Mises Stress Distribution for Bearings Load Case – 5

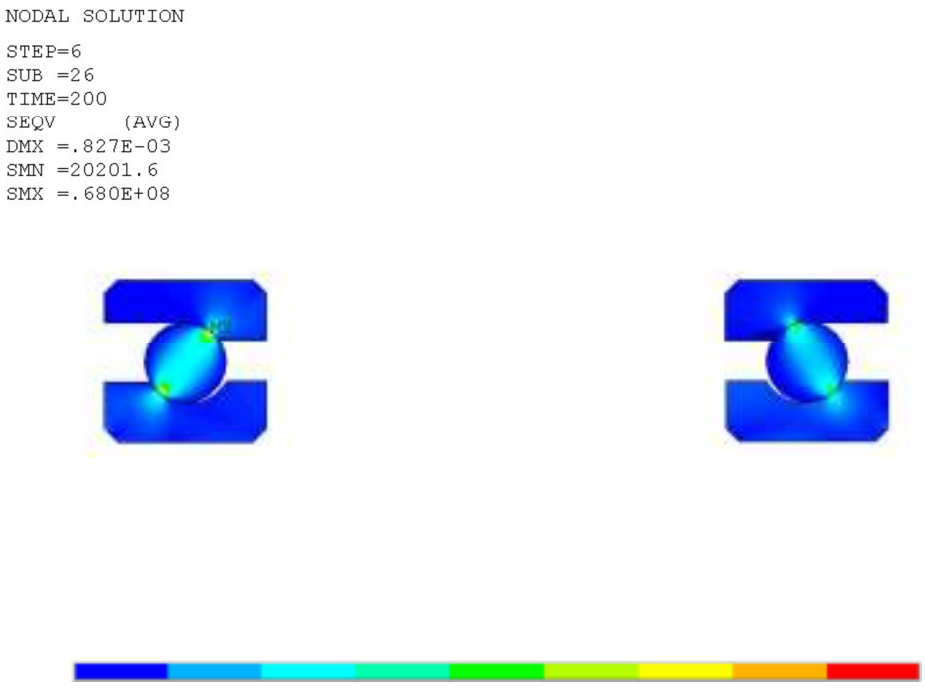

Figure B. 6. Von-Mises Stress Distribution for Bearings Load Case – 6

B.2. Von-Mises Stress Distribution for Part-1

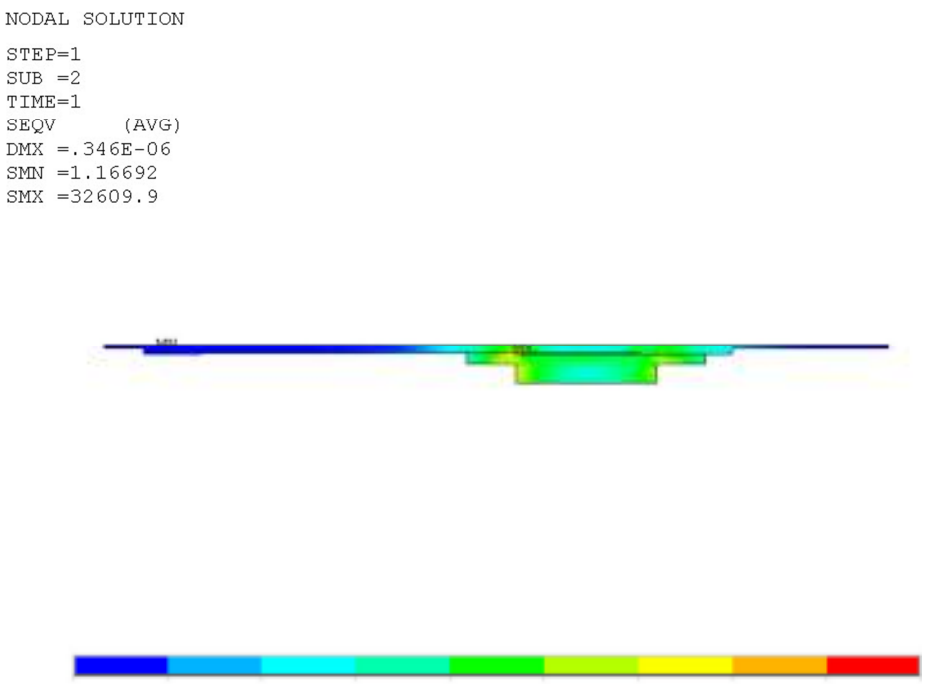

Figure B. 7. Von-Mises Stress Distribution for Part-1 Load Case – 1

NODAL SOLUTION

STEP=2
SUB =8
TIME=2
SEQV (AVG)
DMX =.500E-04
SMN =99.4059
SMX =.281E+07

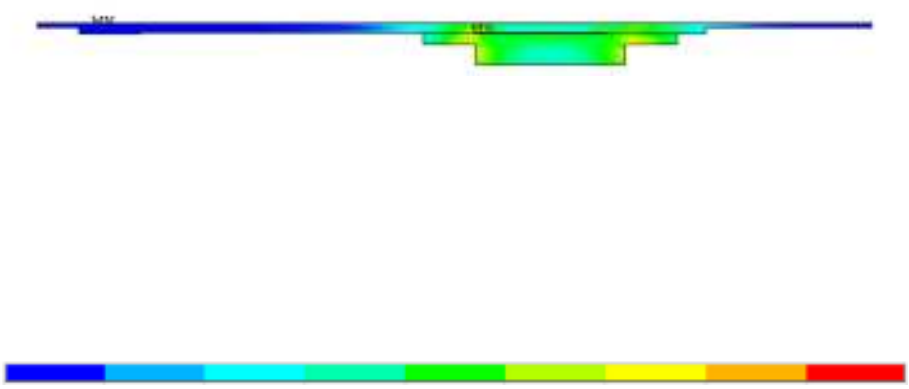

Figure B. 8. Von-Mises Stress Distribution for Part-1 Load Case – 2

NODAL SOLUTION

STEP=3
SUB =2
TIME=3
SEQV (AVG)
DMX =.697E-04
SMN =473.342
SMX =.491E+07

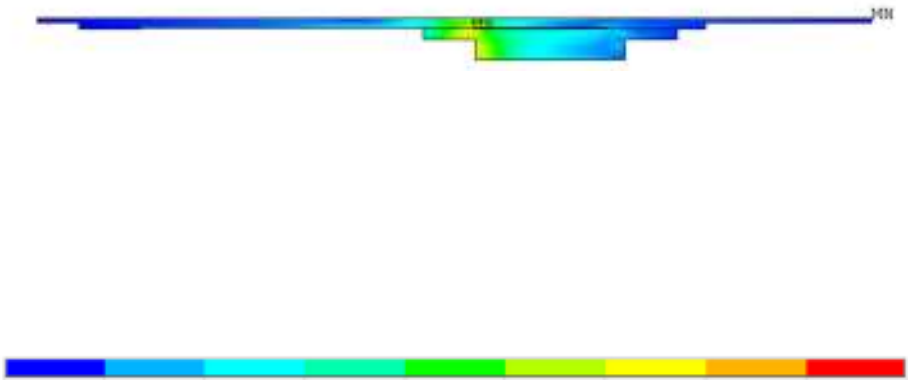

Figure B. 9. Von-Mises Stress Distribution for Part-1 Load Case – 3

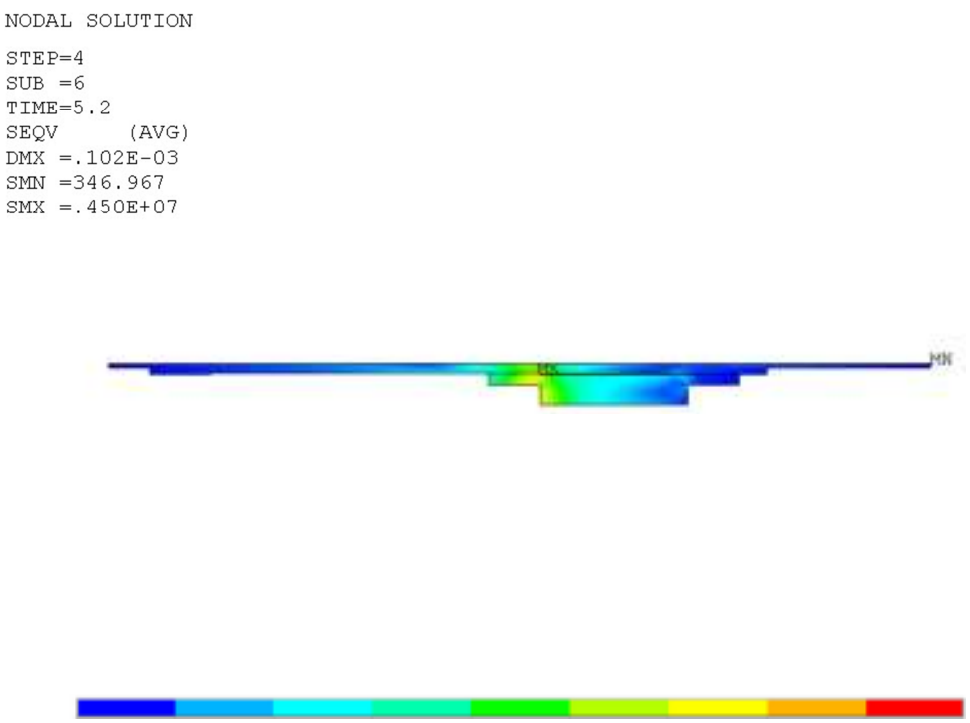

Figure B. 10. Von-Mises Stress Distribution for Part-1 Load Case – 4

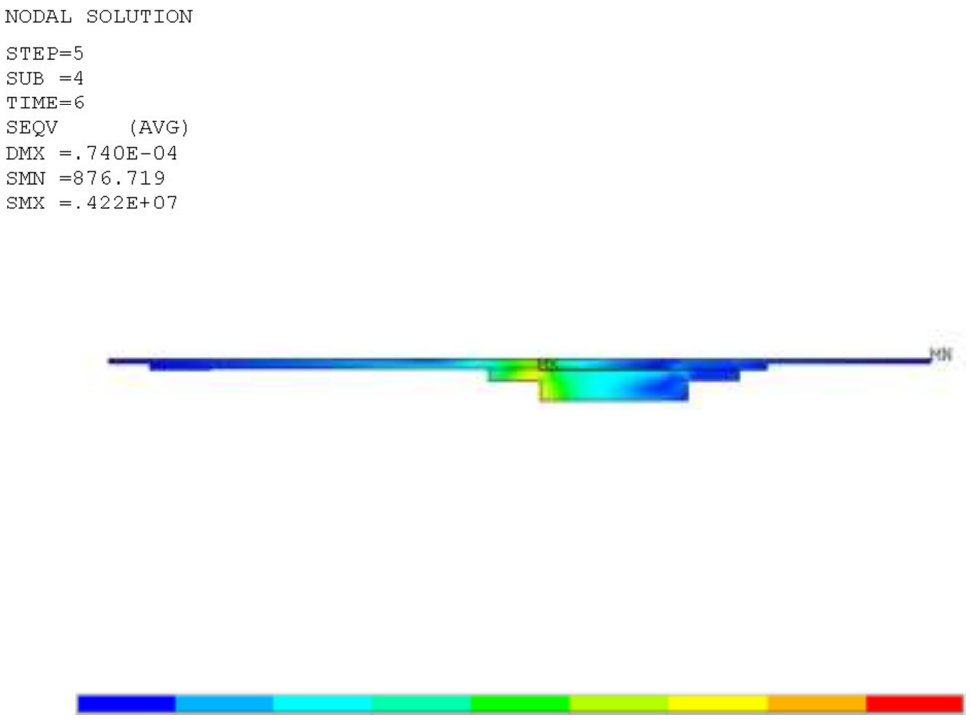

Figure B. 11. Von-Mises Stress Distribution for Part-1 Load Case – 5

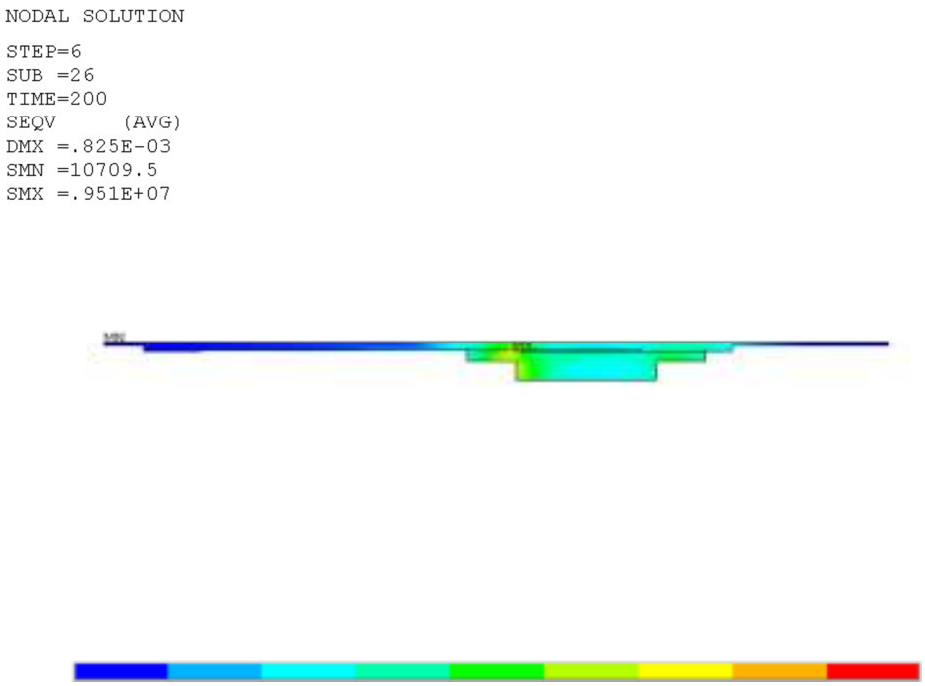

Figure B. 12. Von-Mises Stress Distribution for Part-1 Load Case – 6

B.3. Von-Mises Stress Distribution for Part-2

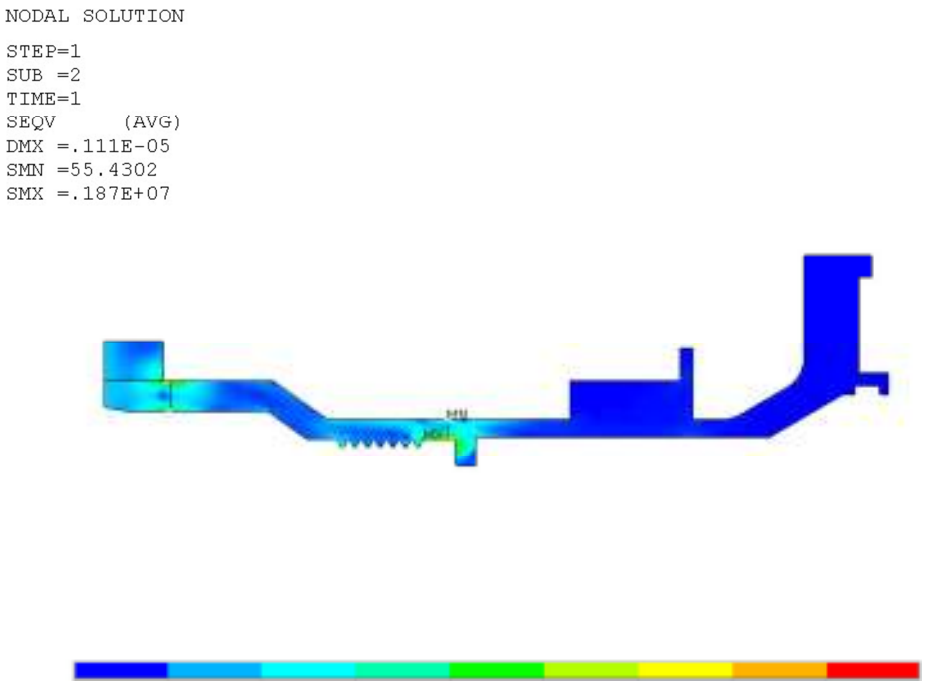

Figure B. 13. Von-Mises Stress Distribution for Part-2 Load Case – 1

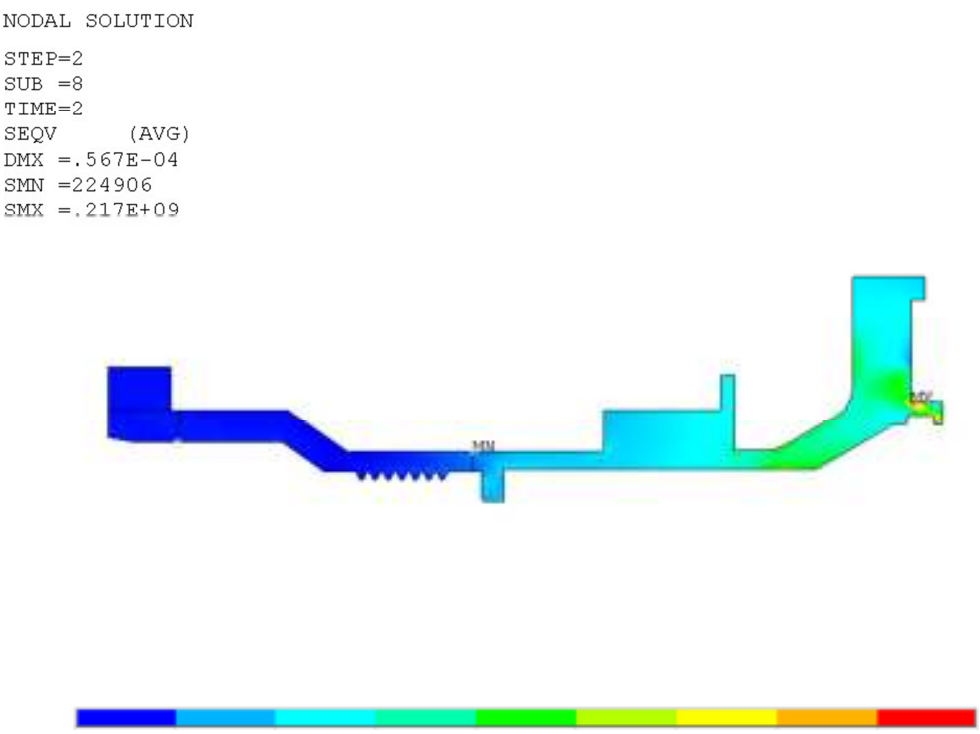

Figure B. 14. Von-Mises Stress Distribution for Part-2 Load Case – 2

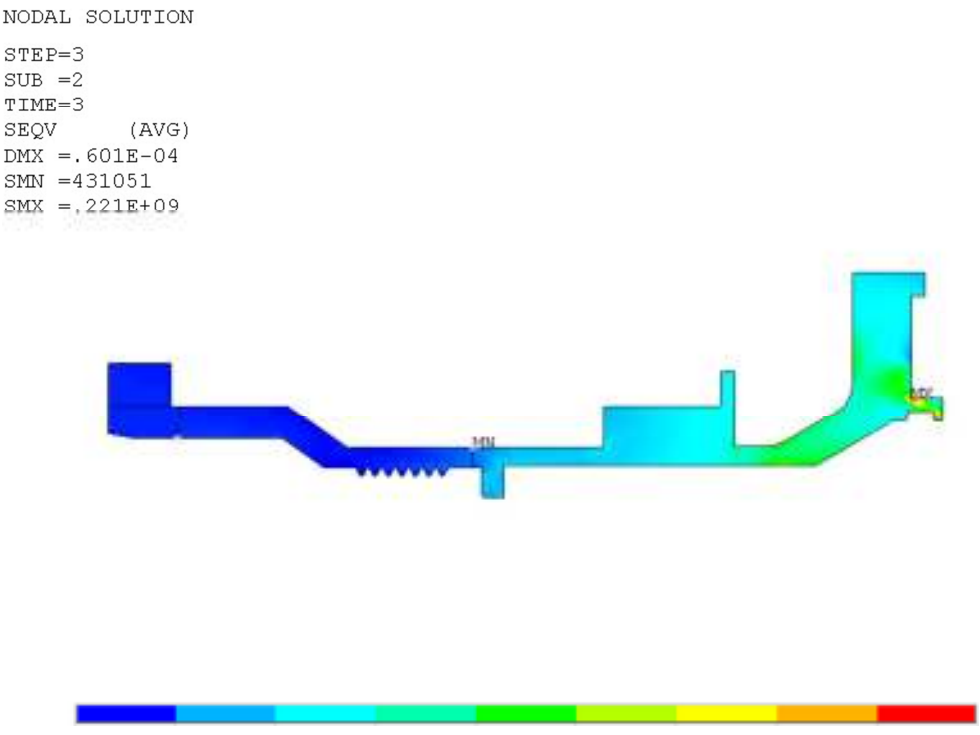

Figure B. 15. Von-Mises Stress Distribution for Part-2 Load Case – 3

NODAL SOLUTION

STEP=4
SUB =6
TIME=5.2
SEQV (AVG)
DMX =.843E-04
SMN =.419E+07
SMX =.341E+09

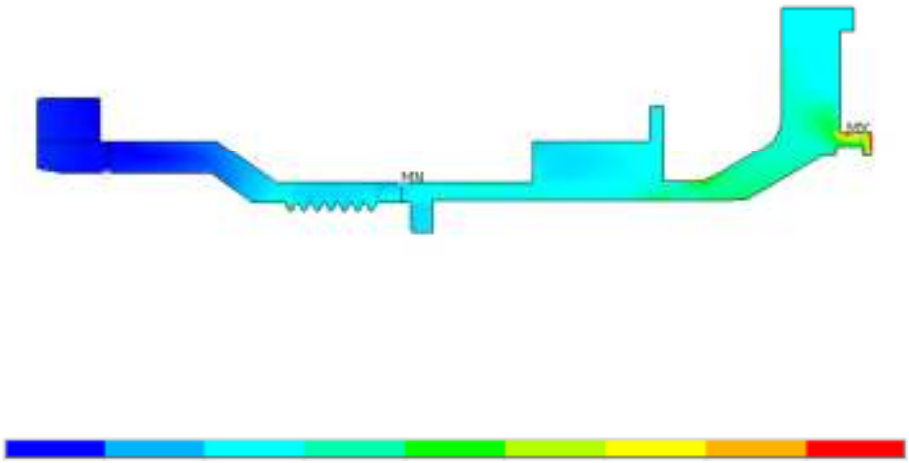

Figure B. 16. Von-Mises Stress Distribution for Part-2 Load Case – 4

NODAL SOLUTION

STEP=5
SUB =4
TIME=6
SEQV (AVG)
DMX =.500E-04
SMN =.368E+07
SMX =.401E+09

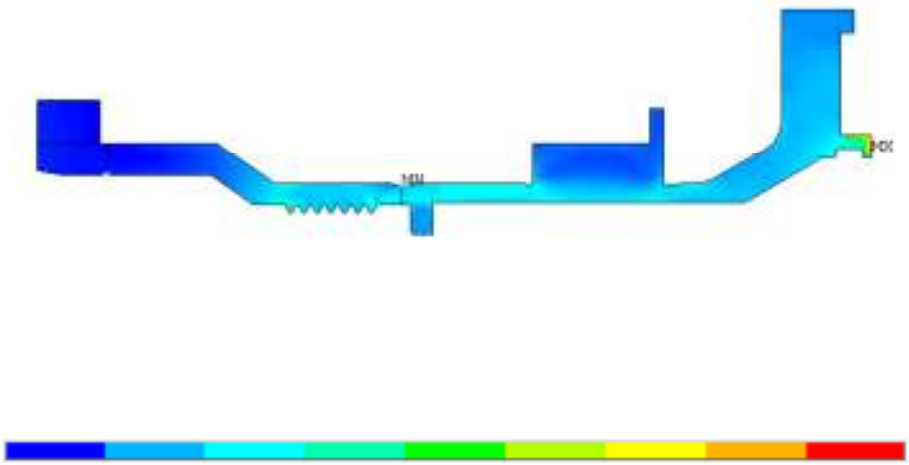

Figure B. 17. Von-Mises Stress Distribution for Part-2 Load Case – 5

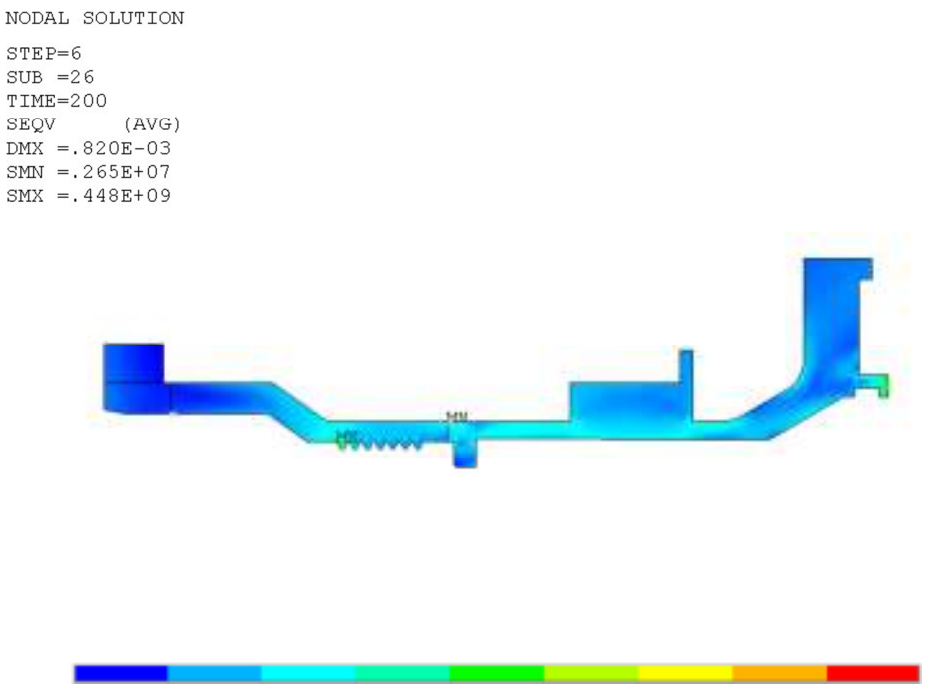

Figure B. 18. Von-Mises Stress Distribution for Part-2 Load Case – 6

B.4. Von-Mises Stress Distribution for Part-4

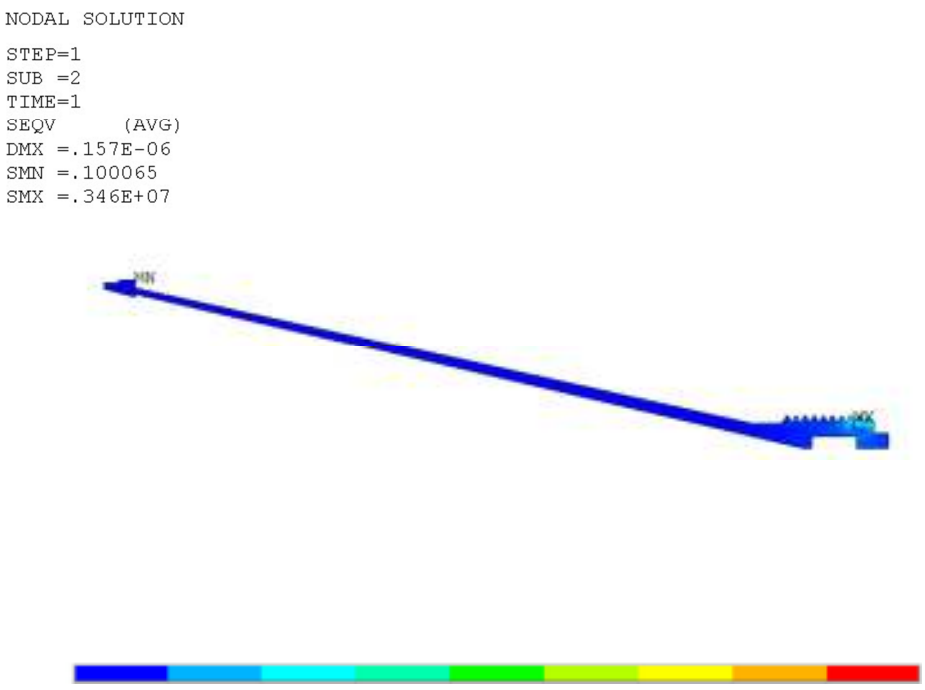

Figure B. 19. Von-Mises Stress Distribution for Part-4 Load Case – 1

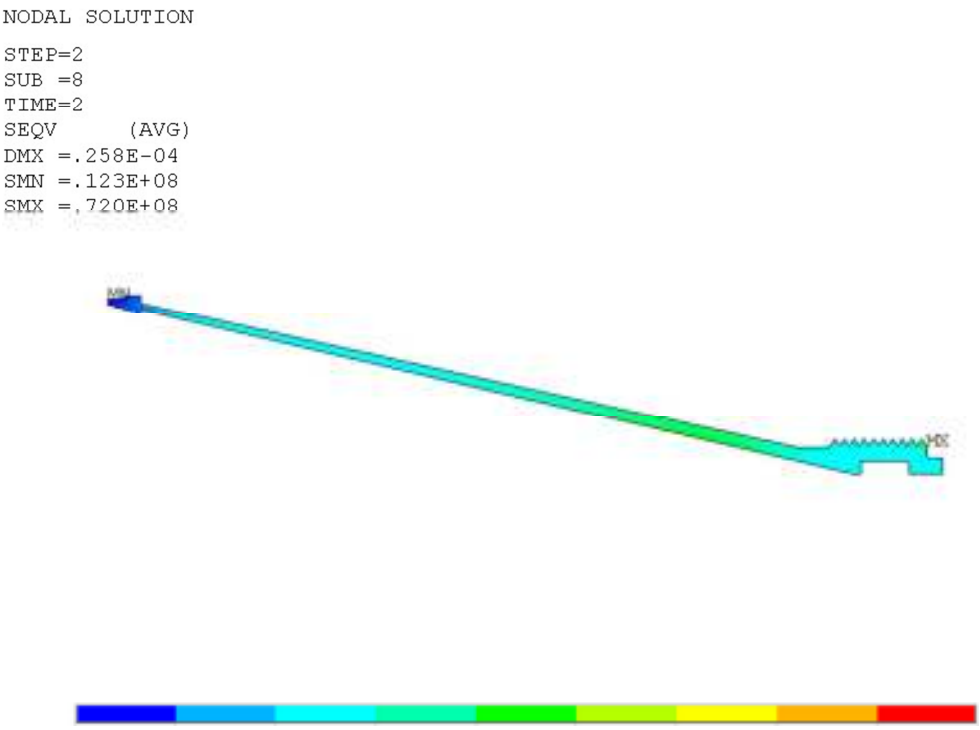

Figure B. 20. Von-Mises Stress Distribution for Part-4 Load Case – 2

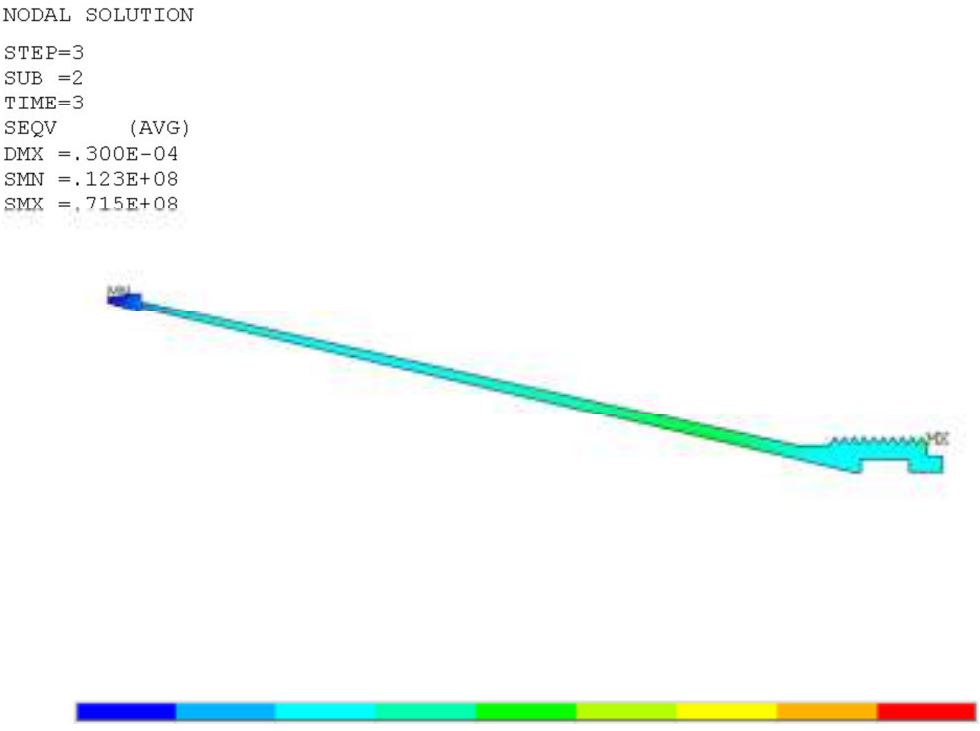

Figure B. 21. Von-Mises Stress Distribution for Part-4 Load Case – 3

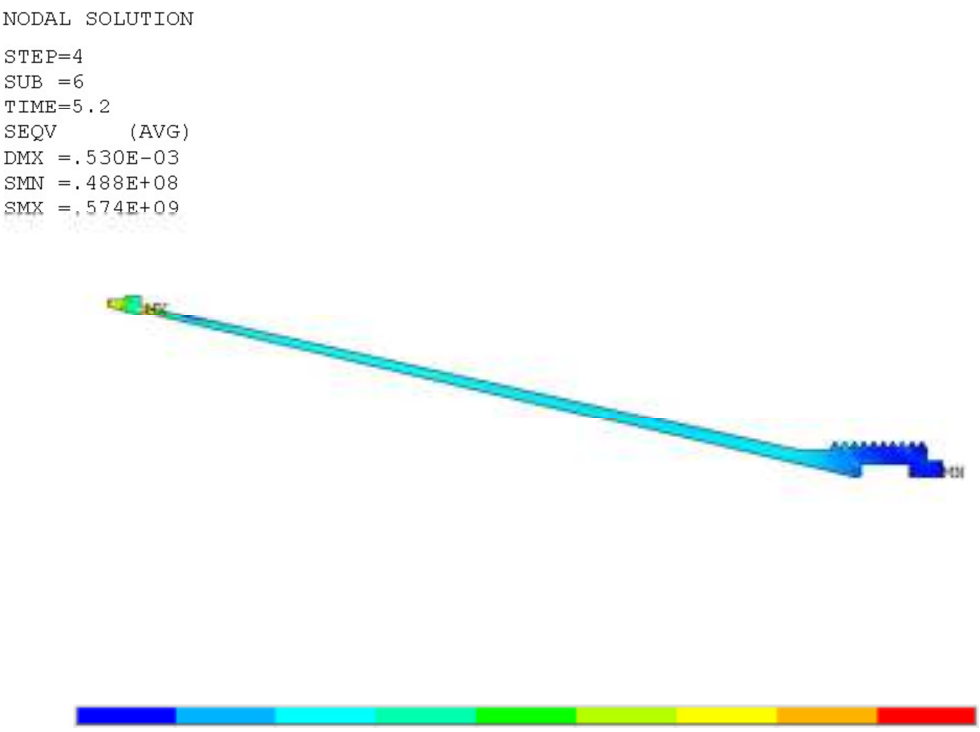

Figure B. 22. Von-Mises Stress Distribution for Part-4 Load Case – 4

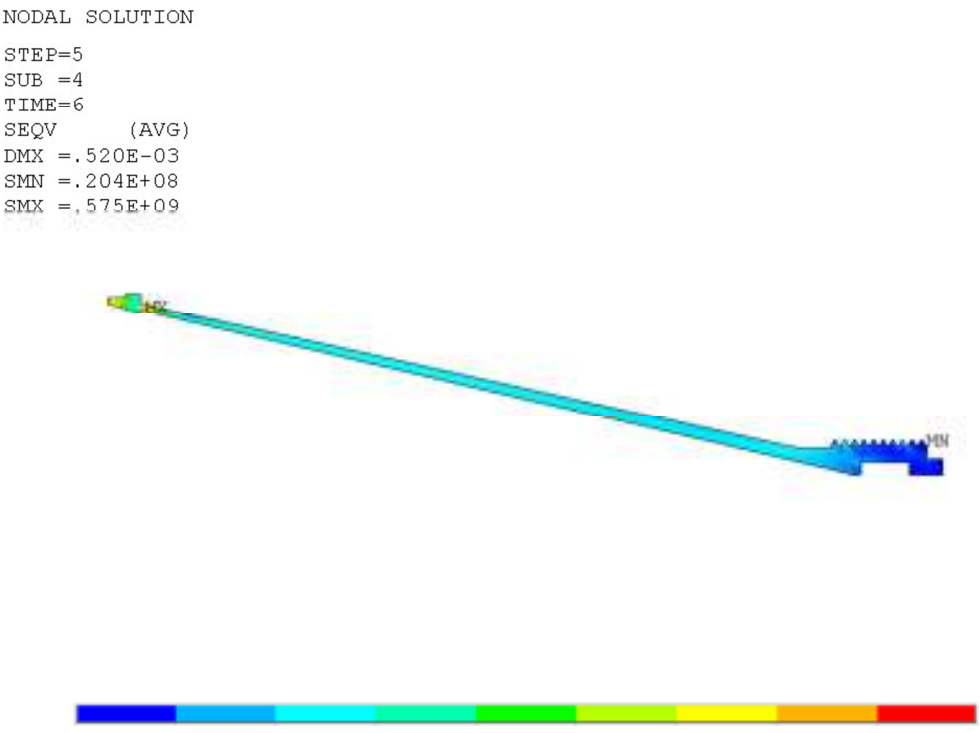

Figure B. 23. Von-Mises Stress Distribution for Part-4 Load Case – 5

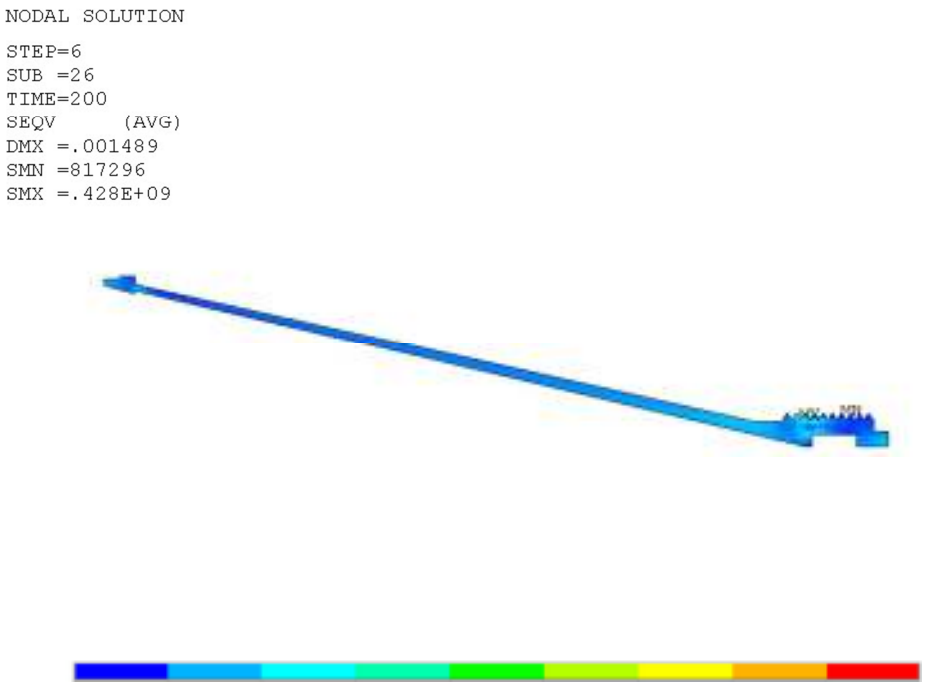

Figure B. 24. Von-Mises Stress Distribution for Part-4 Load Case – 6

B.5. Von-Mises Stress Distribution for Part-5

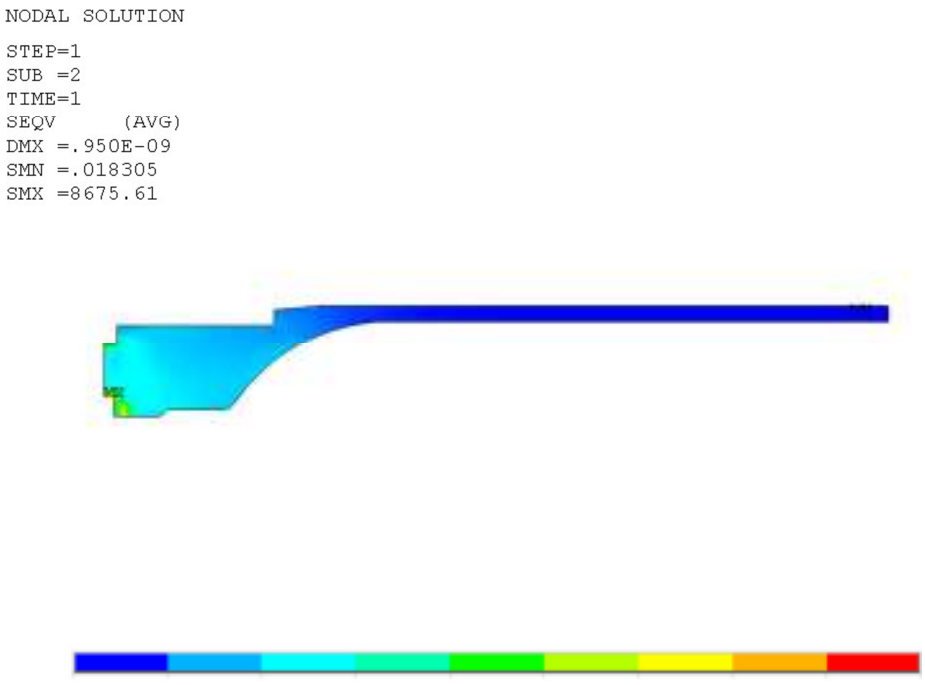

Figure B. 25. Von-Mises Stress Distribution for Part-5 Load Case – 1

NODAL SOLUTION

STEP=2
SUB =8
TIME=2
SEQV (AVG)
DMX =.352E-03
SMN =.327E+08
SMX =.488E+09

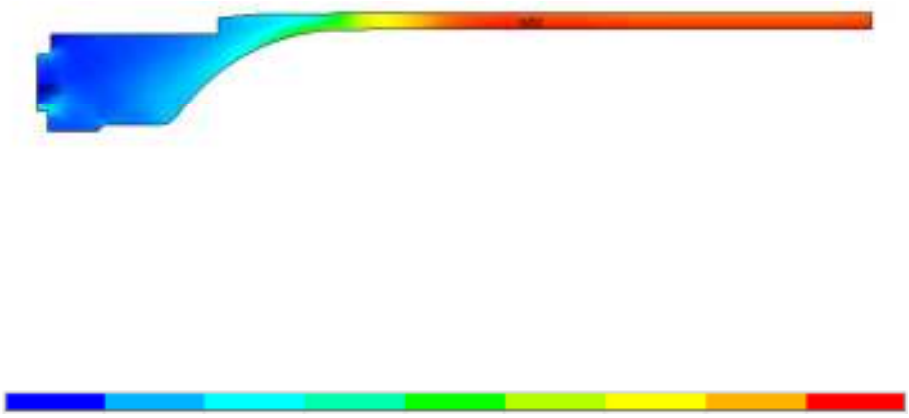

Figure B. 26. Von-Mises Stress Distribution for Part-5 Load Case – 2

NODAL SOLUTION

STEP=3
SUB =2
TIME=3
SEQV (AVG)
DMX =.352E-03
SMN =.322E+08
SMX =.488E+09

Figure B. 27. Von-Mises Stress Distribution for Part-5 Load Case – 3

NODAL SOLUTION

STEP=4
SUB =6
TIME=5.2
SEQV (AVG)
DMX =.353E-03
SMN =.794E+08
SMX =.487E+09

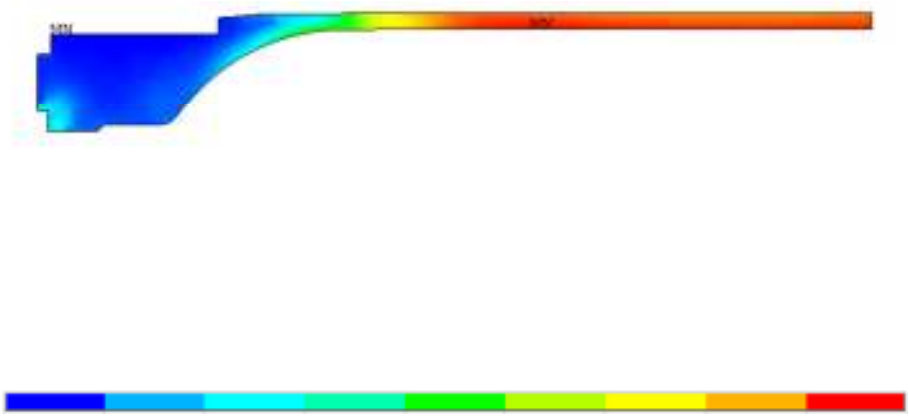

Figure B. 28. Von-Mises Stress Distribution for Part-5 Load Case – 4

NODAL SOLUTION

STEP=5
SUB =4
TIME=6
SEQV (AVG)
DMX =.382E-04
SMN =.109E+07
SMX =.173E+09

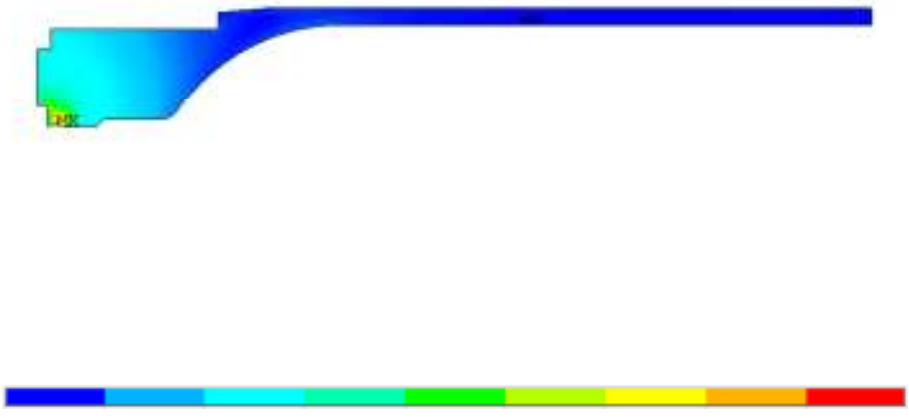

Figure B. 29. Von-Mises Stress Distribution for Part-5 Load Case – 5

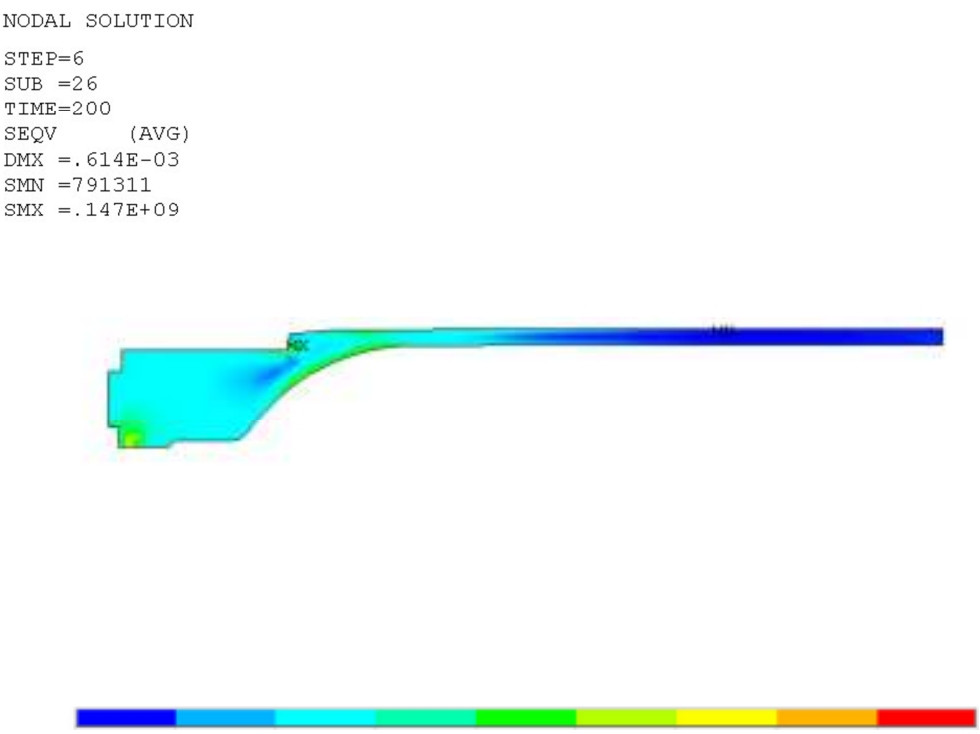

Figure B. 30. Von-Mises Stress Distribution for Part-5 Load Case – 6